LBL-5077
c.2

TWO-PROTON PICKUP STUDIES WITH THE (^{6}Li, ^{8}B) REACTION

Robert Benjamin Weisenmiller
(Ph. D. thesis)

December 3, 1976

Prepared for the U. S. Energy Research and
Development Administration under Contract W-7405-ENG-48

LBL-5077
c.2

TWO-PROTON PICKUP STUDIES WITH THE (^{6}Li,^{8}B) REACTION

Contents

TWO-PROTON PICKUP STUDIES WITH THE (^{6}Li,^{8}B) REACTION

Robert Benjamin Weisenmiller

Nuclear Science Division
University of California
Lawrence Berkeley Laboratory
Berkeley, California 94720

ABSTRACT

The (^{6}Li,^{8}B) reaction has been investigated on targets of ^{26}Mg, ^{24}Mg, ^{16}O, ^{13}C, ^{12}C, ^{11}B, ^{10}B, and ^{9}Be at a bombarding energy of 80.0 MeV, and on targets of ^{16}O, ^{12}C, ^{9}Be, ^{7}Li, and ^{6}Li at a bombarding energy of 93.3 MeV. Only levels consistent with a direct, single-step two-proton pickup reaction mechanisms were observed to be strongly populated. On $T_z = 0$ targets, the spectroscopic selectivity of this reaction resembles that of the analogous (p,t) reaction. Additionally, these data demonstrate the dominance of spatially symmetric transfer of the two protons. On $T_z > 0$ targets the (^{6}Li,^{8}B) reaction was employed to locate two previously unreported levels (at 7.47 $\pm$ 0.05 MeV and 8.86 $\pm$ 0.07 MeV) in the $T_z = 2$ nuclide ^{24}Ne and to establish the low-lying 1p-shell states in the $T_z = 3/2$ nuclei ^{11}Be, ^{9}Li, and ^{7}He. However, no evidence was seen for any narrow levels in the $T_z = 3/2$ nuclide ^{5}H nor for any narrow excited states in ^{7}He.

The angular distributions reported here are rather featureless and decrease monotonically with increasing angle. This behavior can be shown by a semi-classical reaction theory to be a consequence of the reaction kinematics. A semi-classical approach also suggests that the kinematic term in the transition matrix element is only weakly

dependent upon the angular momentum transfer (which is consistent with simple Distorted Wave Born Approximation calculations). However, only qualitative agreement was obtained between the observed relative transition yields and semi-classical predictions, using the two-nucleon coefficients of fractional parentage of Cohen and Kurath, probably due to the limitations of the semi-classical reaction theory.

I. INTRODUCTION

A major part of the focus of nuclear physics has been the attempt to explain adequately the interaction between nucleons. This nuclear interaction can be usefully described by a central potential with an additional "residual interaction" to describe detailed behavior. The dominant component of the residual interaction in light nuclei with an excess of protons or neutrons is pairing correlations (Ri 68) which can be investigated by two-nucleon transfer reactions. Such reactions have been a particularly fruitful field for nuclear spectroscopic studies (See Gl 75 and An 72 for examples). Light-ion two-nucleon transfer reactions have been used to study all types of two-particle and, also, two-hole states except for two-proton-hole levels. A two-proton pickup reaction would complement the existing two-proton stripping reaction studies, since pickup reactions preferentially populate levels below the Fermi sea, while stripping reactions populate those above it.

The (^{6}Li,^{8}B) reaction would seem to be the optimum two-proton pickup reaction for studies in the 1p-shell. No lighter reaction pair is of general utility (due to the limitations of neutron beams for the (n,^{3}He) reaction and the difficulties of detecting particle-unstable nuclides in reactions such as (α,^{6}Be)). Any heavier reaction pair would result in more severe kinematic contributions to the experimental energy resolution, would often have bound excited states so that the energy spectra would have "shadow peak" ambiguities (this would be the case for the (^{9}Be,^{11}C), (^{12}C,^{14}O), and (^{18}O,^{20}Ne) reactions, but not for the (^{11}B,^{13}N) reaction), and would present more of a challenge to detector telescopes for adequate particle identification (see Section II for a more

complete discussion of particle identification and other experimental considerations). The (^{6}Li,^{8}B) two-proton pickup reaction is well-suited to counter telescope experiments since both ^{7}B and ^{9}B are particle unstable, which allows a clean separation of the ^{8}B events from other isotopes. The difficulties with these other reactions is evidenced the few other published examples of two-proton pickup (Si 72, Ch 73, Sc 74a, and Je 74).

This work constitutes the first study of all 1p-shell targets readily available in solid form. This region is particularly suited for an initial survey, since it has been investigated thoroughly with other two-nucleon transfer reactions and the coefficients of fractional parentage (cfp) relevant to two-nucleon transfer have been calculated (Co 70). Both of these results provide a convenient base for establishing the reaction mechanism. Of particular interest was the degree of anti-symmetric pair transfer (Ku 72 and Lk 70). The two-particle cfp for $^{8}B \rightarrow {}^{6}Li + 2p$ (Ku 75) indicate that there is a larger amplitude for the proton pair to be in a spatially anti-symmetric (^{3}P) state than in a symmetric (^{1}D) state relative to the ^{6}Li core (see Section III). The simplest cluster transfer mechanism corresponds to an internal ^{1}S state (as in the (p,t) reaction) for the transferred nucleons, which for the (^{6}Li,^{8}B) reaction can only arise from the ^{1}D component. If anti-symmetric transfer is important, then the expected symmetry between the (^{6}Li,^{8}B) reaction and the analogous (p,t) reaction on $T_z = (N - Z)/2 = 0$ targets might be distorted. While most of the two-proton-hole states in the 1p-shell can be populated by both types of transfer symmetries, there are a few known levels which would be fed predominantly by spatially anti-symmetric transfer,

and two examples of this will be discussed with the experimental results in Section IV.

From this comparison of the experimental data from the (^{6}Li,^{8}B) reaction on T_z = 0 targets to both the two nucleon cfp's and the earlier (p,t) results, it is possible to demonstrate that this reaction has the anticipated spectroscopic selectivity. This selectivity in the population of states in the final nuclei was then exploited on neutron-excess targets to indicate the location of low-lying 1p-shell states in the T_z = 3/2 nuclei ^{7}He, ^{9}Li, and ^{11}Be. This series of nuclei is near the edge of particle stability, so that these levels present information on the two-body interaction in a relatively unexplored region. Also, this reaction was employed for further study of ^{4}H and ^{5}H; since many ambiguities remain in the current description of these nuclides (Fi 73 and Aj 74), any new experimental approach towards elucidating more of their character is of interest. Finally, data will be presented for ^{22}Ne and the T_z = 2 nuclide ^{24}Ne. These data on 2s-1d-shell nuclei illustrate the possible extension of this work to heavier nuclei.

II. EXPERIMENTAL DETAILS

While two-nucleon transfer reactions have been thoroughly investigated, this work involved an extension of many aspects of the experimental techniques employed in these earlier studies. These differences occurred in the production of a lithium beam (Section A), detection and identification of ^{8}B particles (Section C), and achieving adequate background reduction in these modest yield reactions (which was accomplished in part through electronic requirements--Section C--and partially by more detailed data analysis based upon multi-parameter recording of each event--Section D). Many of these differences resulted from the heavy-ion character of both ^{6}Li and ^{8}B. The yields placed these particular reaction studies as intermediate between more conventional spectroscopic studies and mass measurement work on relatively inaccessible nuclei, so that the experimental techniques resemble more closely those employed in the mass measurement studies, while the information and interest resemble those of conventional spectroscopic studies.

A. Ion Source, Cyclotron, Beam Transport, and Experimental Area

These experiments were conducted with the variable-energy, sector-focused Lawrence Berkeley Laboratory 88-inch cyclotron, which provided the required high energy beams (high energies are needed due to the very negative Q-values of these reactions, the kinematic conditions, and particle identification constraints). This cyclotron can produce a maximum energy of 140 Q^2/A MeV for heavy-ions of charge state Q and mass A. For $^{6}Li^{+2}$ ions this corresponds to 93.3 MeV, which was employed for the studies of the ^{6}Li and ^{7}Li targets and for a portion

of the investigation with the ^{9}Be target. The remainder of this work was conducted with an 80 MeV $^{6}Li^{+2}$ beam.

As there is no suitable gaseous lithium compound, lithium ions have not generally been accelerated in cyclotrons, so that the development of an appropriate lithium vapor source was required for this work. These beams were produced at the cyclotron by a Penning Ion Gauge (PIG) type source (see Cl 72) with arc-heated cathodes (see Fig. II-1). The lower source cathode consisted of a mixture of isotopically-separated ^{6}LiF (40%) and tantalum powered (60%), which was fused at high pressure. In addition, a tantalum sleeve, coated with fused ^{6}LiF was placed inside the anode chamber. A carrier gas (typically $^{14}N_2$) was employed to strike and maintain the source arc. This arc eroded the cathodes and heated the sleeves, thus vaporizing the lithium.

This beam was accelerated by the cyclotron operating on the first harmonic at a frequency of 8.5 MHz, so that successive beam pulses (5-ns wide) were separated by about 120 ns. The cyclotron, beam transport systems, and the experimental area are shown in Fig. II-2. A beam energy analysis of $dE/E \sim 0.14\%$ was obtained by bending the beam with a switching magnet through an angle of 39.5^{o} onto a 1.5 mm wide analyzing slit. Absolute beam energies were measured with a high precision analyzing magnet (Hi 69) with a $dE/E = 0.02\%$, which was calibrated for absolute energies by scattering molecular hydrogen ion beams on ^{12}C and observing the T = 3/2 resonance in ^{13}N at 14.232 MeV (Ba 71). (This system is located in an adjacent experimental area and is not shown in Fig. II-2.) Typical beam spots of 1.5 x 2.0 mm^2 were obtained on target in the 0.5-m scattering chamber.

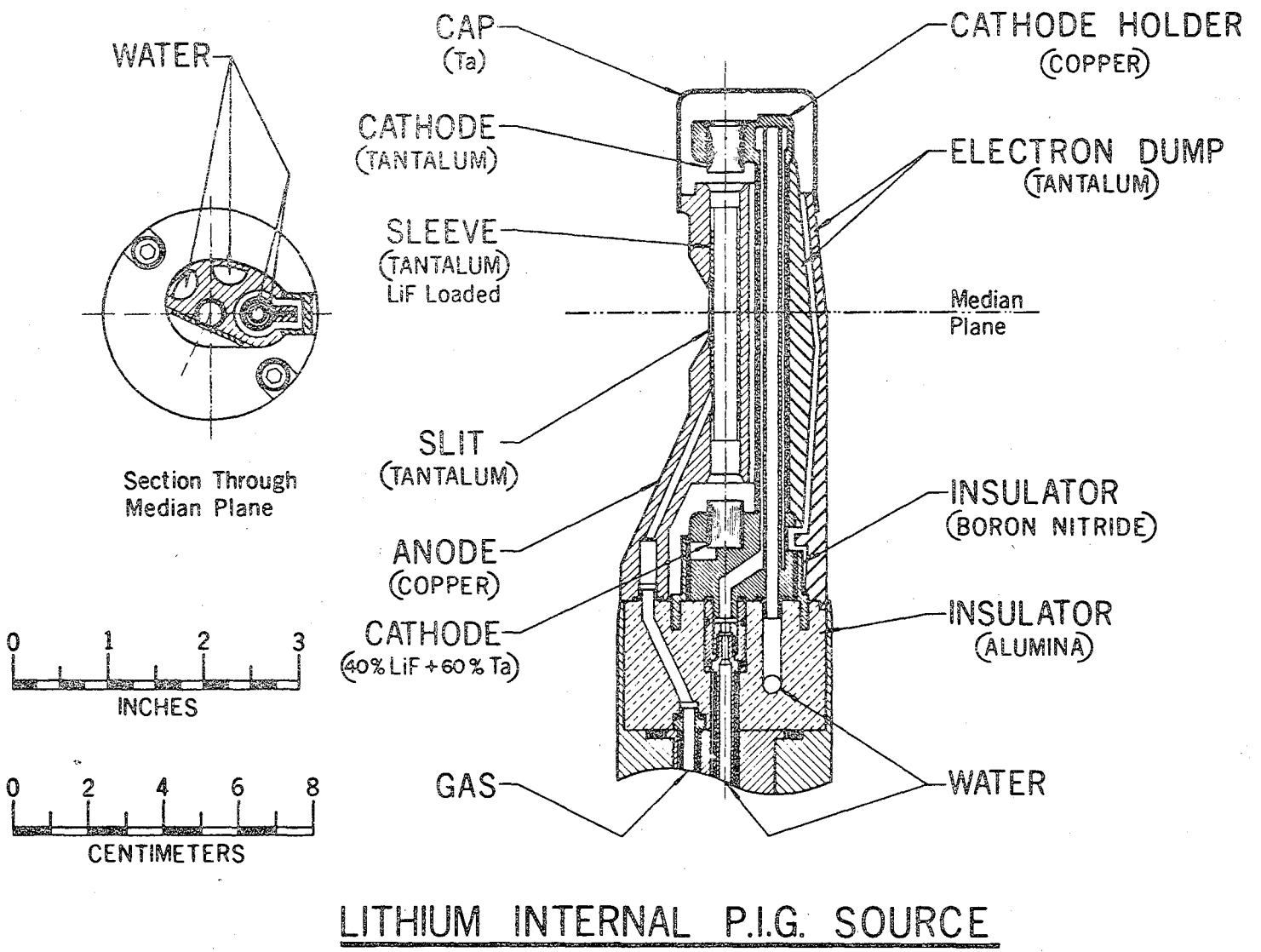

XBL 7410-15368

Fig. II-1. A cross-section of the internal PIG source illustrating the doped cathodes and anode sleeve insert employed to produce lithium ions.

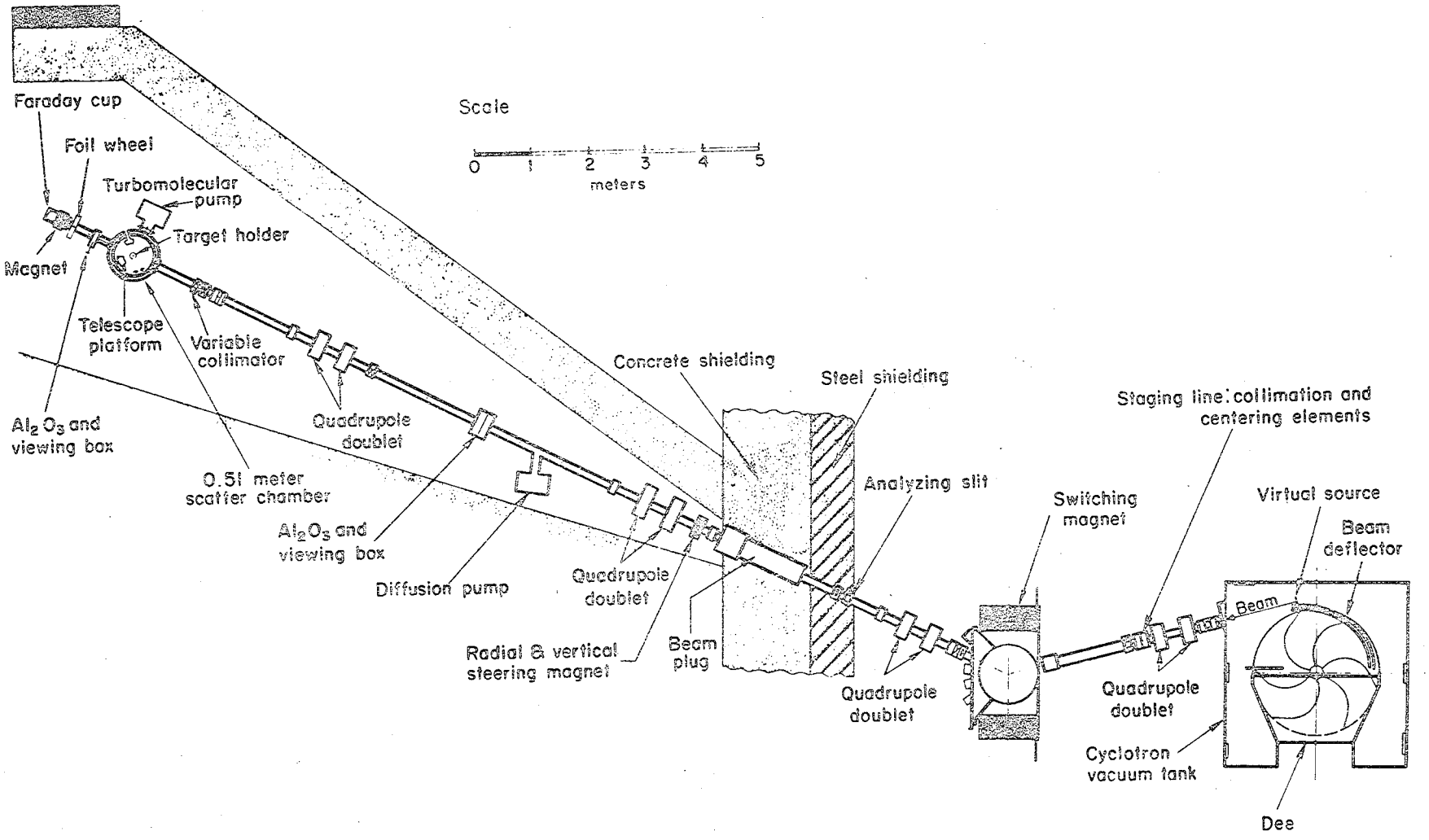

Fig. II-2. A schematic diagram of the 88 inch cyclotron, beam transport system, and Cave 2 experimental area.

Within this chamber detectors were mounted about 15 cm from the target on two independently movable platforms located on either side of the beam. An aluminum housing with tantalum shielding on the upstream side enclosed the counter telescope, and a 600 gauss permanent magnet was placed in front of the collimators to deflect low energy electrons produced in the target. In some of the experiments the detectors were cooled by a thermoelectric cooler to -20°C to reduce thermal noise and leakage current. The scattering chamber pressure was typically 4×10^{-5} Torr; carbon buildup was reduced by employing a series of liquid nitrogen cooled traps.

B. Targets

Self-supporting isotopically enriched targets were used in these experiments (see Table II-1 for further details). Target thicknesses were determined from the energy loss of alpha-particles from ^{212}Po and ^{212}Bi. For targets of natural isotopic composition or those which were rapidly oxidized, portions were weighed on a microbalance. These determinations are estimated to be accurate to about 15% due to inhomogeneities in the target and the presence of target contaminants. The amounts of contaminants (typically carbon and oxygen) were determined by comparison of either their reaction or elastic yield relative to weighable samples.

C. Detectors and Electronics

Each detector telescope consisted of four counters. The first two of these detectors—denoted as ΔE2 and ΔE1—were Ortec surface-barrier transmission detectors (of 34 and 24 μm thickness, respectively). The remaining counters were fabricated at LBL. The E detectors in

Table II-1. Target information and detector geometry.

	Targets		Detector Collimation	
	Isotopic Purity (%)	Thickness (mg/cm^2)	Angular Acceptance (degrees)	Solid Angle (msr)
^{6}Li	99.3	0.40	0.6	0.27
			0.6	0.27
^{7}Li	99.99	0.33	Same as for ^{6}Li	
^{9}Be	100.0	0.13	0.6	0.31
			0.6	0.19
^{10}B	96.0	0.14	Same as for ^{9}Be	
^{11}B	98.0	0.21	Same as for ^{6}Li	
^{12}C	98.89	0.22	0.7	0.43
			0.8	0.45
^{13}C	90.0	0.14	Same as for ^{9}Be	
^{16}O	99.8	0.12 (^{16}O thickness)	Same as for ^{6}Li	
^{24}Mg	99.7	0.15	1.0	0.65
			1.0	0.38
^{26}Mg	99.4	0.45	Same as for ^{24}Mg	

these two telscopes were 200-μm phorphorus-diffused counters. Finally, a 1-mm thick lithium-drifted detector was employed to reject those events which did not stop in the E-counter.

Signals from these detectors fed charge-sensitive pre-amplifiers (PA) (see Fig. II-3). The PA signals were then delay-line shaped (400 ns) into bipolar signals in the linear amplifiers. This form of shaping gives fast baseline recovery and a narrow pulse width (~1 μs), which produced a dead time of about 5% at a counting rate of 20 kHz. (The dead time was measured by the ratio of randomly-strobed pulse triggers to the number of pulser events observed in the final data.) Events were limited to one beam burst by a pile-up rejector (PUR) with a pulse pair resolving time of 50-ns and an inspection time of 1-μs. Events were further limited to the particles of interest by single channel analyzer (SCA) windows around the energy signals in each detector. The slowest component of the electronics, the particle identifier, required stretched signals (~5-μs). However, signals were stretched only if there was a 40-ns fast coincidence between SCA's in all three amplifiers, plus a valid event signal from the PUR within 40-ns, and there was no event in the Rej amplifier within 1-μs. In this particle identification unit, the energy signals from all three counters were added to produce the total energy signal (E_{total}) for each event.

The resolution of this total energy signal was determined by a combination of the natural level width, the spread in the cyclotron beam energy, the electronic resolution, the target thickness, and the finite angular acceptance of the collimators. All these effects can

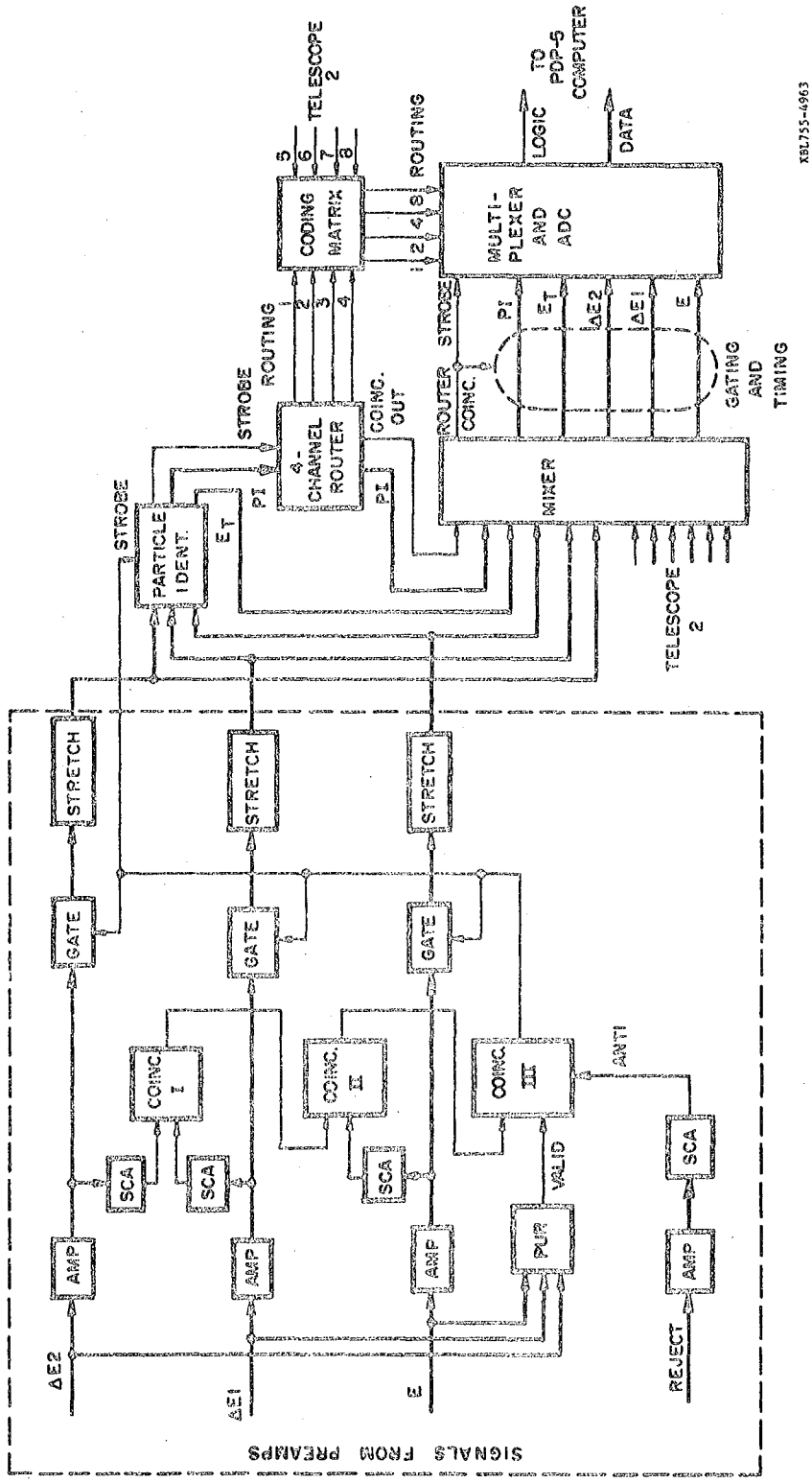

Fig. II-3. A schematic electronics block diagram for these experiments.

be considered to add in quadrature, although some have rectangular distributions (Mo 66, Ma71); typically, the dominant contributions were from the last two effects. The resolution in these experiments was usually 200-300 keV.

The particle identifier was a Goulding-Landis three-counter, double identification system (see Go 66 and Ce 66a). This method of identification is based upon the empirical relationship that the range of a charged particle is given by

$$R = AE^b \qquad \text{(II-1)}$$

above a certain energy threshold. A is a constant characteristic of the particle type, E is the particle energy, and b is a constant that is weakly dependent upon the Z of the detected particles. For boron isotopes, this last constant is about 1.6 (Po 76), but the constant b is empirically optimized at the beginning of each experiment for the particles of interest. If a charged particle passes through a transmission detector of thickness T and deposits ΔE in this counter and then stops in the E counter losing E amount of energy in the latter, then, it can be demonstrated that

$$T/A = (E + \Delta E)^b - E^b = (E_{total})^b - E^b \qquad \text{(II-2)}$$

and this T/A is an energy independent particle identification (PI) signal (see Go 64).

The resolution of this signal is obviously directed proportional to the uniformity of the transmission detector. Detectors normally cannot be made with a non-uniformity less than 0.5-1 micron and a

typical limit is ~2 microns (Wa 75), which will lead to relatively poorer identification with 20-μm detectors than 200-μm ones as transmission detectors. Also, it can be demonstrated that A is proportional to MZ^2, which implies poorer separation for heavier elements. Since the energy loss of charged particles is proportional to MZ^2/E, these rather low energy ^8B particles (in the region from 40 to 70 MeV) have a range of at most 300-μm in silicon, so that rather thin transmission detectors (35 and 25 μm thick) were employed. Thus, for detected heavy-ions, the particle identifier gives particle spacings smaller than for lighter particles and the thinner transmission counters led to poorer particle resolution.

One can achieve lower background by employing a second transmission detector, as is illustrated in Fig. II-4, so that two independent determinations of the particle type can be generated. To the extent that a misidentification occurs in either counter due to non-statistical fluctuations in the rate of energy loss (for example, caused by channeling, blocking, or anomalously high energy loss due to the Landau process), then the ratio of these particle determinations will be anomalous. The particle identification unit generated a particle identification signal (from the summed energy losses in the transmission detectors) by an analog circuit employing a logarithmic element and also a ratio signal of the two independent identifications (since each PI signal = T/A (Eq. II-2) and thus, $PI_1/PI_2 = T_1/T_2$, this ratio corresponds to the ratio of equivalent detector thicknesses). We have examined alternative means of gating this ratio to improve the particle identification. The gating can be performed either on-line (which

Three counter particle identifier

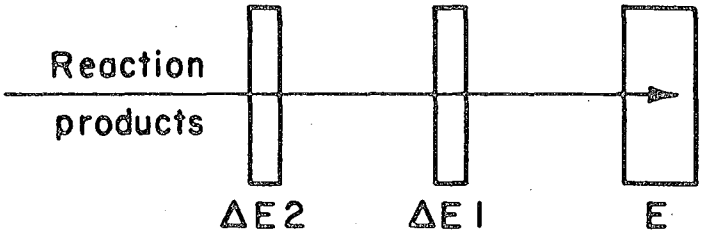

Different identification modes of the particle identifier

	ctr(s) used as "ΔE" ctr	ctr(s) used as "E" ctr
A.	ΔE2	ΔE1 + E
B.	ΔE1	E

if the ratio A/B is within a chosen percentage, then the final output is C

C.	ΔE2 + ΔE1	E

MUB-9885

Fig. II-4. An illustration of the operation of the three-counter particle identifier.

allows a better evaluation of the data during the experiment, but suffers from irreversibility), or off-line. With on-line gating the percentage of events rejected was carefully monitored, since slight gain shifts in either transmission detector system can cause drastic increases in the rejection rate. Typically, 10 to 20% of the events were rejected by this gate.

We have examined the effects of this selection process as a function of energy, because of the interest in this work in both angular distributions and cross sections as a function of excitation energy. Along with the anomalous identifications due to non-statistical fluctuations, there is a general energy dependence in the particle identification signal. We have determined that the majority of the rejected events were in the low energy portion of the spectrum ($E(^8B) \lesssim 40$ MeV). This can be investigated on-line by using the E SCA to vary the energy region of events entering the particle identifier, or by off-line gating of the ratio signal. From these investigations we have determined that if a ^8B event loses more than 15 MeV in the E counter (equivalent to about 45 MeV total energy for the typical transmission counters employed), its particle identification signal is reasonably energy independent. This is in agreement with theoretical range-energy calculations of the PI signal employing the computer code LZY (Ma 70). Accordingly, we will limit our presentation of data for individual energy levels to this region.

A typical PI spectrum is shown in Fig. II-5. As can be seen from this spectrum, a clean separation of the ^8B's from other boron isotopes was readily achieved.

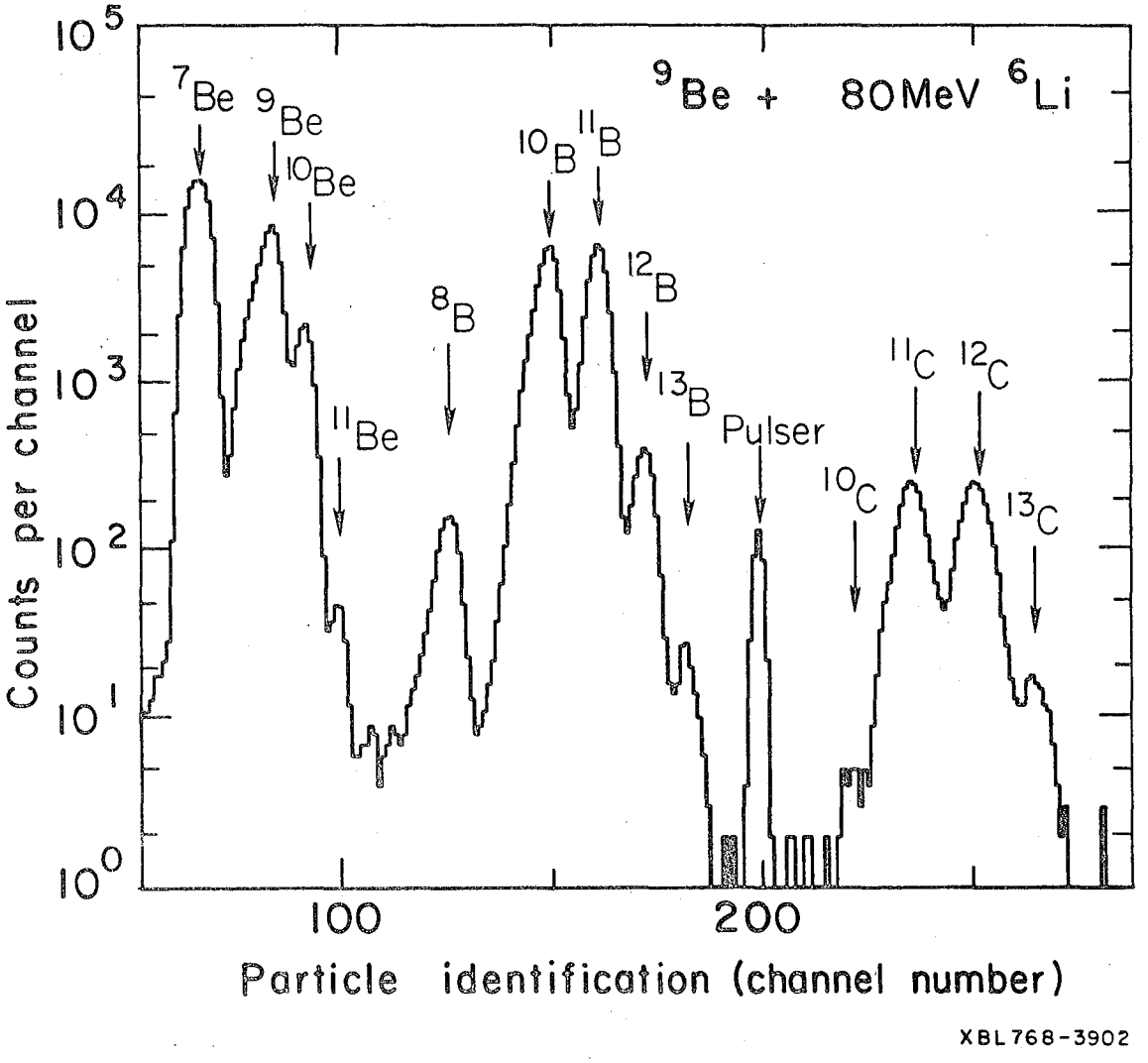

Fig. II-5. A particle identification spectrum resulting from bombarding a ^{9}Be target with an 80 MeV ^{6}Li beam.

D. Data Acquisition and Analysis

For each event, four parameters (either $\Delta E2$, $\Delta E1$, E_{total}, and the PI signal generated from the summed energy losses in the ΔE's; or the ratio of the PI signals, E, E_{total}, and PI_{total} signals) were sent via a multiplexer and an analog-to-digital converter to an on-line PDP-5 computer. The energy spectra were displayed during the experiment on a CRT and the events were written on magnetic tape for subsequent analysis. In this off-line analysis on an SCC-660 computer, the multi-parameter sorting and gating program CHAOS (Ma 74) was employed to set more stringent PI requirements and to generate the resulting energy spectra. These spectra were then analyzed with the peak-fitting program DERTAG (Ma 71), which computed the peak centroids, integrals, and widths. These quantities were then used in the program LORNA (Ma 71) on a CDC-7600, which calculates a least-squares fit to the known energy calibation points and assigns excitation energies to other levels.

Definite assignments of peaks to a particular reaction were made only if they were seen at several angles with the appropriate kinematic shift. Early investigations were made of carbon and oxygen targets, so that spectra from the basic target contaminants were well-understood. As an aid in the analysis, all the data on each target were kinematically shifted to one angle and summed by the program SUMSHIFT on the SCC-660. Also, the data for unbound light systems (e.g., ^{4}H, ^{5}H) were compressed by a factor of 4 (from ~100 keV to ~400 keV) to improve the statistical analysis of broad levels (see Appendix A for a description of some considerations in the analysis of unbound systems).

Finally, the measured angular distributions will be presented with only statistical error bars on the data points; this indicates the relative error, although the absolute error could be as large as 30%.

III. THEORETICAL CONSIDERATIONS

While, in general, these studies represent an extension of earlier two-nucleon transfer investigations to include two-proton pickup, the heavy-ion nature of the incoming and outgoing particles adds a distinct character to these studies. Much of this difference arises due to the possibility for transfer of two nucleons in various coupling configurations. In spite of these additional possibilities, the observated selectivity in the population of states in the residual nuclei suggests that the dominant configuration of the two transferred protons remains the ^1S relative state, the predominance of which is expected from the fundamental nature of the pairing interaction. While the transferred pair is an internal ^1S cluster, its total wave function is ^1D with respect to the ^6Li core; the extended nature of this state means that finite-range effects will be important in describing the reaction kinematics. These finite-range effects, along with the large number of partial waves (and the angular momentum mismatch) of the incoming and outgoing particles, cause the reaction to exhibit characteristic heavy-ion reaction features, which suggest the appropriateness of semi-classical treatment of the reaction process.

A. General Features of Two-Nucleon Transfer Reactions

Studies of light-ion tow-nucleon transfer reactions have been legion and the reader is referred to the numerous general articles discussing spectroscopic studies with these reactions (for example, Gl 63, Gl 65, Gl 75, To 69, An 72, and Br 73).

The transition matrix element of a nuclear reaction can be described in terms of a nuclear structure component and a transfer amplitude, the product of which is summed and averaged over the appropriate quantum numbers. For two-nucleon transfer reactions, this includes a coherent addition of these amplitudes over the internal quantum numbers of the transferred nucleons. This introduces a sensitivity of the transition strength not only to the magnitude, but also to the sign of small admixtures into the wave functions of the "core" plus "cluster" systems (To 69). (In the case of heavy-ion reactions, such as (^{6}Li,^{8}B), we must consider the "core" plus "cluster" system in both the target and in the outgoing ^{8}B.)

Typically, the interest is in the nuclear structure factor term, which is called the spectroscopic factor of the transition. This factor is proportional to the square of the two-nucleon coefficients of fractional parentage (2-cfp), where this coefficient, in the case of pickup, describes the target ground state wave function in terms of states of the final nucleus coupled to two nucleon states with appropriate values of relative angular momentum between the "cluster" and the "core".

For a single-step direct reaction, these spectroscopic factors are a measure of the probability of two-nucleons forming a particular cluster through their spatial correlation (the transition strength will also depend upon the probability density of the cluster wave function in the region where the transfer occurs). For two (or more)

nucleons these spatial correlations arise from, not only the nucleon-nucleon force (or the pairing interaction), but also from the angular momentum coupling (Gl 63). (For example, the spatial correlation of two identical nucleons with angular momentum j, which are coupled to J, is larger if the classical orbits of these particles are co-planar (i.e., if J is 0) rather than tilted with respect to each other.) However, the transition strength will be largest when the transferred pair retains the same relative state; which would select essentially only the ^1S clusters in the target for pickup into a triton in the (p,t) reaction, but could allow other cluster configurations to match the ^8B ground state wave function in the (^6Li,^8B) reaction.

Although light-ion two-nucleon transfer reactions often have a possible small component of ^1D as well as ^1S cluster transfer (e.g., the expansion of the triton ground state wave function has a ^1D component, which offers this possibility to the (p,t) reaction), the ^1S state dominates these reactions (Br 71). In heavy-ion reactions the more complicated structure of the projectile-outgoing particle-pair could result in transfer of "clusters" not only in the relative ^1S state, but also with ^1D or ^3P configurations, if the structure of the other system contains these relative configurations. This will be discussed in greater detail in Section III-B. Similarly, the transition strengths will depend upon slight admixtures in the target ground state wave function in this pickup reaction, and examples of this sensitivity will be presented in Section IV (in particular, with respect to the first excited state of ^9Li).

B. Structural Features

It is clear that the transition strength is dependent upon the structure of both the target and ^{8}B. A heavy-ion aspect of the (^{6}Li,^{8}B) reaction is the more complicated structure of the projectile-outgoing particle pair than for the light-ion reactions. One of the more interesting features of this reaction is that it provides a means of investigating anti-symmetric pair transfer. This type of transfer process has been the subject of some theoretical speculation (Ku 72, Lk 70). There is a great weight of evidence that light-ion two-nucleon transfer reactions occur only through the transfer of a pair coupled predominantly in a spatially symmetric (^{1}S) configuration rather than a ^{1}D state. However, it would be useful to learn whether this arises because of the limited structural possibilities of the light-ion reactions, or because of the more prevalent nature of the ^{1}S state due to the pairing interaction. This test requires that the structure, both of the reaction pair and the target, provide an opportunity for anti-symmetric transfer, and we will discuss each system in turn.

The (^{6}Li,^{8}B) reaction is a good probe for determining the importance of the spatially anti-symmetric (^{3}P) configuration in the transfer process, since ^{8}B has a higher percentage of a ^{3}P pair relative the ^{6}Li core than a ^{1}D cluster. (See Table III-1 for the magnitude of these symmetric and anti-symmetric transfer terms for some heavy-ion two-nucleon pickup reactions--the SMAG, PMAG, etc., notation will be discussed below.) This can be seen from the ground state configurations and spins of ^{6}Li and ^{8}B (see Table III-2). The dominant ground state configurations (^{2S+1}L) can be connected only by

Table III-1. Spectroscopic factors for 1p-shell heavy-ion two-nucleon transfer reactions.

	Symmetric		Anti-Symmetric		
Reaction	SMAG	DMAG	PMAG 0	PMAG 1	PMAG 2
(^{6}Li, ^{8}B or ^{8}Li)	0	0.032	0	0.141	0.494
(^{9}Be, ^{11}C or ^{11}Be)	0	0.747	0	0.888	0.720
(^{10}B, ^{12}N or ^{12}B)	0	1.354	0	0	0.039
(^{11}B, ^{13}N)	0	2.061	0	1.806	0.472
(^{11}B, ^{13}B)	0.637	0.043	0.101	0	0.004
(^{12}C, ^{14}O or ^{14}C)	0.597	0	0.101	0	0
(^{13}C, ^{15}O)	1.002	0	0.300	0	0
(^{10}B, ^{8}Li or ^{8}B)	0	0.732	0	0.295	1.428
(^{11}B, ^{9}Li)	0.667	1.443	0.022	0.143	1.984
(^{12}C, ^{10}Be or ^{10}C)	2.747	0	0.032	0	0
(^{13}C, ^{11}Be)	1.959	0	0.090	0.001	0
(^{14}C, ^{12}Be)	1.784	0	0.111	0	0
(^{13}C, ^{11}C)	0	2.061	0	1.806	0.472
(^{14}C, ^{12}C)	0.597	0	0.101	0	0
(^{14}N, ^{12}B or ^{12}N)	0.033	2.415	0.008	0.388	0.361
(^{15}N, ^{13}B)	0	3.737	0	2.755	0.955
(^{15}N, ^{13}N)	1.002	0	0.300	0	0
(^{16}O, ^{14}C or ^{14}N)	2.212	0	0.788	0	0

Table III-2. ^{2S+1}L components of the ground state wave functions of ^{6}Li and ^{8}B (from Ba 66).

^{6}Li g.s.;1^{+}	$0.992\ ^{3}S - 0.028\ ^{3}D + 0.120\ ^{1}P$
^{8}B g.s.;2^{+}	$0.922\ ^{3}P - 0.242\ ^{3}D + 0.060\ ^{3}F + 0.241\ ^{1}J - 0.148\ ^{3}D$ $- 0.032\ ^{3}P + 0.084\ ^{5}P$

(Note that in ^{8}B the ^{3}P and ^{3}D configurations are repeated, since the group theoretic symmetries are different for the two cases of these configurations.)

(^{6}Li $\otimes$ 2p = ^{8}B) ^{3}S $\otimes$ ^{3}P = ^{3}P; since for the L-values, only $\vec{0} + \vec{1} = \vec{1}$, and two identical fermions must have S=1 for odd L and T=1. Symmetric transfer must arise through other than the dominant configurations, such as in ^{3}S $\otimes$ ^{1}D = ^{3}D. One can see that symmetric transfer can only occur by a ^{1}D configuration (relative to the ^{6}Li core) since $\vec{1} \otimes \vec{0}$ ($^1S_0$) $\neq \vec{2}$.

These configurations relative to the core can be decomposed by the Talmi brackets, that have been tabulated by Brody and Moshinsky (Br 60), into the internal relative angular momentum λ and the center-of-mass angular momentum Λ of the pair relative to the core, where

$$\vec{L} = \vec{\lambda} + \vec{\Lambda} \qquad \text{(III-1)}$$

The ^{3}P configuration (L = 1) can be decomposed into only $\lambda = \Lambda = 1$. The ^{1}D configuration (L = 2) can be transformed with equal amplitude ($\sqrt{2}/2$) into either $\lambda = 0$, $\Lambda = 2$, or $\lambda = 2$, $\Lambda = 0$. (Since the Talmi transformation brackets are for harmonic oscillator wave functions, they are expressed only in terms of L.) For the anti-symmetric component, since S = 1, the L = 1 term can correspond to J = 0, 1, or 2, while for symmetric transfer each L corresponds to a unique J.

As previously mentioned, for a test of the strength of transitions through the anti-symmetric components one needs not only a reaction pair with a large component of anti-symmetric transfer, but also a target that contains a large portion of anti-symmetric transfer strength to a particular final state. The 2-cfp's for the 1p-shell in a jj-basis have been tabulated by Cohen and Kurath (Co 70) based upon their intermediate coupling wave functions (Co 65 and Ku 56). As part of this work (Co 70), Cohen and Kurath have tabulated the transition

strengths for $J = L = \Lambda = 0$ transfer (denoted in their notation as SMAG or S magnitude) and for $J = L = \Lambda = 2$ transfer (called DMAG for D magnitude) for a relative ^1S cluster ($\lambda = 0$). We have extended this work of Cohen and Kurath by calculating and tabulating the analogous quantities for anti-symmetric transfer (with $\Delta T=1$) for their wave functions, which we will denote in a similar fashion as PMAG 0, PMAG 1, and PMAG 2 (for $L = \Lambda = \lambda = 1$ with $\Delta J = 0$, 1, or 2 respectively). These values are listed in Table III-1 for various two-nucleon transfer reactions and in Section IV for the targets studied in this work. (A more complete listing of transitions with the 1p-shell is available from the author.)

This transformation consists of first converting the 2-cfp's from the jj-basis into an L·S representation, and then squaring them. Finally, these quantities are weighted by a statistical factor for the available number of pairs for the transition ($\sqrt{N[N-1]}$) where N is the number of 1p-shell nucleons in the initial nucleus for pickup reactions and in the final nucleus for stripping reactions. Because of the importance of these spectroscopic factors for this work, these relationships between the jj and L·S 2-cfp's are listed in Table III-3. It should be noted from this table that the $\Delta J = 1$ transitions are only possible through PMAG 1, while $\Delta J = 0$ or 2 transitions are possible through either the symmetric or anti-symmetric transfer configurations.

In fact, SMAG and PMAG 0 (and similarly, DMAG and PMAG 2) are orthogonal combinations of the jj-basis wave functions. Accordingly, these states accessible through anti-symmetric transfer of two nucleons are fairly common, but they typically exist at rather high excitation

Table III-3. The conversions between the jj and L·S representations of the two-nucleon fractional-parentage-coefficients.

$$\Theta^{01}({}^1S_0) = \frac{\sqrt{2}\,\Theta^{01}(33) + \Theta^{01}(11)}{\sqrt{3}}$$

$$\Theta^{21}({}^1D_2) = \frac{\Theta^{21}(33) + \sqrt{2}\,\Theta^{21}(31)}{\sqrt{3}}$$

$$\Theta^{11}({}^3P_1) = \Theta^{11}(31)$$

$$\Theta^{21}({}^3P_2) = \frac{\sqrt{2}\,\Theta^{21}(33) - \Theta^{21}(31)}{\sqrt{3}}$$

$$\Theta^{01}({}^3P_0) = \frac{-\Theta^{01}(33) + \sqrt{2}\,\Theta^{01}(11)}{\sqrt{3}}$$

The notation employed is the same as in Co 70, and is $\Theta^{JT}(1j_1 2j_2)$ for the jj-representation and ${}^{JT}({}^{2S+1}L_J)$ for the L·S representation.

energy. These levels are rather inaccessible because of their unusual configuration, so that only a few states of this type have been located. The symmetric states occur at lower excitation energies and typically have been well investigated. This level ordering might be expected from the sign and size of the pairing interaction, which can be viewed as splitting these states. Fortunately, we found two good test cases (in the $^{10}B(^{6}Li,^{8}B)$ and the $^{16}O(^{6}Li,^{8}B)$ reactions) which provide a good test for the importance of anti-symmetric transfer.

Another type of test for the importance of this reaction process (and also for multi-step transitions) is to compare the results of this reaction with that of the (p,t) reaction on $T_z = 0$ nuclei. For this type of target, the two reactions populate mirror final nuclei, so that they are quite analogous (see the numerous discussions of isospin, such as Cerny (Ce 68) and references therein, for a justification of these expectations). If the symmetry of the transferred cluster were different in these two reactions, then a lack of correspondence might be observed. However, the differing kinematic aspects of the two reactions will tend to make the agreement between them inexact, i.e., one would expect the same qualitative selectivity, but the relative transition strengths might be quantitatively different. We will present examples of this similarity on ^{6}Li, ^{10}B, ^{12}C, ^{16}O, and ^{24}Mg targets.

C. Selection Rules

A useful way of characterizing reactions is by their selectivity in the population of states in the final nuclei. These selection rules may suggest values for the spin and parity of populated levels. For example, the $(^{6}Li,^{8}B)$ reaction populates strongly only levels with

the same parity as the target ground state, so that data from this reaction will suggest the location of negative parity states in ^{7}He, ^{9}Li, and ^{11}Be. Moreover, the reaction selectivity in the population of states in the final nuclei will reflect the reaction mechanism, so that it is possible to differentiate most easily among direct reactions and more complicated mechanisms by the type of levels preferentially populated (for example, see Ce 64 and Ma 71).

For simplicity, this discussion will be limited to 1p-shell levels, thus, the dominant configuration of the ground state of a 1p-shell target of atomic number A may be described as $(1s)^{4}(1p)^{A-4}\ J_i$. If the (^{6}Li,^{8}B) reaction proceeds by a direct single-step pickup mechanism on such a target, then only levels with the configuration $(1p)^{A-6}\ J_f$ may be populated (assuming for this discussion that the 1s-orbitals remain inert during the reaction, which deletes for now reactions on both the ^{6}Li and ^{7}Li targets). Since this reaction involves the pickup of an even number of nucleons, the parity of the final levels ($\pi_f = \pi_i(-1)^{A-2}$) must be the same as that of the target ground state. Similarly, the pickup of two identical 1p-shell nucleons can change the value of J_i by at most 2, so $\vec{J}_f = \vec{J}_i + \vec{2}$. However, in a sequential transfer the parity might be changed and in the pickup of two nucleons in different shells the parity must be change.

If one denotes the initial state in the target nucleus and the final state in the residual nucleus by their total angular momentum and isospin quantum numbers ($\vec{J}_i$, $\vec{T}_i$) and ($\vec{J}_f$, $\vec{T}_f$) respectively, and also describes the single particle orbitals of the transferred nucleons by their orbital and total angular momenta ($\vec{l}_1$, $\vec{j}_1$) and ($\vec{l}_2$, $\vec{j}_2$);

then with only the assumption of a direct reaction one can again derive (see To 69) that

$$|J_i - J_f| \leq j_1 + j_2 \qquad \text{(III-2a)}$$

For the pickup of two 1p-shell protons this relationship is

$$|J_i - J_f| \leq 2 \qquad \text{(III-2b)}$$

If one denotes the orbital angular momentum, intrinsic angular momentum, total angular momentum, and isospin quantum numbers of the transferred pair by $\vec{L}$, $\vec{S}$, $\vec{J}$, and $\vec{T}$ respectively, then (To 69)

$$\vec{L} = \vec{l}_1 + \vec{l}_2 = \vec{\lambda} + \vec{\Lambda} \qquad \text{(III-3)}$$

and

$$\vec{S} = \vec{s}_1 + \vec{s}_2 \qquad \text{(III-4)}$$

and

$$\vec{T} = \vec{t}_1 + \vec{t}_2 \qquad \text{(III-5)}$$

and

$$\vec{J} = \vec{j}_1 + \vec{j}_2 = \vec{L} + \vec{S} \qquad \text{(III-6)}$$

and for the transfer of two protons

$$\vec{T} = \vec{1} \qquad \text{(III-5)}$$

These relationships have one solution for symmetric transfer and another for anti-symmetric transfer, since the fermion nature of the two protons requires for an anti-symmetric (with respect to change) total wave function that if L is even then

$$S + T \text{ is odd} \qquad \text{(III-7a)}$$

and if L is odd then

$$S + T \text{ is even} \qquad \text{(III-7b)}$$

Then for symmetric transfer

$$\vec{L} = \vec{2} = \vec{\lambda} + \vec{\Lambda} \qquad \text{(III-3)}$$

so either

$$\vec{\lambda} = 2, \ \vec{\Lambda} = 0$$

or

$$\vec{\lambda} = 0, \ \vec{\Lambda} = 2$$

and

$$\vec{S} = \vec{0} \qquad \text{(III-4)}$$

so finally

$$\vec{J} = \vec{L} = \vec{2} \qquad \text{(III-6)}$$

and for anti-symmetric transfer

$$\vec{L} = \vec{1} = \vec{\lambda} + \vec{\Lambda} \qquad \text{(III-3)}$$

so

$$\vec{\lambda} = \vec{\Lambda} = \vec{1}$$

and

$$\vec{S} = \vec{1} \qquad \text{(III-4)}$$

so finally

$$\vec{J} = \vec{L} + \vec{S} = \vec{\lambda} + \vec{\Lambda} + \vec{1} \qquad \text{(III-6)}$$

The necessity of retaining the same cluster configuration in both systems of core plus cluster requires that

$$\vec{J}_f = \vec{J}_i + \vec{J} = \vec{J}_i + \vec{L} + \vec{S} \qquad \text{(III-8)}$$

and so for symmetric transfer

$$\vec{J}_f = \vec{J}_i + \vec{L} \qquad \text{(III-8)}$$

The experimental results indicate that only symmetric transfer occurs, so $\vec{J}_f = \vec{J}_i + \vec{L}$. The allowed L-values are identical to those of the (p,t) reaction. There are few cases in which more than one L-value will be allowed, and where the spin-orbit interaction would cause a coherence in the reaction amplitude.

The (^{6}Li,^{8}B) reaction data provide a test of whether the relative transition strengths simply arise from a "Q-window" effect (which is unlikely at these beam energies and values of the Sommerfeld parameter (see Section D)). The best matching of the incoming and outgoing Coulomb orbits occur at some optimum Q-value (see Appendix B-1 for the formula for Q_{opt}). For this reaction all the Q-values are negative, while the most favored Q-values would be positive (except for targets with $Z \leq 5$). This could lead to transitions with lower Q-values being enhanced. As a test that the relative yields do not simply reflect this kinematic hindrance, we have employed two cases (^{10}B and ^{13}C, see Section IV) where an excited state should be populated more strongly than the ground state (due to spectroscopic considerations), which was in agreement with the experimental results. While there should be a general dependence in the transfer amplitude upon the Q-value of the transition (see Sections D and E), the relative transition strengths do not arise completely from this effect.

Another aspect of the reaction mechanism that can be explored from the selectivity of this reaction in the population of states in the final nucleus is the strength of multi-step transitions which involve an inelastic excitation of states in the initial (or final) nucleus

before (or after) the two-proton pickup. By comparison of the form factors and a coupled channel calculation, Sørenson (Sø 74) has proposed that these indirect processes are an important component of transitions to excited states in the $^{26}Mg(^{16}O,^{14}C)^{28}Si$ reaction. These processes could be indicated by the population of unnatural parity levels, as the excited states would by populated proportional to their collective strengths. Although the $^{24}Mg(^{6}Li,^{8}B)^{22}Ne$ reaction is an appropriate test for this mechanism, since several multi-particle-hole levels in ^{22}Ne are known (Ol 71, En 73) to be very collective, we found no evidence for these transitions. This is in agreement with the 1p-shell results ($\Delta\pi = +$, $\vec{J}_f = \vec{J}_i + \vec{2}$), since the observed selection rules were derived assuming only a direct single-step pickup of the proton pair.

D. Kinematic Considerations

The spectroscopic selectivity of the $(^{6}Li,^{8}B)$ reaction demonstrates that it is predominantly a direct, single-step pickup reaction, which would be expected by the high energy (over 13 MeV/nucleon) employed in these studies. This selectivity illustrates the importance of kinematic aspects in determining the features of the reaction. We will explore in this Section the effects of kinematic variables on the angular distribtions of this reaction, and in the following Section their effect upon the transfer amplitudes.

Kinematic effects upon angular distributions can be seen in two extreme limits of the degree of localization of the incoming wave-packet Sc 73, Sc 74b, Sc 75). A light-ion direct reaction has an extended projectile, emphasizing the particule's wave nature. This extended projectile, along with the limited L's of the transition, leads to

a diffractive angular distribution. "Traditional" heavy-ion reactions have possessed a localized incoming wave-packet, emphasizing the projectile's particle character. In these heavy-ion reactions the wavelength of the projectile is much less than the interaction radius (R_{int}) (which is slightly larger than the touching radius of the two spheres) and R_{int} is large enough so that the effective potential felt by the incoming and outgoing particles is primarily the Coulomb potential. Accordingly, the transition yield is maximized by the greatest overlap of the incoming and outgoing Coulomb orbits. (This matching condition differs in emphasis from the conditions of Brink's formulism, which will be discussed below. In the present approach, the Coulomb orbits of the incident and outgoing particles are well matched, while in the discussion below the orbits of the cluster, with respect to the core in the initial and final systems, are matched. In general, the requirements of these two conditions are different, although in many cases the consequences are similar.) Interactions that occur at a distance closer than R_{int} are absorbed into the compound system, while for those further out than R_{int} the transition probability is reduced by the exponential fall-off of the nucleon probability densities. This leads to a bell-shaped angular distribution, with the maximum probability at a radius corresponding to the grazing angle (θ_c).

These conditions for either a diffractive or a Gaussian angular distribution can be expressed in terms of kinematic variables. The critical variables are the wavenumber (k), R_{int}, the grazing L-values (roughly $k \cdot R_{int}$) or the number of contributing partial waves, and the Sommerfeld parameter (η). (These kinematic parameters are defined

in Appendix B-1.) A Gaussian distribution arises when the wavelength is much less than R_{int} or equivalently $k \cdot R_{int} >> 1$ (and accordingly, there are many contributing partial waves) and when there is a well defined Coulomb orbit for the incoming and outgoing particles, or $\eta >> 1$.

For high-energy heavy-ion reactions, such as $(^6Li, ^8B)$, on light targets the angular distributions follow a simple, monotonically decreasing pattern with increasing angle as shown in Fig. III-1 (see Bi 67, Na 73, Yo 73, Do 65, Do 66, Gr 70, and An 74). In these cases $k \cdot R_{int} >> 1$, but $\eta \approx 1$. This distribution shape might be viewed as arising from the grazing angle being at an inaccessibly forward angle or equivalently from the localized particles again either forming a compound system below some R_{int} or beyond R_{int} sampling the exponentially decreasing nuclear tail density, but with no focusing of the projectile onto a particular Coulomb orbit at R_{int} for a certain θ_c because of the low η.

The $(^6Li, ^8B)$ reaction exhibits this monotonically decreasing angular distribution on light targets (see Section IV), as might be expected from its kinematic parameters (see Appendix B-2 for a listing of the variables of interest for some representative targets studied with this reaction). For the $(^6Li, ^8B)$ reaction on 1p-shell targets, $k \cdot R_{int} \sim 30$, $\eta \sim 1$, $\theta_c \sim 5^o$ (c.m.), $\Delta\theta_{min} \sim 10^o$ (c.m.), and $L \sim 7$. Finally, it should be noted that on the much heavier target ^{142}Nd, where η was quite large, the angular distribution was the expected bell-shaped peak at the grazing angle (We 75). Accordingly, the angular distributions of the $(^6Li, ^8B)$ reaction only reflect the kinematic aspects

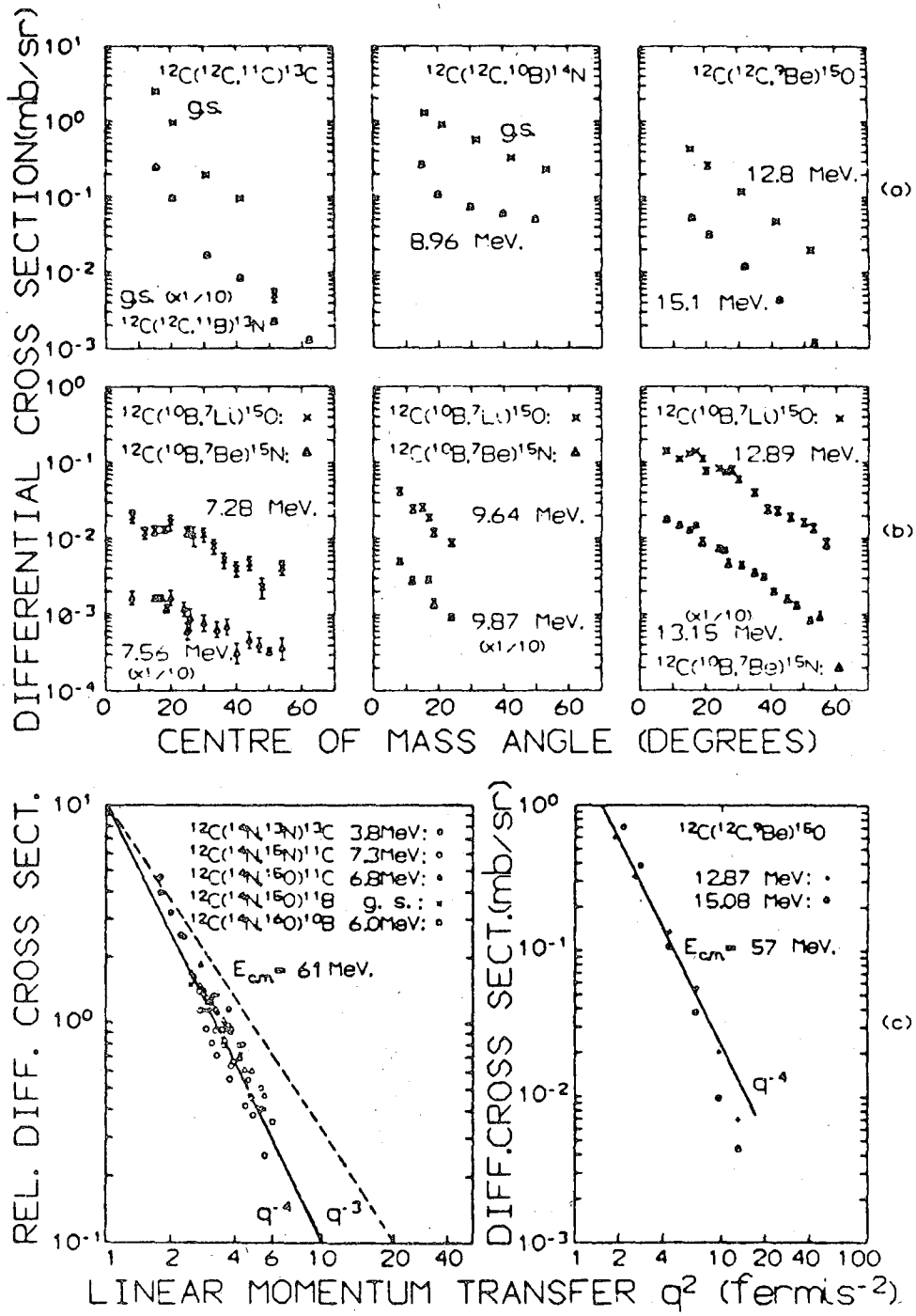

XBL769-10511

Fig. III-1. Angular distributions for one, two, and three nucleon reactions induced on a ^{12}C target (An 74): (a) Reactions induced with a 114 MeV ^{12}C beam, and (b) reactions induced with a 100 MeV ^{10}B beam. (c) Differential cross sections for a range of transfer reactions as a function of transferred momentum. The theoretical curves of q^{-3} and q^{-4} are based upon the calculations of Dodd and Greider (Do 65, Do 66, Gr 70).

of the reaction, instead of conveying structural information. Spectroscopic information can be obtained from this reaction only in the relative transition strengths.

E. Relative Kinematic Hindrances

To extract spectroscopic structural information from the relative transition strengtrhs, it is necessary to be able to estimate the dependence of the transfer amplitudes upon the J (or L) of the reaction and the particular Q-values of the transition. In this Section we will discuss an approach that provides an estimate of the relative hindrance factors of transitions as a function of the properties of the final states in the residual nucleus.

These hindrance factors are analogous to the transfer amplitudes of the transition matrix element that were discussed in Section A. In light-ion two-nucleon transfer reactions the transfer amplitudes are calculated by Distorted Wave Born Approximation (DWBA) computer codes, such as DWUCK (Ku 74a). We will not employ this approach because the degree of momentum mismatching calls into question its utility; moreover, because of the novelty of high-energy lithium beams, the appropriate optical model parameters are unavailable; and, finally, the magnitude of the recoil terms (finite range effects) in these systems indicates that a more sophisticated (and costly) DWBA code such as LOLA (De 73), which includes recoil effects, should be employed. A brief test of DWUCK confirmed that it did not reproduce the experimentally determined angular distributions, and suggested that the kinematic term in the transition matrix element is only slightly dependent upon the J of the transitions. (These will be described

as simple calculations since they employed optical model parameters from 135 MeV ^{6}Li scattering on ^{28}Si (Go 75) for both the ^{6}Li and ^{8}B particles in this reaction on ^{12}C, ignored finite range effects, treated both ^{6}Li and ^{8}B as spinless particles, and were not optimized by varying the parameters to describe the observed angular distributions.) It has been suggested (An 74) that, with the assumption that the transfer occurs near the surface of the target nucleus, the magnitude of the quantity $k_o \cdot R_t$ (where k_o is the wavenumber of the transferred cluster and R_t is the target radius) provides a check of the size of recoil effects, since this quantity is approximately equal to the phase factors (which contain the recoil effects) in the transition matrix element of the formalism of Dodd and Greider (Gr 70, Do 65, Do 66). Recoil effects are negligible if $k_o \cdot R_t$ is much less than 1, but for the (^{6}Li,^{8}B) reaction on 1p-shell targets this quantity is about 5.

All of these difficulties are circumvented by employing a semi-classical treatment (SCT) of the transfer amplitudes. This approach has been generally successful for reactions with similar kinematic conditions (An 74), although these conditions might seem to indicate that a SCT would not be adequate (see Section D). This theory is based upon a series of criteria that have been proposed as a measure of the relative hindrance (Br 72). These rules are for a reaction

$$a_1 + c_2 = (c_1 + k) + c_2 \rightarrow c_1 + (c_2 + k) = c_1 + a_2$$

where a cluster "k" is transferred from a beam "a_1" to a target "c_2" forming a final nucleus "a_2" and an outgoing "c_1". (To treat pickup reactions in this formalism one uses the time-reversed reaction.)

The initial and final states of the cluster with respect to the core are described by

$$\psi_1 = u_1(r_1)\ Y_{l_1\lambda_1}(\Theta_1,\phi_1)$$

for $\underline{k}$ in a_1 and

$$\psi_2 = u_2(r_2)\ Y_{l_2\lambda_2}(\Theta_2,\phi_2)$$

for k in a_2, where $u_1(r_1)$ and $u_2(r_2)$ are radial wavefunctions and $Y_{l\lambda}$'s are spherical harmonics. For this reaction system, the optimum kinematic matching occurs when

$$1. \quad \Delta K = k_o - \lambda_1/R_1 - \lambda_2/R_2 \sim 0 \qquad \text{(III-9)}$$

where k_o is again the wavenumber of the transferred cluster, the λ_i's are the substates of the cluster's total angular momentum relative to the cores, and the R_i's are the radius of the beam and the target. The above equation requires that the y-component of the momentum of the transferred cluster should be almost conserved (see Fig. III-2 for the coordinate system employed).

$$2. \quad \Delta L = \lambda_2 - \lambda_1 + 0.5k_o(R_1 - R_2) + Q_{eff}\ R/\hbar v \sim 0$$

where the expression for Q_{eff} is listed in Appendix B-1. This condition requires that the change in the z-component of the total angular momentum be almost 0, or that the total angular momentum be conserved within the limitations of the uncertainty principle.

$$3. \quad l_1 + \lambda_1 = \text{even}$$

$$l_2 + \lambda_2 = \text{even}$$

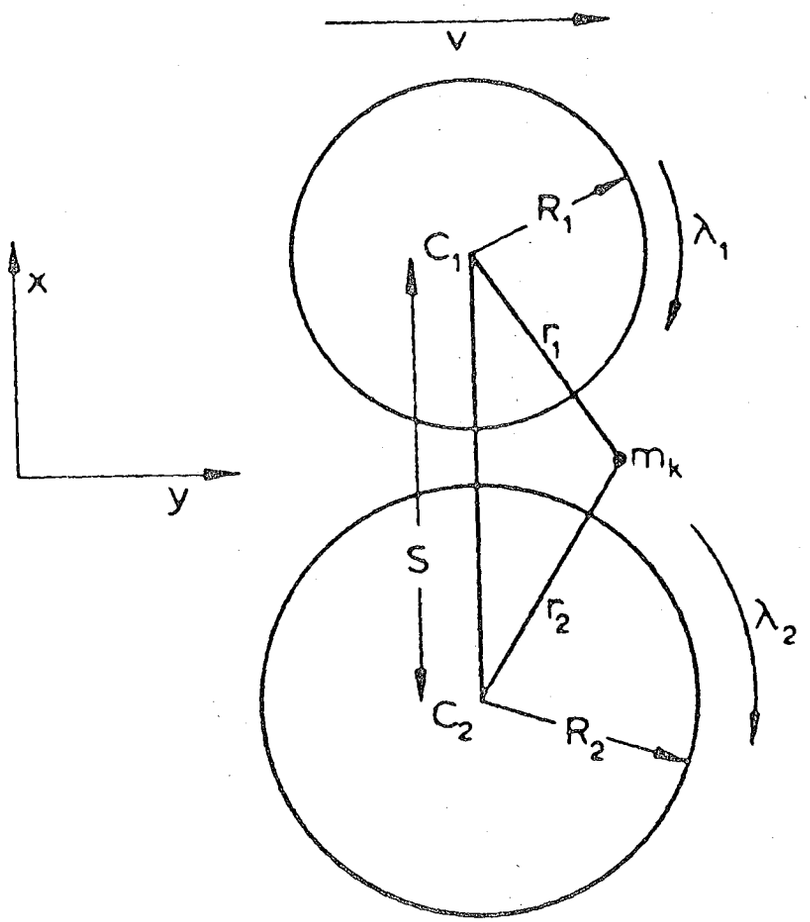

Fig. III-2. Co-ordinate system employed in this semi-classical approach.

where l_1 and l_2 are the total angular momentum of the cluster with respect to the cores (for a spinless cluster) and λ_1 and λ_2 are the magnetic substates of these vectors in the initial state $(l_1\ \lambda_1)$ and in the final state $(l_2\ \lambda_2)$. This condition requires that the transferred nucleon be near the reaction plane, or that $\theta_1 = \theta_2 = \pi/2$ and $\phi=0$ in the wavefunctions ψ_1 and ψ_2, since $Y_{l\lambda}\ (\pi/2,0) = 0$ unless $l+\lambda$ is even.

Given these equations, one can derive an expression that incorporates these conditions and calculates relative hindrance factors. The transition probability from an initial state $(l_1\lambda_1)$ to a final state $(l_2\lambda_2)$ can be expressed (An 74) by

$$P(\lambda_2,\lambda_1) = P_o(R)\left|Y_{l_1\lambda_1}(\pi/2,0)\ Y_{l_2\lambda_2}(\pi/2,0)\right|^2 x \exp\left[-\left(\frac{R\Delta K}{\sigma_1}\right)^2\left(\frac{\Delta L}{\sigma_2}\right)^2\right] \qquad \text{(III-9)}$$

where ΔK and ΔL were defined in conditions 1. and 2., the widths of σ_1 and σ_2 are roughly π and $(\gamma R)^{1/2}$ respectively, with $\gamma^2 = m_k \in/\hbar^2$, and $\in$ is the average of the binding energies of the clusters in the initial and final nuclei (but both are typically treated as adjustable parameters with $\sigma_1 = \sigma_2 \sim 2.5$), R is the touching radius, and $P_o(R)$ is a function of the radial wavefunctions and R. This assumes that the cluster k has zero spin, the centers of the nuclei c_1 and c_2 move along well defined classical paths, and the z-axis is perpendicular to the reaction plane.

This approach can be extended to include the general case in which the cluster and the cores both have non-zero spin (see An 74). For a cluster with spin S_k and isospin T_k and angular momentum configurations

$(L_1 J_1 M_1)$ and $(L_2 J_2 M_2)$ in the initial and final nuclei, the transition probability is

$$P_{21} = \frac{2J_{a_2} + 1}{2J_{c_2} + 1} \sum_{\substack{J_1 M_1 \\ J_2 M_2}} \frac{1}{(2J_1 + 1)(2J_2 + 1)} \sum_{L_1 L_2 L_k T_k}$$

$$\left| B_{S_k T_k}(J_2 L_2 M_2, J_1 L_1 M_1) \Theta^{(1)}(L_1 S_k T_k J_1)\ \Theta^{(2)}\ (L_2 S_k T_k J_2) \right.$$

$$\left. \langle T_{a_2} T_{3_{a_2}} | T_{c_2} T_{3_{c_2}} T_k T_{3_k} \rangle \langle T_{a_1} T_{3_{a_1}} | T_{c_1} T_{3_{c_1}} T_k T_{3_k} \rangle \right|^2$$

This expression consists of the spectroscopic amplitudes [i] for the decomposition of $a \rightarrow c + k$ for particular states of k described by $L_i S_k T_k J_i$, Clebsch-Gordon coefficients (symbolized by $\langle T_{a_1} T_{3_{a_1}} | T_{c_1} T_{3_{c_1}} T_k T_{3_k} \rangle$) for coupling the isospin vectors, and a transfer amplitude factor $B_{S_k T_k}$ for each transition term between states $(J_1 L_1 M_1)$ and $(J_2 L_2 M_2)$. This transfer amplitude factor is relation to expression (III-9) by

$$B_{S_k T_k}(J_2 L_2 M_2, J_1 L_1 M_1) = \sum_{\lambda_1 \lambda_1 m_s} \langle J_1 M_1 | L_1 \lambda_1 S_k M_s \rangle \qquad \text{(III-11)}$$

$$\langle J_2 M_2 | L_2 \lambda_2 S_k M_s \rangle\ P(\lambda_2, \lambda_1)$$

with some more Clebsch-Gordan coefficients and another sum over magnetic substates (see An 74 for a more detailed derivation).

This expression (III-10) is evaluated by the computer code HIPROB (Hu 75). The quantity $P_o(R)$ in expression (III-9) is calculated by a standard Coulomb bound-state wavefunction routine. The results of these calculations will be discussed in Section IV; employing the parameters listed in Table III-4.

Table III-4. Input perameters for the program HIPSOB.

For illustration we will employ the $^{12}C(^{6}Li,^{8}B)^{10}Be$ reaction. Since this program is designed for stripping reactions, this case is calculated as the $^{6}Li(^{12}C,^{10}Be)^{8}B$ reaction with an appropriate (c.m.) beam energy.

$$\sigma_1 = \sigma_2 = 2.5 \ , \ r_o = 1.4 \text{ fm}$$

	Core Plus Cluster System				Bound State Wave Function (Volume Wood Saxon Potential)								
	L	$J_{cluster}$	J_{core}*	J_{final}	Nodes	L	J	S	V_r	r_o	a_r	V_{SO}	V_{so}
				J = 0									
Initial	0	0	0	0	1	0	0	0	-1.	1.25	0.65	25.0	0
Final	2	0	1	2	0	2	2	0	-1.	1.25	0.65	25.0	0
				J = 2									
Initial	2	0	0	2	0	2	2	0	-1.	1.25	0.65	25.0	0
Final				Same as Above									

* This quantity is not a direct input parameter.

It is possible to qualitatitively evaluate conditions 1 and 2 for their effects upon the reaction selectivity. Expression (1),

$$\Delta K = k_o - \lambda_1/R_1 - \lambda_2/R_2 \sim 0 \qquad (1)$$

for this (^{6}Li,^{8}B) reaction on 1p-shell target can be reduced to

$$k_o R_1 - \lambda_1 - \lambda_2 \sim 0$$

since $R_1 \sim R_2$. Typically, the equivalent stripping reaction for ^{6}Li on 1p-shell targets has a $k_o R_1 \sim 5$, so we have

$$5 - \lambda_1 - \lambda_2 \sim 0 \qquad (1)$$

Similarly, expression (2),

$$\Delta L = \lambda_2 - \lambda_1 + 0.5k_o(R_1 - R_2) + Q_{eff}\, R/\hbar v \sim 0 \qquad (2)$$

can be reduced to

$$\lambda_2 - \lambda_1 - 5 \sim 0$$

Both expressions, if solved simultaneously, are zero for $\lambda_1 = 0$ and $\lambda_2 = 5$. For allowed values of both λ's, expression (1) is smallest if $\lambda_2 = \lambda_1 = -2$, and expression (2) is smallest if $\lambda_2 = -\lambda_1 = 2$, which are mutually exclusive. The minimum value of the sum of expressions (1) and (2) is when $\lambda_1 = 0$ and $\lambda_2 = 2$. The transition strength will be proportional to the negative exponent of the sum of the squares of these expressions and other terms will not be very significant. Since pickup reactions are treated by their equivalent stripping reactions, λ_1 is the magnetic substate of the two-protons with respect to the actual target core, and therefore, relative transition strengths will be comparable for L=0 or 2 (or 1). However, with higher excitation energy Q_{eff} increases, so that expression (2) will become mismatched.

Therefore, there will be a general decrease in relative transition strengths with increasing excitation.

This kinematic dependence is in contrast to the stripping reactions reported in An 74, since in these cases the hindrance was minimized at some higher excitation energy. The transition probabilities for these stripping reactions resembled Gaussian distributions and the peak in these calculations corresponded to the observed dominant transition. Moreover, in these stripping reactions, lower J transitions were hindered relative to high-spin states. For these pickup reactions the transition probabilities are simply the tail regions of the Gaussian distributions. The slight differences in the transition strength for the various spin transitions is reproduced by exact calculations of expression (III-10) and also by DWUCK calculations.

In summary, we have demonstrated that the transfer amplitude term in the transition matrix element enhances low excitation levels and depends only slightly upon the spin of the transition. Accordingly, the observed transition strengths within a limited range of excitation energy are a reasonable measure of the relative spectroscopic factor. This is useful to note for Section IV, where the energy spectra will be presented. Also, in Section IV, we will present some calculations of the total transition strength (expression III-10) and compare these with the observed relative yields.

IV. EXPERIMENTAL RESULTS

As discussed in the previous section, the observed relative yields to levels in the final nuclei of the (^{6}Li,^{8}B) reaction are roughly indicative of the two-proton spectroscopic amplitudes of these states. The energy spectra, which will be presented in this section, will indicate these relative transition strengths, since these relative yields are independent of angle. The selectivity of the two-proton transfer will demonstrate that this reaction proceeds primarily through a direct, single-step pickup. In general, the dominant observed transitions are only to levels with a significant predicted two-nucleon spectroscopic factor. The observed angular distributions, which will also be presented here, illustrate the lack of any obvious spectroscopic utility of this aspect of the reaction. A summary of the experimental investigations is presented in Table IV-1.

Excitation energies and the associated spins and parities of the levels populated in this reaction were obtained by comparing the observed excitation energies to the previously measured ones (tabulated in Aj 74, Fi 73, En 73, etc). The uncertainties in the measured excitation energies indicate primarily the extent of reproducibility in these observations. Similarly, it should again be noted that the uncertainty indicated in the angular distributions represents only the statistical error; the absolute error could be as much as 30%.

As a measure of the strength of anti-symmetric transfer we will employ both the 1^{+} levels in ^{14}C and ^{8}Li and overall comparison of the spectroscopic selectivity of the (^{6}Li,^{8}B) and (p,t) reactions.

Table IV-1. Summary of experimental investigations.

Target	Q-Value (MeV)	Beam Energy (MeV)	Angular Range Studied (deg) ($\theta_{c.m.}$)	Final Nucleus	Observed Energy Levels (MeV)
^{6}Li	-21.17	93.3	31-46	^{4}H	0.0
^{7}Li	-25.02*	93.3	27-40	^{5}H	- - -
^{9}Be	-23.5974	93.3	32-49	^{7}He	0.0
^{9}Be	-23.5974	80.0	22-40	^{7}He	0.0
^{10}B	-17.7300	80.0	22-44	^{8}Li	0.0,1.0,2.2,6.5
^{11}B	-25.1330	80.0	20-32	^{9}Li	0.0,2.6,4.4,6.4
^{12}C	-21.4429	80.0	18-49	^{10}Be	0.0,3.3,5.9,7.5,9.4,11.8
^{12}C	-21.4429	93.3	18-29	^{10}Be	0.0,3.3,5.9
^{13}C	-25.8865	80.0	18-36	^{11}Be	0.3,2.7,4.0
^{16}O	-16.5914	80.0	17-29	^{14}C	0.0,6.1,6.9,8.3,10.4
^{16}O	-16.5914	93.3	15-25	^{14}C	0.0,6.9,8.3,10.4
^{24}Mg	-14.7410	80.0	14-30	^{22}Ne	0.0,1.3,3.4,4.5,5.4, 5.9,6.3,6.9,7.5
^{26}Mg	-19.1002	80.0	11-28	^{24}Ne	0.0,2.0,3.9,7.5,8.9

* This Q-value is for transitions to a final ^{5}H system with zero binding energy for breakup to t + 2n.

Other tests are possible, such as the predicted 2_3^+ state in ^{10}Be (see Table IV-2), but this work seems to have utilized the most satisfactory test cases. The results for the ^{8}Li case are particularly unambiguous since the location of at least the 1_1^+ state is well established (unlike the cases in ^{11}Be and ^{9}Li) and this level is at a low excitation energy so that the configuration should be reasonably pure (unlike the 2_3^+ state in ^{10}Be where even the 2_2^+ strength is fragmented). While the 1^+ level in ^{14}C is not definitely located and is at a high excitation energy, it has a very large predicted transition strength so that it should clearly be in evidence (see Table IV-3). Finally, the overall comparison between the spectroscopic utility of the (^{6}Li,^{8}B) and (p,t) reactions does not depend upon any one level, so that it removes the ambiguity associated with the uncertainty in the configuration of any particular level.

This section is divided into four parts. The first portion consists of data for the $T_z = 0$ 1p-shell targets ^{12}C, ^{16}O, and ^{10}B, which will be compared to the earlier data from the analogous (p,t) reaction on these targets. The second part contains data from reactions on the neutron-excess targets ^{13}C and ^{11}B, which will be compared with data from the (t,p) reaction leading to the same final nuclei. The third portion consists of data for reactions on ^{9}Be, ^{6}Li, and ^{7}Li targets, which lead to unbound final systems that have yet to be completely characterized in a non-controversial and unambiguous fashion (Aj 74, Fi 73). It should be noted that the hierarchy among the three 1p-shell sections reflects a trend towards an increasing neutron to proton ratio with a corresponding decrease in the knowledge of the final system.

Table IV-2. Summary of experimental and theoretical results for ^{10}Be.

Low-Lying Known Levels[a]		Levels Observed in This Work		Predicted Levels				Transition Strength[e]					Cross Sections[f] at $\theta_{c.m.} \sim 25^{\circ}$
								Cohen and Furath					
J^{π}	MeV	MeV	± keV	J^{π}	Boyarkina[b]	Horton and Goldhammer[c]	Cohen and Furath[d]	SPAG	UPAG	PPAG 0	PPAG 1	PPAG 2	μb/sr
0^+	0	0		0^+	0	0	0	2.747	0	0.032	0	0	5.4 ± 0.3
2^+	3.37	3.33	60	2^+	3.39	3.85	4.16	0	1.215	0	0	2.432	3.2 ± 0.2
2^+	5.958	5.96	60	2^+	5.89	6.39	5.81	0	4.544	0	0	0.256	1.4 ± 0.1
1^-	5.960												
0^+	6.18												
2^-	6.26												
3^-	7.37												
2^+	7.54	7.53	60										0.5 ± 0.2
(4^-)	9.27												
(2^+)	9.4	9.42	70	2^+	8.59	9.52	9.16	0	0.004	0	0	4.066	0.8 ± 0.2
				3^+	9.39	9.50							
≥1	10.7			1^+	10.19	9.10	8.13	0	0	0	0.222	0	
				4^+	10.99	12.34							
	(11.75)	11.79	70	0^+	11.29	10.86	11.05	0.004	0	0.011	0	0	0.6 ± 0.2
				2^+	11.29	11.52							
				1^+	11.29	11.22	10.22	0	0	0	1.452	0	
				0^+	14.59	12.27							

a Ref. Aj 74.
b Ref. Bo 64.
c Ref. Ho 71.
d Ref. Co 70.
e SPAG and UPAG are from Ref. c, PPAG 0, PPAG 1, and PPAG 2 are this work, see text.
f The differential cross sections decreased monotonically with angle, see text.

Finally, the fourth part consists of data for the 2s-1d-shell targets ^{24}Mg and ^{26}Mg, which represent an example of the possible extension to heavier targes of the work presented in the earlier parts. In all cases these results will be compared to available theoretical spectroscopic amplitudes and level predictions.

A. $T_z = 0$ 1p-Shell Targets

1. The $^{12}C(^6Li, ^8B)^{10}Be$ Reaction

An energy spectrum of the $^{12}C(^6Li, ^8B)^{10}Be$ reactions is shown in Fig. IV-1a. These data were collected with an 80.0 MeV beam from a 0.22 mg/cm^2 target. This particular spectrum is a composite of data collected between $\theta_{lab} = 12.8^o$ and 16.8^o, in which the data were kinematically shifted to $\theta_{lab} = 15.8^o$. Data were also collected with a 93.3 MeV beam energy as a calibration for the studies employing ^6Li and ^7Li targets; both the selectivity and the yields were essentially unaltered by the difference in beam energy (as is expected for a direct reaction at similar bombarding energies).

As indicated by this spectrum, the dominant transitions are to the 0^+ ground state and to the first excited level, at 3.36 MeV (2_1^+). The next peak (2_2^+ at 5.96 MeV) probably corresponds to the 2^+ member of the 2^+, 1^- doublet at this excitation energy, since the 1^- level must have a cross-shell configuration and this type of state would be unlikely to have substantial parentage in the ^{12}C ground state wave function. Weaker transitions are seen to a state at 7.54 MeV (2_3^+), a probable 2^+ level at 9.4 MeV (Aj 74), and a known state at 11.8 MeV excitation. These experimental results are summarized in Table IV-2. The rather featureless angular distributions of the first two transitions

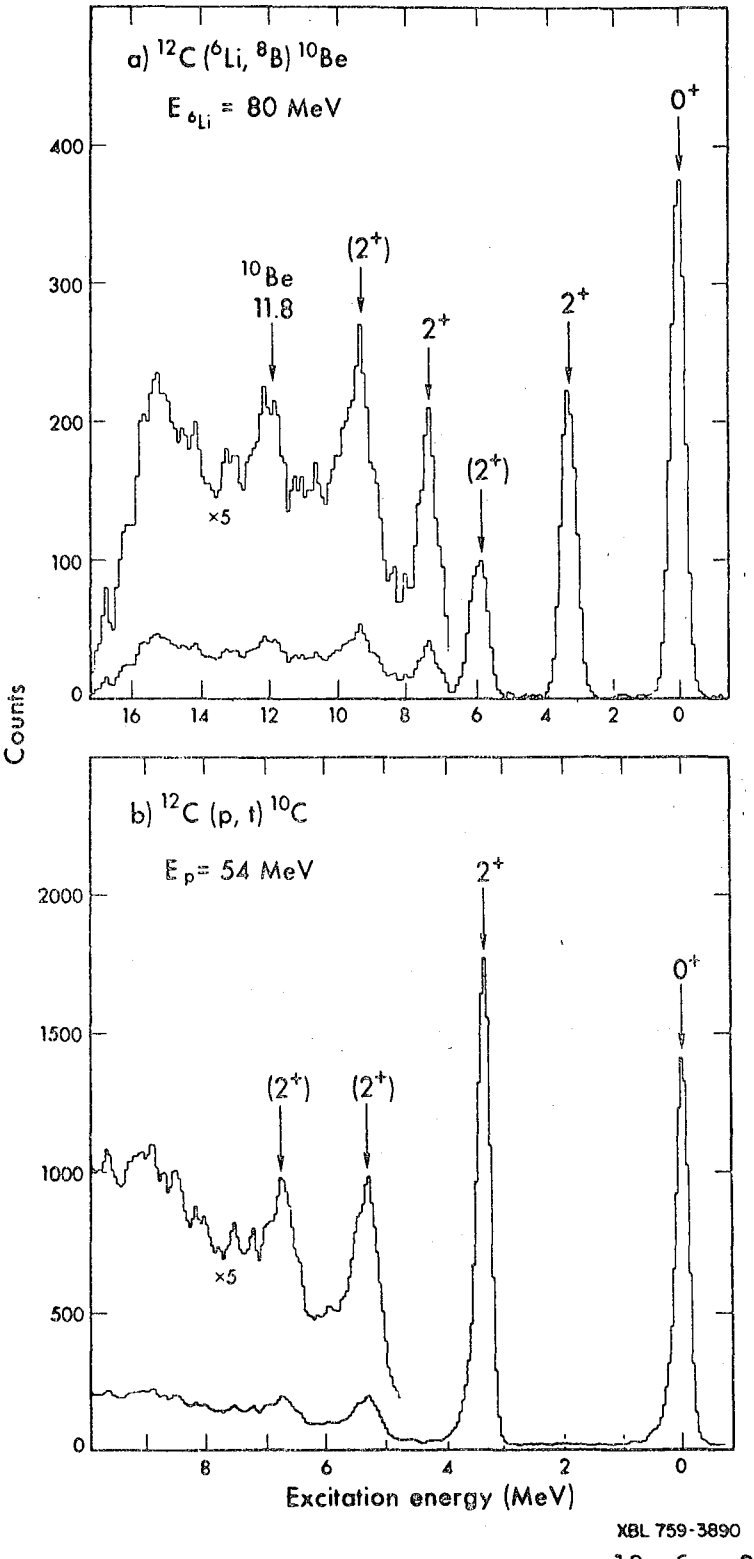

Fig. IV-1. (a) A composite spectrum of the $^{12}C(^{6}Li, ^{8}B)^{10}Be$ reaction between θ_{lab} = 12.8° and 16.8° (with $E(^{6}Li)$ = 80 MeV), in which the data were kinematically shifted to θ_{lab} = 15.8°. (b) The $^{12}C(p,t)^{10}C$ reaction induced by 54 MeV protons at θ_{lab} = 19.5° (as 75). (This angle lies at the first minimum in the ^{10}C g.s. angular distribution.)

are shown in parts (a) and (b) of Fig. IV-2.

One sees a strong similarity between these results and those of the $^{12}C(p,t)^{10}C$ reaction (As 75, Be 67), which are shown in Fig. IV-1b. These data were collected at the first minimum in the ^{10}C ground state angular distribution. The comparison between these energy spectra suggests the location of the analog levels in these two final nuclei. Both of the higher excited levels at 5.28 and 6.60 MeV in ^{10}C have angular distributions which are consistent with L = 2 (As 75). In the first case this supports the suggestion that the 5.96 MeV level, populated in the $^{12}C(^{6}Li,^{8}B)^{10}Be$ reaction, corresponds to the 2^+ member of the 2^+, 1^- doublet (denoted by 2_3^+). In the second case, it supports the suggestion that the 6.60 MeV level in ^{10}C is the analog of the known 2^+ state (2_3^+) at 7.54 MeV in ^{10}Be. Finally, analogs of the two higher lying transitions (at 9.4 and 11.8 MeV excitation in ^{10}Be) were seen as a by product of the $^{14}C(p,t)^{12}C$ investigation (As 76) due to ^{12}C target contamination. Although the differing transfer emplitudes lead to a relative enhancement of the yield to higher lying levels in the ($^{6}Li,^{8}B$) data compared to the (p,t) reaction, there is a strong similarity in the selectivity of these two reactions.

The various theoretical predictions for both the energy levels and the transition strengths for two-nucleon transfer are also summarized in Table IV-2. (As the transfer amplitudes are ignored, the comparison between these predicted transition strengths and the observed yield is meant to be very qualitative.) One sees reasonable qualitative agreement between the various level predictions and the experimental results. Major disagreement between theory and experimental results

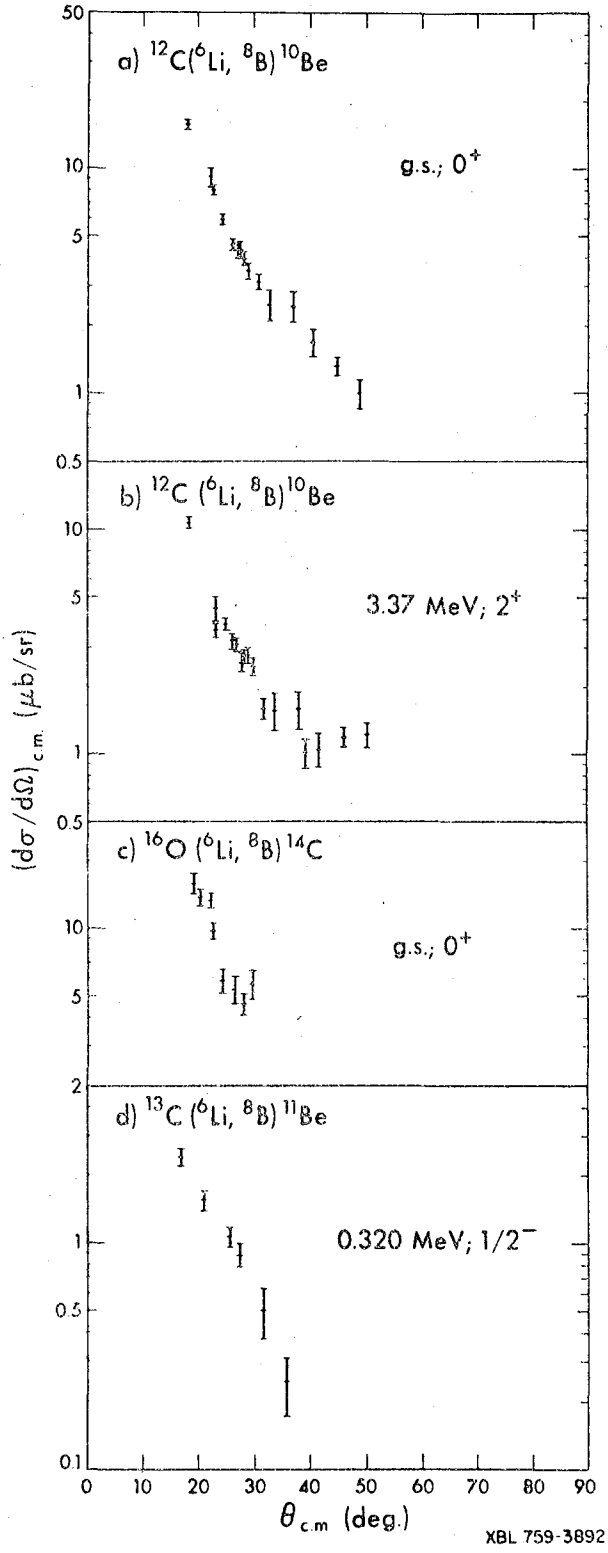

Fig. IV-2. Angular distributions for reactions induced by an 80 MeV ^{6}Li beam: (a) $^{12}C(^{6}Li,^{8}B)^{10}Be$ g.s.; (b) $^{12}C(^{6}Li,^{8}B)^{10}Be^*$ (3.37 MeV, 2^+); (c) $^{16}O(^{6}Li,^{8}B)^{14}C$ g.s., and (d) $^{13}C(^{6}Li,^{8}B)^{11}Be^*$ (0.320 MeV, $1/2^-$).

appears for the transition to the 2_3^+ level (at 7.54 MeV), which is not an expected 1p-shell level; also, the 2_2^+ state at 5.96 MeV has a large spectroscopic factor (relative to the 2_1^+ level), but a relatively weak transition strength. The 2_3^+ state is felt to be primarily an sd-shell "intruder" level (Al 69). Its population in this reaction might indicate that the predicted 2_2^+ 1p-shell configuration is split among the observed 2_2^+ and 2_3^+ states, which could explain the observed transition strength to the 2_2^+ level.

The close correspondence between the theoretical predictions and the experimental results would suggest that the theoretical 2_3^+ state corresponds to the probable 2^+ level at 9.4 MeV excitation and that the theoretical 0_2^+ state corresponds to the 11.8 MeV peak; this would be consistent with these levels being populated, along with the other transitions seen in this work, in the $^7Li(^7Li,\alpha)^{10}Be$ (Gl 71) and $^9Be(p,\pi^+)^{10}Be$ (Da 73) reactions. While the 2_3^+ state may be populated by anti-symmetric transfer (see Table IV-2 for the predicted relative magnitude of the symmetric and anti-symmetric transfer components), it is more likely that its possibly relative enhanced yield reflects either the effect on the transition strength of either admixtures in the ^{12}C ground state wave function or configuration mixing in the final level. Of course, these two transitions could also correspond to the predicted two 1^+ levels, whose locations have not been experimentally determined, but this is rather unlikely, as will become obvious from the discussion of similar states in ^{14}C and ^8Li.

2. The $^{16}O(^{6}Li,^{8}B)^{14}C$ Reaction

An energy spectrum of the $^{16}O(^{6}Li,^{8}B)^{14}C$ reaction is shown in Fig. IV-3a. These data were collected with a 93.3 MeV beam from a 16% oxidized (by atom) 0.34 mg/cm^2 ^{7}Li target at $\theta_{lab} = 13.5^{o}$. Carbon contamination gave rise to the ^{10}Be states; the spectrum is cut-off before possible transitions could arise from the ^{7}Li component of the target. Data were collected at 80.0 MeV with both a 0.21 mg/cm^2 SiO_2 target and a 100% oxidized (by atom) ^{142}Nd target. The reaction yield and selectivity again were essentially unchanged with the different beam energies.

The dominant transition is to the ^{14}C ground state and the next strongest transitions are to a series of 2^+ levels at 7.01, 8.32 and 10.0 MeV excitation. In this particular spectrum the ^{10}Be contaminant state obscured possible further transitions to the 1^- level at 6.09 MeV and a 0^+ state at 6.58 MeV (which is predominantly an sd-shell level (Al 69)), but these transitions were seen in the investigations with the other targets. By analogy to the $^{16}O(p,t)^{14}O$ reaction (Fl 71), shown in Fig. IV-3b, one would expect that the peak near 7.0 MeV corresponds to not only the 2^+ state at 7.01 MeV, but that is also has an unresolved component corresponding to the 3^- level at 6.73 MeV (this is consistent with both the measured excitation energy and width of this peak, which was often barely resolved from the transition to the 0^+ state at 6.59 MeV). The experimental results are summarized in Table IV-3; the ground state angular distribution is shown in Fig. IV-2c.

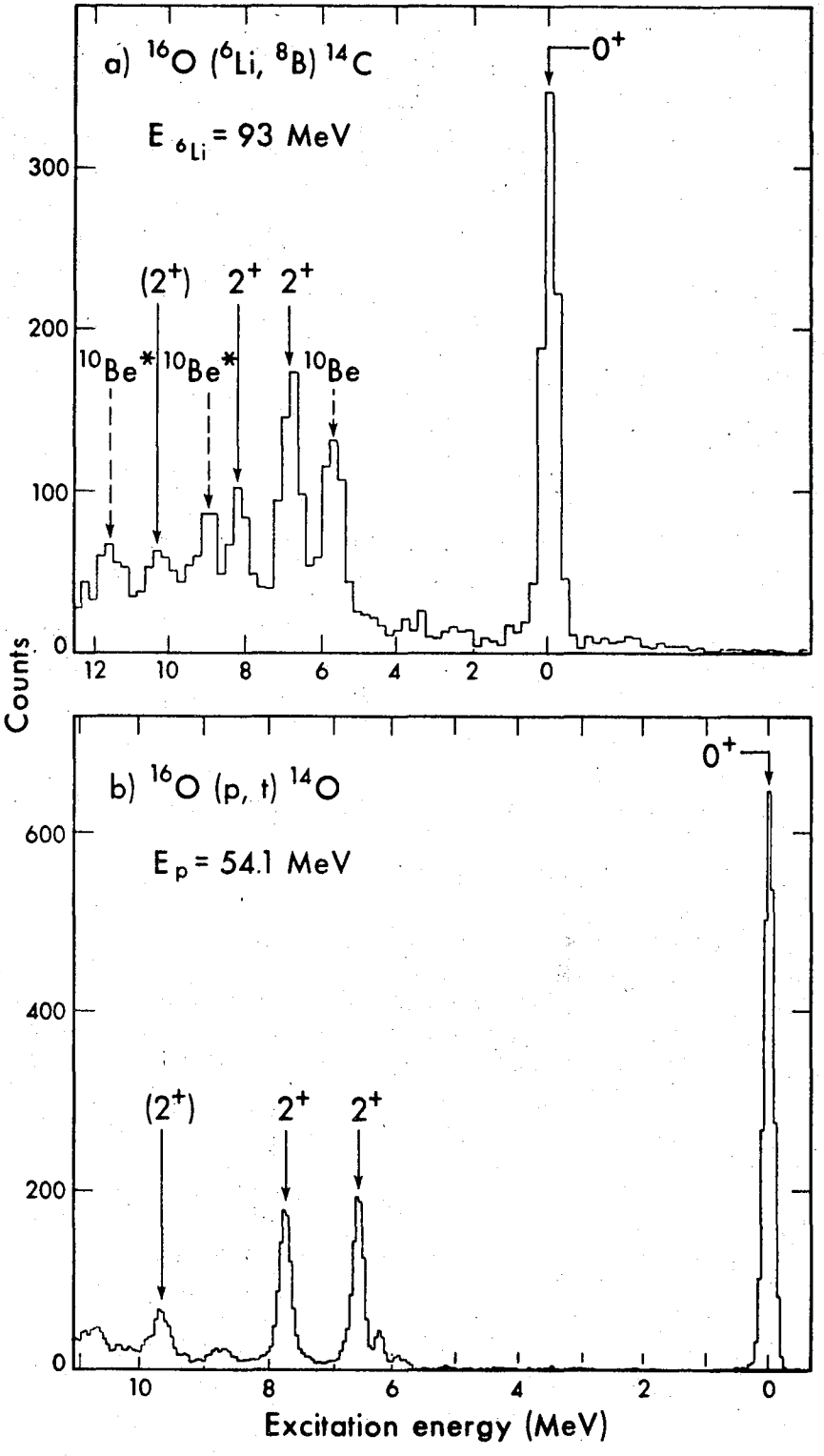

XBL 759-3889

Fig. IV-3. (a) An energy spectrum from a partially oxidized Li target for the $^{16}O(^{6}Li,^{8}B)^{14}C$ reaction. These data were collected at θ_{lab} = 13.5° with a 93.3 MeV ^{6}Li beam. Carbon contamination gave rise to the ^{10}Be states. (b) The $^{16}O(p,t)^{14}O$ reaction induced by 54.1 MeV protons at θ_{lab} = 27° (Fl 71).

Table IV-3. Summary of experimental and theoretical results for ^{14}C.

Low-Lying Known Levels[a]		Levels Observed in This Work		Predicted Levels						Transition Strength[g]					Cross Sections[h] at $\theta_{c.m.} \sim 22^{\circ}$
										Cohen and Kurath					
J^{π}	MeV	MeV	± keV	J^{π}	Boyarkina[b]	Lie[c]	True[d]	Horton and Goldhammer[e]	Cohen and Kurath[f]	SPSG	DPSG	PPSG 0	PPSG 1	PPSG 2	μb/sr
0^+	0	0		0^+	0	0	0	0	0	2.212	0	0.788	0	0	9.7 ± 0.8
1^-	6.09	6.09	50												0.5 ± 0.2
0^+	6.59														
3^-	6.73														
0^-	6.90														
2^+	7.01	6.94[i]	60	2^+	6.2	7.19	7.18	6.56	6.83	0	12.721	0	0	2.277	3.4 ± 0.4[i]
2^-	7.34														
2^+	8.32	8.30	70												1.5 ± 0.3
(3,1)	9.80														
$(2^+,3)$	10.44	10.40	90												1.0 ± 0.3
(6^+)	10.51														
	10.74														
(1^+)[j]	11.35			1^+	9.6	9.69	13.64	14.09	9.09	0	0	0	9.001	0	≥0.5
				0^+	12.9	5.8	5.52	16.68	13.63	0.788	0	2.212	0	0	
				2^+	15.3	7.43	9.37	16.72	15.19	0	2.277	0	0	12.721	
				2^+		9.25	12.96								

a Ref. Aj 73.
b Ref. Bo 64.
c Ref. Li 72.
d Ref. Tr 63.
e Ref. Ho 71.
f Ref. Co 70.
g SPSG and DPSG are from Ref. f, PPSG 0, PPSG 1, and PPSG 2 are from this work see text.
h The differential cross sections decrease monotonically with angle, see text.
i By analogy to the (p,t) results, this peak should correspond to transitions to the 0^+, 3^-, and 2^+ levels, see text.
j Ref. Ra 71.

As can be seen from Fig. IV-3b, the dominant transition in the $^{16}O(p,t)^{14}O$ reaction is to the ^{14}O ground state. This level is followed in strength by the triplet of 2^+ states. Finally, the two cross-shell 1^- and 3^- levels and the sd-shell 0^+ state are also populated; thus, these higher-shell configurations are components of the ^{16}O ground state wave functions.

The theoretical predictions of the energy levels and transition strengths are also summarized in Table IV-3. The theoretical predictions of the energy levels are not completely comparable, since both Boyarkina (Bo 64) and, also, Cohen and Kurath (Co 70) employ calculations with only a 1p-shell basis, while both True (Tr 63) and Lie (Li 72) included configuration mixing from 2s-1d-shell levels. These latter calculations agree more completely with the known levels. One effect of these higher configurations can be seen in the triplet of 2^+ states, which is felt to arise from the strength of the 2^+ configuration being split among these three levels (Fl 71, Tr 63, Li 71). This configuration has a very large spectroscopic factor, so this suggested fragmentation of the transition strength leads to better agreement between these results (and those of the (p,t) reaction (Fl 71)) with the predicted spectroscopic factors (Co 70).

Reactions on this target also provide a convenient test for anti-symmetric transfer processes. The predicted 1^+ level can only be populated by anti-symmetric transfer (since $\Delta J = 1$). It has been proposed by Kaschl (Ka 71) that this state is located in ^{14}C at 11.29 MeV excitation (based upon results from the $^{15}N(d,^3He)^{14}C$ reaction).

This region is obscured by a contaminant peak at the angle shown in Fig. IV-3a, but no strong transition is seen to this level in any of the other spectra, indicating that anti-symmetric transfer does not play an important role in this reaction.

3. The $^{10}B(^{6}Li,^{8}B)^{8}Li$ Reaction

An energy spectrum of the $^{10}B(^{6}Li,^{8}B)^{8}Li$ reaction is shown in Fig. IV-4. These data were collected with an 80.0 MeV beam from a 0.14 mg/cm^2 target; this particular spectrum is a composite of data collected between $\theta_{lab} = 9.7^{o}$ and 20.3^{o}, in which the data were kinematically shifted to $\theta_{lab} = 9.7^{o}$. The ^{14}C levels arose from ^{16}O contamination of the target.

The dominant transition is to the 3^+ level at 2.26 MeV. Weaker transitions are seen to the 2^+ ground state, a 1^+ level at 0.98 MeV, and to the known (Aj 74) state at 6.53 MeV excitation. These experimental results are summarized in Table IV-4; the angular distributions are shown in Fig. IV-5.

The same qualitative selectivity in the relative transition strengths was observed in the $^{10}B(p,t)^{8}B$ reaction (Sq 70), which is not reproduced here. This (p,t) study could only observe the lower-lying transitons, so that the analog of the 6.53 MeV state was not observed.

The various theoretical predictions of the energy levels and transition strengths are also summarized in Table IV-4. In general, the theoretial calculations indicate that there should be an extremely high level density in ^{8}Li (and ^{8}B), but relatively few states have been located. However, ^{8}Li is unbound above $\approx$2 MeV, and several of

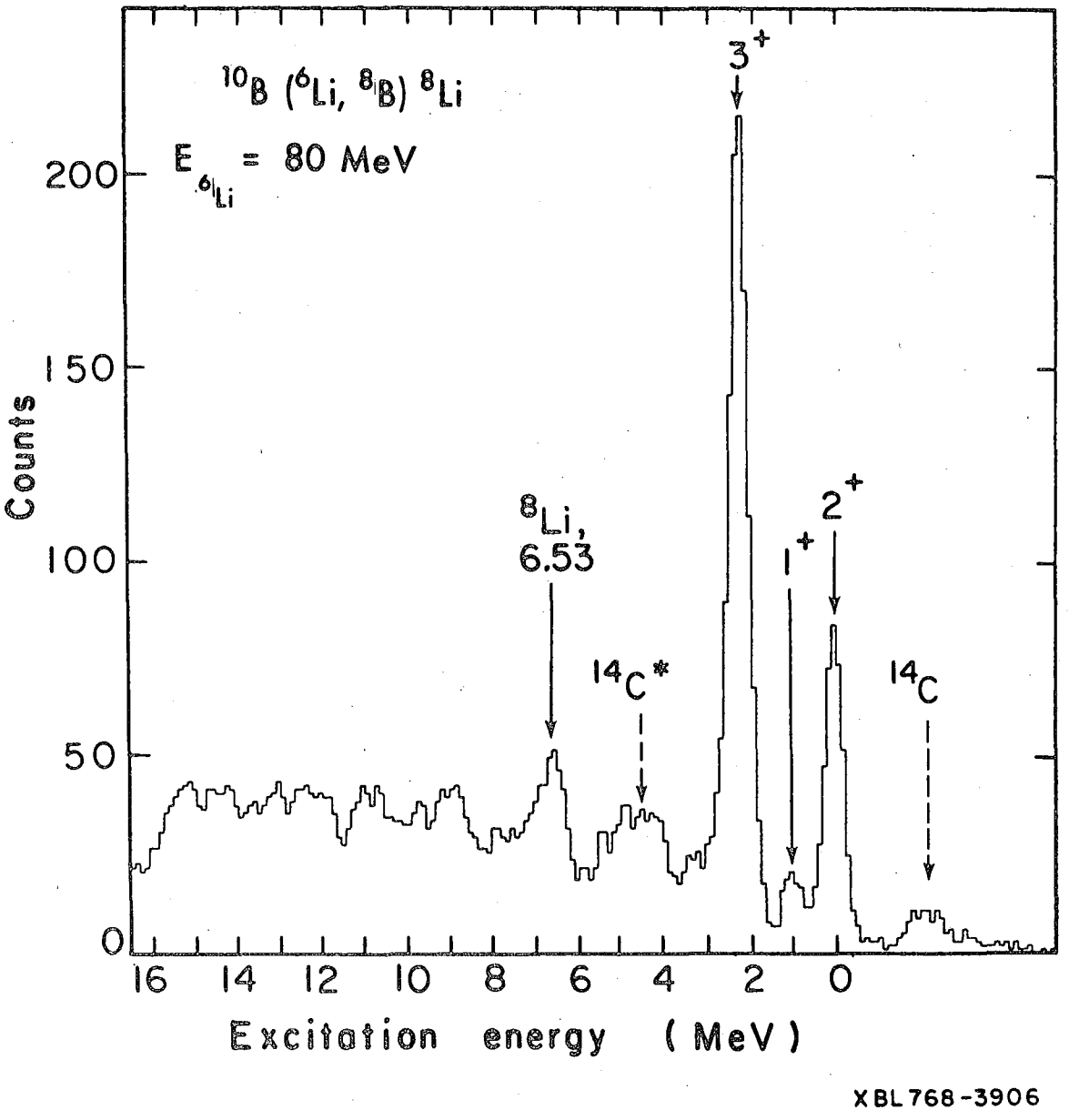

Fig. IV-4. A composite spectrum of the $^{10}B(^{6}Li,^{8}B)^{8}Li$ reaction between θ_{lab} = 9.7° and 20.3° (with $E(^{6}Li)$ = 80 MeV), in which the data were kinematically shifted to θ_{lab} = 9.7°. Oxygen contamination gave rise to the ^{14}C transitions.

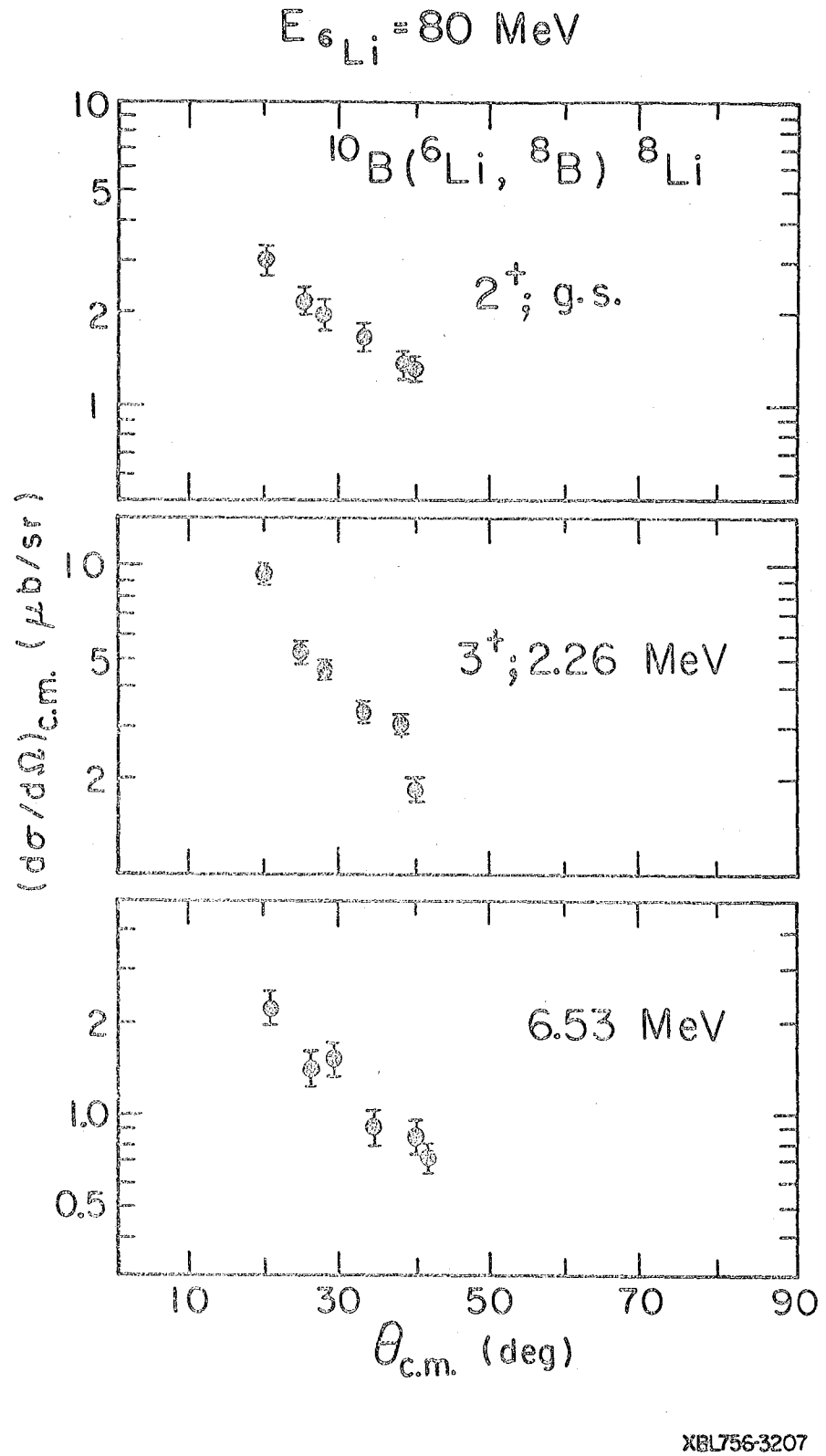

Fig. IV-5. Angular distributions for reactions induced by an 80 MeV ^{6}Li beam: (a) $^{10}B(^6Li, ^8B)^8Li$ g.s.; (b) $^{10}B(^6Li, ^8B)^8Li^*$ (2.26 MeV, 3^+), and (c) $^{10}B(^6Li, ^8B)^8Li^*$ (6.53 MeV).

Table VI-4. Summary of experimental and theoretical results for ^{6}Li.

Known Levels[a]		Levels Observed in this Work		Predicted Levels						Transition Strength[g]					Cross Sections[h] $\theta_{c.m.} \sim 25^{o}$
								Morton and	Cohen	Cohen and Kurath					
J^{π}	MeV	MeV	± keV	J^{π}	Boyarkina[b]	Barker[c]	Kumar[d]	Goldhammer[e]	and Kurath[f]	SPAG	DPAG	PPAG 0	PPAG 1	PPAG 2	μb/sr
2^{+}	0	0		2^{+}	0	0	0	0	0	0	0.732	0	0.295	1.428	2.3 ± 0.2
1^{+}	0.99	0.95	40	1^{+}	1.2	0.83	0.92	1.53	0.91	0	0.002	0	0	0.408	0.5 ± 0.1
3^{+}	2.26	2.24	40	3^{+}	2.8	2.09	2.19	1.92	1.63	0.750	1.305	0.018	0.069	0.871	5.3 ± 0.4
1	3.21			1^{+}	3.0	2.65	4.28	5.37	2.78	0	0.021	0	0	0.873	
				0^{+}	3.1	2.89	3.95	4.32	5.32						
$(2^{+},3^{+})$	5.4			2^{+}	3.4	2.96	4.05	4.05	2.95	0	0.003	0	0.001	0.120	
				3^{+}	4.5				5.59	0.27	0.482	0.015	0.009	0.053	
				1^{+}	4.6	4.33	5.74								
				1^{+}	5.2		8.39	6.15							
				2^{+}	5.4	4.74	5.33	6.15							
	6.1			2^{+}	6.2										
				3^{+}	6.3	6.51	7.81								
	6.93	6.52	150	4^{+}	8.9	5.57	5.79	6.39	5.55	0	0.346	0	0.010	0.33	1.6 ± 0.4
	7.1														
	(9.)														

a Ref. Aj 74.
b Ref. Bo 64.
c Ref. Ba 66.
d Ref. Ku 74b.
e Ref. Mo 71.
f Ref. Co 70.
g SPAG and DPAG are from Ref. f, PPAG 0, PPAG 1, and PPAG 2 are from this work, see text.
h The differential cross sections decrease monotonically with angle, see text.

the known states are quite broad, so that it would be difficult to identify many of these levels.

This nucleus provides a good test for the importance of anti-symmetric transfer, since both of the low-lying 1^+ levels can be populated essentially solely through spatially anti-symmetric transfer. However, since the 1^+ level at 0.98 MeV is weakly populated, little evidence for this transfer mode is seen. Similarly, if one assume that the second 1^+ state corresponds to the known spin 1 level (Aj 74) at 3.21 MeV, then this conclusion is further confirmed. Finally, one sees from the transition strengths that the 3^+ state's strong population relative to the ground state also provides supporting evidence that anti-symmetric transfer is unimportant (since this 2^+ level has a larger possible anti-symmetric component than the 3^+ state). In summary, then, we have seen no evidence for anti-symmetric transfer either in the yield of the 1^+ level in ^{14}C, or the known 1^+ state in ^{8}Li, or a possible 1^+ level in ^{8}Li, or in overall comparisons between the (^{6}Li,^{8}B) and the (p,t) reactions.

The relative transition strengths of the ground state and the 3^+ level indicate that the observed population ratio reflects the spectroscopic factors, instead of solely the reaction kinematics. The only other cases in the 1p-shell where an excited state should be populated more strongly than the ground state are in transitions leading to ^{11}Be (which will be discussed below) and those leading to ^{12}Be (in this last case, data from the $^{14}C(^{6}Li,^{8}B)^{12}Be$ reaction (Wi 74), which was employed in an attempted mass measurement, were consistent with the population of the first excited state, but only an upper limit

could be determined for the ground state transition).

From the spectroscopic factors of Cohen and Kurath (Co 70), one could suggest that the 6.53 MeV level is either a 3+ or a 4^+ state, and these high spins would be consistent with the known (Aj 74) narrow width of this level ($\leq$40 MeV).

B. $T_z > 0$ 1p-Shell Targets

1. The $^{13}C(^6Li,^8B)^{11}Be$ Reaction

An energy spectrum of the $^{13}C(^6Li,^8B)^{11}Be$ reaction is shown in Fig. IV-6. These data were collected with an 80.0 MeV beam from a 0.14 mg/cm^2 target; this particular spectrum is a composite of data collected between $\theta_{lab} = 9.4^o$ and 20.3^o for a total of 32,900 μC, in which the data were kinematically shifted to $\theta_{lab} = 14.3^o$. The ^{10}Be and ^{14}C levels arose from the ^{12}C and ^{16}O contaminants in the target, respectively.

The dominant transition is to the first excited state of ^{11}Be, a $1/2^-$ level at 0.320 MeV excitation, which is the lowest 1p-shell level (Aj 75). The predominant population of this state, instead of the known $1/2^+$ ground state (Aj 75), was established by the known ^{10}Be contaminant transitions. More weakly populated levels are seen at 2.69 and 4.0 MeV (this last peak may correspond to both members of the known doublet near this excitation). These experimental results are summarized in Table IV-5; the angular distribution of the first excited state is shown in Fig. IV-2d.

The selectivity of this reaction can be contrasted with that of the $^9Be(t,p)^{11}Be$ reaction (Aj 72), which populates all the known levels in ^{11}Be. While the $(^6Li,^8B)$ reaction can only populate 1p-shell levels,

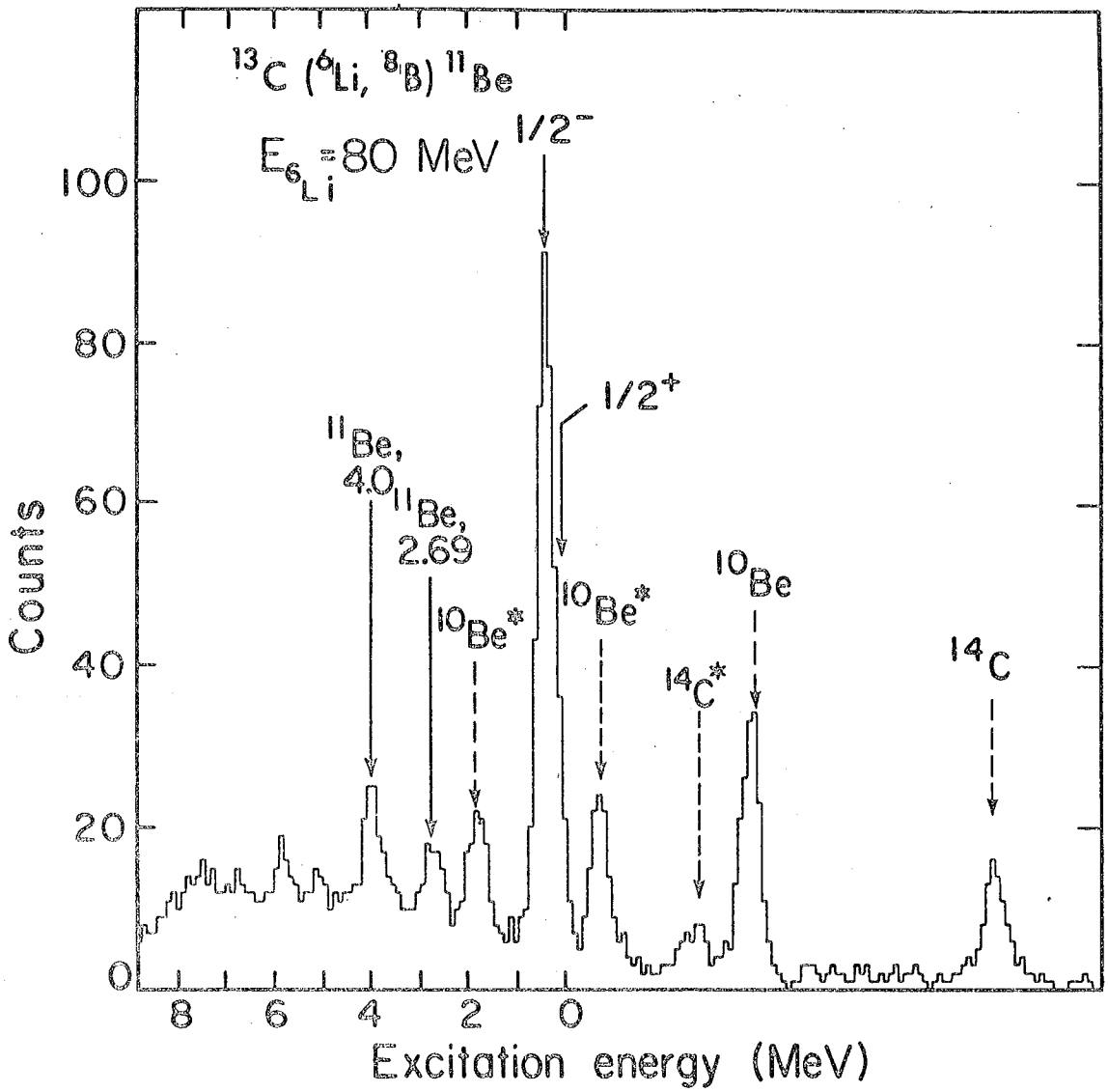

Fig. IV-6. A composite spectrum of the $^{13}C(^{6}Li,^{8}B)^{11}Be$ reaction collected between θ_{lab} = 9.4° and 20.3° for a total of 32,900 μC (with $E(^{6}Li)$ = 80 MeV), in which the data were kinematically shifted to θ_{lab} = 14.3°. Oxygen contamination gave rise to the ^{14}C states.

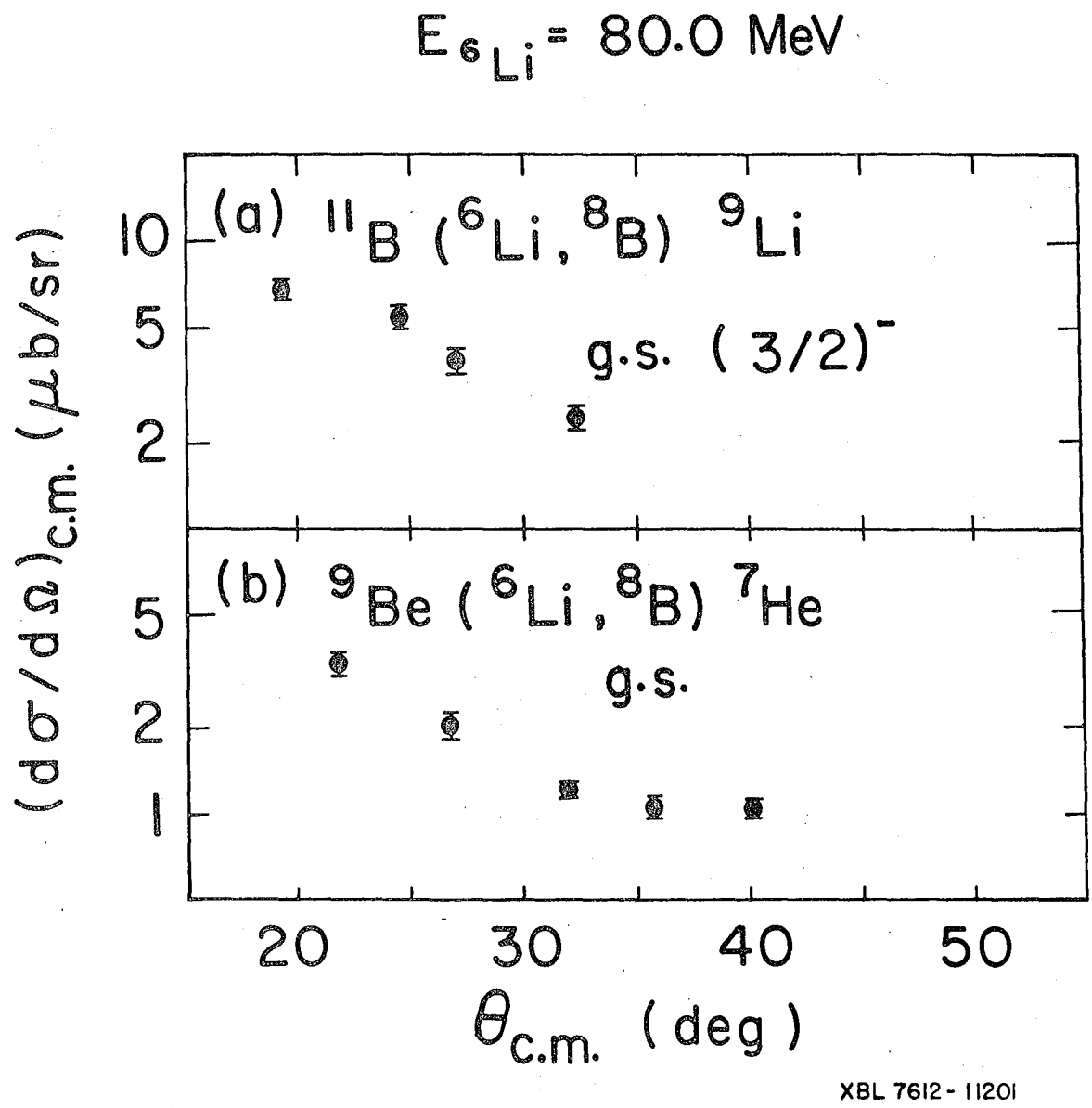

Fig. IV-7. Angular distributions for reactions induced by an 80 MeV ^6Li beam: (a) $^{11}B(^6Li,^8B)^9Li$,g.s., and (b) $^9Be(^6Li,^8B)^7He$,g.s.

Table IV-5. Summary of experimental and theoretical results for ^{11}Be.

Known Levels[a]		Levels Observed in This Work		Predicted Levels				Transition Strength[e]					Cross Sections[f] at $\theta_{c.m.} \sim 25^{\circ}$
								Cohen and Kurath					
J^{π}	MeV	MeV	± keV	J^{π}	Boyarkina[b]	Norton and Goldhammer[c]	Cohen and Kurath[d]	SPSG	DPSG	PPSG 0	PPSG 1	PPSG 2	μb/sr
$1/2^{+}$	0												
$1/2^{-}$	0.32	0.30		$1/2^{-}$	0	0	0	1.959	0	0.090	0.001	0	1.1 ± 0.1
$(1/2,3/2,5/2)^{+}$	1.79												
$(1/1,3/2,5/2)^{+}$	2.69	2.66	40	$3/2^{-}$	2.9	3.79	2.28	0	0.191	0	0.011	0.900	0.2 ± 0.1
$(1/2,3/2,5/2)^{+}$	3.41												
	3.89												
	3.96	4.00	100	$5/2^{-}$	3.9	3.68	4.66	0	1.842	0	0	1.499	0.2 ± 0.1
	5.29			$3/2^{-}$	7.6	6.46	4.93	0	1.395	0	0.002	0.699	
	(5.85)												
	6.51			$7/2^{-}$	12.6		7.99						
	6.72												
	7.03												
	8.04												

a Ref. Aj 75.
b Ref. Bo 60.
c Ref. No 71.
d Ref. Co 70.
e SPSG and DPSG are from Ref. d, PPSG 0, PPSG 1, and PPSG 2 are from this work, see text.
f The differential cross sections decrease monotonically with angle, see text.

Table IV-6. Summary of experimental and theoretical results for ^{9}Li.

Known Levels[a]		Levels Observed in this Work		Predicted Levels						Transition Strengths[f]					Cross Sections[h] $\theta_{c.m.} \sim 25^{o}$
								Norton and	Cohen and	Cohen and Kurath					
J^{π}	MeV	MeV	± keV	J^{π}	Boyarkina[b]	Barker[c]	Kussar[d]	Goldhammer[e]	Kurath[f]	SFPG	DFPG	FFPG 0	FFPG 1	FFPG 2	μb/sr
$(3/2)^{-}$	0	0		$3/2^{-}$	0	0	0	0	0	0.667	1.443	0.022	0.143	1.984	5.8 ± 0.4
$(1/2^{-})$	2.69	2.59	100	$1/2^{-}$	2.1	2.89	2.22	3.23	3.88	0	0.032	0	0.110	0.229	0.6 ± 0.1
	4.31	4.36	100	$5/2^{-}$	2.6	2.89	3.08	5.16	3.79	0	0.508	0.	0.155	0.042	0.7 ± 0.1
	5.38			$3/2^{-}$	3.6	4.31	4.65	5.97	4.88	0.143	0.062	0.063	0.042	0.042	>0.3
	6.41	6.38	120	$7/2^{-}$	5.4		5.20	6.81	6.18	0	0.001	0	0	0.094	0.8 ± 0.2

a Ref. Aj 74.
b Ref. Bo 64.
c Ref. Ba 66.
d Ref. Ru 76b.
e Ref. No 71.
f Ref. Co 70.
g SFPG and DFPG are from Ref. f. FFPG 0, FFPG 1, and FFPG 2 are from this work, see text.
h The differential cross sections decrease monotonically with angle, see text.

which must have negative parity, the (t,p) reaction can also populate states with higher configurations and positive parity. An example of such a level is the $1/2^+$ ground state of ^{11}Be. This unusual level ordering of a 2s-1d-shell state below the 1p-shell levels has been explained by Talmi and Unna (Ta 60) as a consequence of the differing interaction energies of the $2s_{1/2}$ and $1p_{1/2}$ neutrons with the $1p_{3/2}$ proton. The lack of population of the ^{11}Be ground state by the $^{13}C(^6Li,^8B)^{11}Be$ reaction is additional confirmation that the level at 0.320 MeV excitation is the lowest 1p-shell state in ^{11}Be. Finally, by the comparison of these two reactions we can suggest that the known levels at 1.79 and 3.41 MeV might have positive parity, since they are not populated in the (^{6}Li,^{8}B) reaction.

These results can be compared with the predicted level spacings and transition strengths shown in Table IV-5. We have located three 1p-shell states below 5 MeV excitation, which agrees with all three calculations (given the lowest level at 0.320 MeV excitation). All three calculations predict a level order of $1/2^-$, $3/2^-$, and $5/2^-$. While the predicted strength of the population of the $3/2^-$ state is quite small, these transition strengths are quite sensitive to small admixtures in the target around state wave function (Ku 76).

2. The $^{11}B(^6Li,^8B)^9Li$ Reaction

An energy spectrum of the $^{11}B(^6Li,^8B)^9Li$ reaction is shown in Fig. IV-8. These data were collected with an 80.0 MeV beam from a 0.21 mg/cm^2 target; this particular spectrum is a composite of data collected at $\theta_{lab} = 12.4^o$ and 16.4^o, in which the latter spectrum was kinematically shifted to $\theta_{lab} = 12.4^o$. The ^{14}C transition arose from

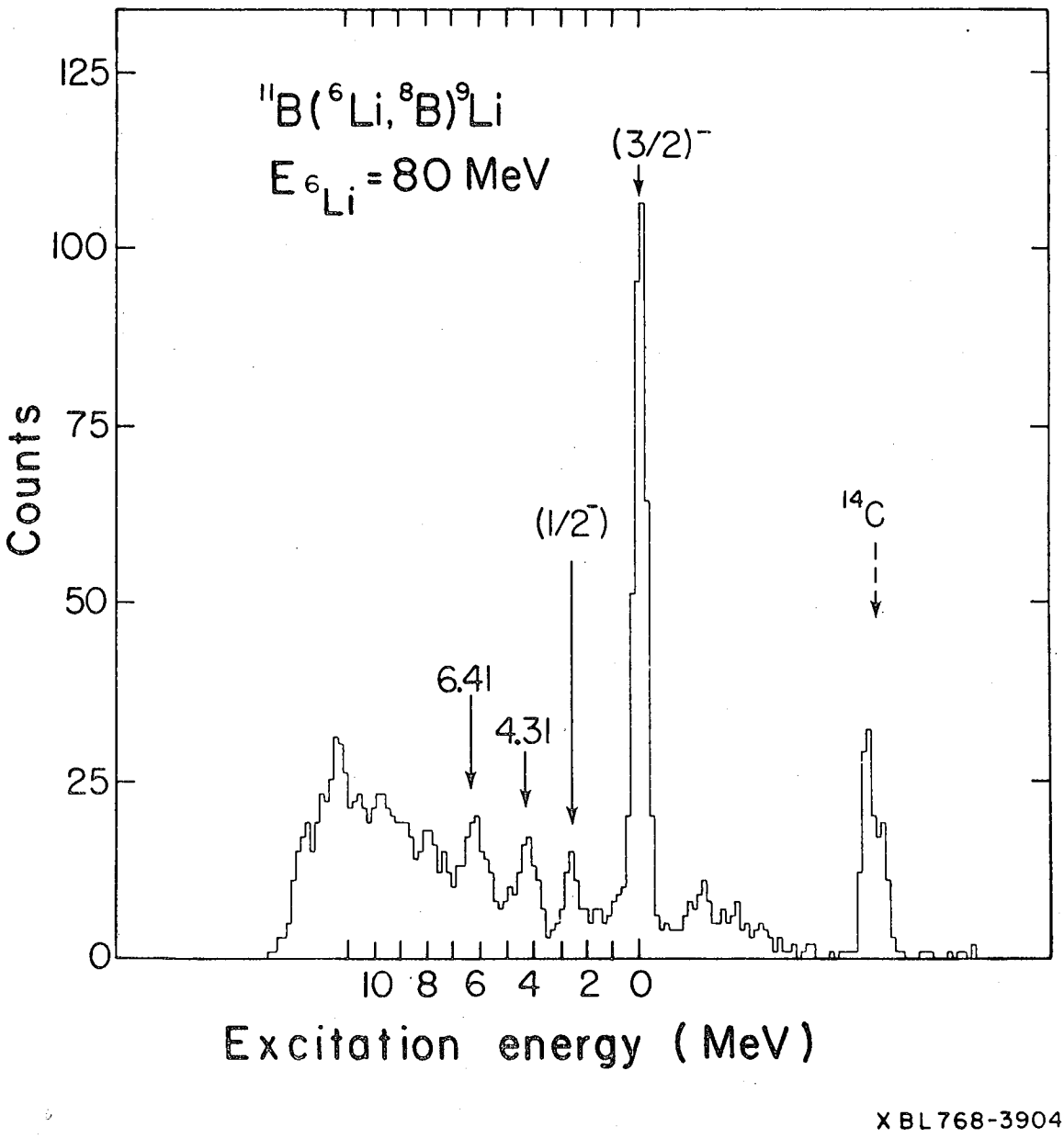

Fig. IV-8. A composite spectrum of the $^{11}B(^{6}Li,^{8}B)^{9}Li$, reaction collected at $\theta_{lab} = 12.4^{o}$ and 16.4^{o} (with $E(^{6}Li) = 80$ MeV), in which the latter data were kinematically shifted to θ_{lab} 12.4^{o}. Oxygen contamination gave rise to the ^{14}C peak.

Table IV-7. Summary of experimental and theoretical results for ^{7}Be.

Known Levels[a]		Levels Observed in this Work		Predicted Levels						Transition Strengths[g]					Cross Sections[h] $\theta_{c.m.} \sim 25^{\circ}$
							Norton and			Cohen and Kurath					
J^{π}	MeV	MeV	$\pm$ keV	J^{π}	Dayarkina[b]	Barker[c]	Kumar[d]	Goldhammer[e]	Kurath[f]	SPG	DPG	PPG 0	PPG 1	PPG 2	μb/sr
	0	0		3/2⁻	0	0	0	0	0	1.172	0.352	0.029	0	0.007	2.1 $\pm$ 0.2
				1/2⁻	2.4	1.46	3.21	4.34	2.55	0	0.012	0	0	0.001	
				5/2⁻	3.3	3.08	4.07	4.34	3.64	0	0.364	0	0.001	0.003	>0.2
				3/2⁻	4.4		5.65	7.80	3.87	0.001	0.046	0	0.002	0.002	
				3/2⁻	10.4				8.43	0.001	0.001	0	0.001	0	

a Ref. Aj 76.
b Ref. Do 64.
c Ref. Ba 66.
d Ref. Ku 76b.
e Ref. Ko 71.
f Ref. Ku 75.
g The notation is based upon Co 70 and this work, the wave functions are from Ref. f.
h The differential cross sections decrease monotonically with angle, see text.

the ^{16}O comtaminant in the target.

The dominant transition is to the $(3/2)^-$ ground state of ^9Li. Weaker transitions are observed to levels at 2.69, 4.31, and 6.41 MeV. The other known state, at 5.38 MeV excitation, is not appreciably populated. While this could indicate that this level has positive parity, a more likely explanation for its absence is that it has negative parity, but a small spectroscopic factor. These data are summarized in Table IV-6; the ground state angular distribution is shown in Fig. IV-7a.

These results can be compared with those of the $^7Li(t,p)^9Li$ reaction (Yo 71), which populated all of the known levels in ^9Li. From a comparison of the observed level spacing and widths with their predicted values by Barker, along with a comparison between the predicted and observed transition strengths in the (t,p) reaction, it was suggested (Yo 71) that the $3/2^-$, $1/2^-$, $5/2^-$, $3/2^-$, and $7/2^-$ states correspond to the observed levels at 0, 2.69, 4.31, 5.38, and 6.41 MeV, respectively. It should be noted that the population of these levels by the $(^6Li,^8B)$ reaction strongly suggests that the populated states have negative parity (although we cannot suggest any spin assignments) and that both reactions generally agree on the location of the lp-shell levels in ^9Li.

These experimental results can be compared with the theoretical predictions of the energy spectrum and transition strengths, which are also summarized in Table IV-6. While there is reasonable agreement among these predictions as to the number of low-lying lp-shell state, there are differences concerning their order. Kumar's work (Ku 74b)

is an improved version of Barker's (Ba 66); it employs the same theoretical techniques, but is based upon more recent experimental data. The level ordering of Boyarkina (Bo 64), Kumar, and Norton and Goldhammer (No 71) agree, but differ with Cohen and Kurath (Co 70) (and also Barker) as regards the order of the first two excited states. The probable $1/2^-$ assignment to the first excited state (Aj 74) agrees with the majority of these calculations. If this level is indeed a $1/2^-$ state, then its transition strength is much greater than might be expected from its very small spectroscopic factor. However, a 1% admixture in the ^{11}B ground state wave function would increase this strength to 0.15 (Ku 76). Similarly, the observed population of the possible $7/2^-$ state at 6.41 MeV rather than the possible $3/2^-$ level at 5.38 MeV (Yo 71) could arise from the sensitivity of the transition strengths to this admixture. In summary, while this reaction does not establish the spin of unknown levels, it does strongly indicate their parity; the (weak) population of the excited state is potentially extremely sensitive to any configuration-mixing in the target ground state wave function.

C. Unbound Final Systems

This section can, for the most part, be viewed as a continuation of the investigation of the light $T_z = 3/2$ nuclides (i.e., the earlier ^{11}Be, ^{9}Li, and now ^{7}He, ^{5}H, and finally 3n (see Ce 74 for the 3n portion of this study); but not ^{4}H which has $T_z = 1$). However, these unbound nuclides are discussed separately from ^{11}Be and ^{9}Li, since the interpretation of these results must consider phase-space distributions and final-state interactions (see Appendix A). Moreover, unbound levels

have broad widths, so these energy spectra are four-channel sums of the original data. Transitions can be obscured not only by the broad widths of these states, but also by the underlying breakup continuum.

1. The $^{9}Be(^{6}Li,^{8}B)^{7}He$ Reaction

An energy spectrum of the $^{9}Be(^{6}Li,^{8}B)^{7}He$ reaction is shown in Fig. IV-9. This particular spectrum was collected with an 80.0 MeV beam from a 0.13 mg/cm^2 target at $\theta_{lab} = 9.7^{o}$ for 9200 μC. The smooth curve in this figure corresponds to the phase-space distribution for the three-body breakup reaction $^{6}Li + {}^{9}Be \rightarrow {}^{8}B + {}^{6}He + n$. Four and five body breakup reactions can also contribute to the underlying continuum above their indicate thresholds. The relationships amoung these thresholds are indicated in Fig. IV-10.

The ground state of ^{7}He, which is unbound to $^{6}He + n$ by 440 keV (Aj 74), is clearly populated. This reaction was investigated not only for a range of angles (from $\theta_{lab} = 9.7^{o}$ to 18^{o}) with an 80 MeV beam, but also at two angles ($\theta_{lab} = 15^{o}$ and 18^{o}) with a 93.3 beam. These studies show no indication of any sharp excited states in ^{7}He below ~10 MeV excitation. However, weak transitions to a possible broad excited state in ^{7}He would have been obscured by the breakup continuum. The experimental results are summarized in Table IV-7; the angular distribution is shown in Fig. IV-7b. This nuclide has been investigated by the $^{7}Li(t,^{3}He)^{7}He$ (St 67) and the $^{7}Li(n,p)^{7}He$ (Li 73) reactions, which also failed to locate any sharp excited states in ^{7}He.

These negative results can be contrasted with the predictions of excited levels of ^{7}He, which are also shown in Table IV-7. However,

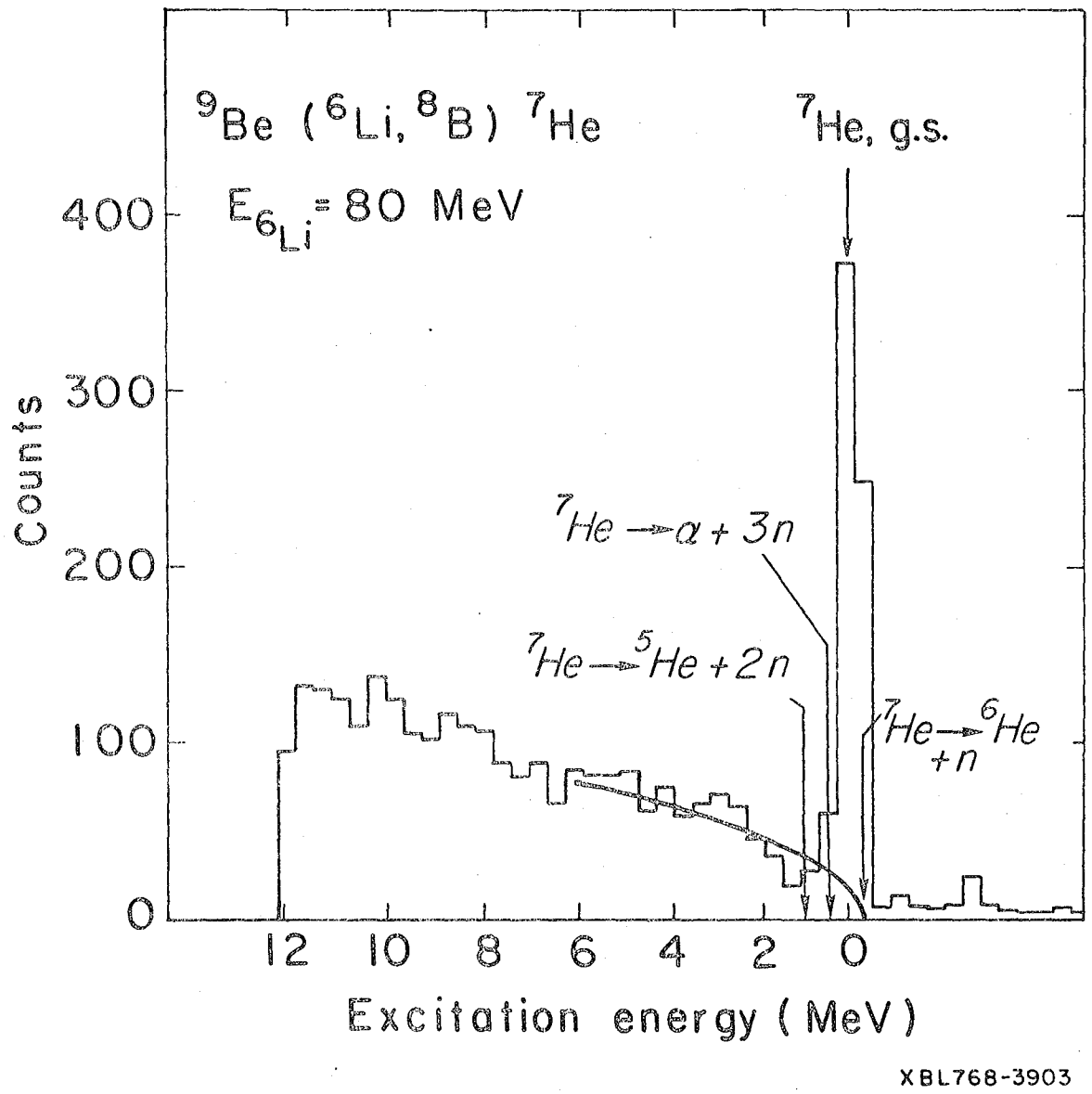

Fig. IV-9. An energy spectrum of the ^{9}Be(^{6}Li, ^{8}B) ^{7}He reaction collected at $\theta_{lab} = 9.7^{\circ}$ for 9200 μC (with E(^{6}Li) = 80 MeV). These data are four channel sums and the smooth curve corresponds to three-body phase-space for the ^{6}Li + ^{9}Be → ^{8}B + ^{6}He + n breakup reaction.

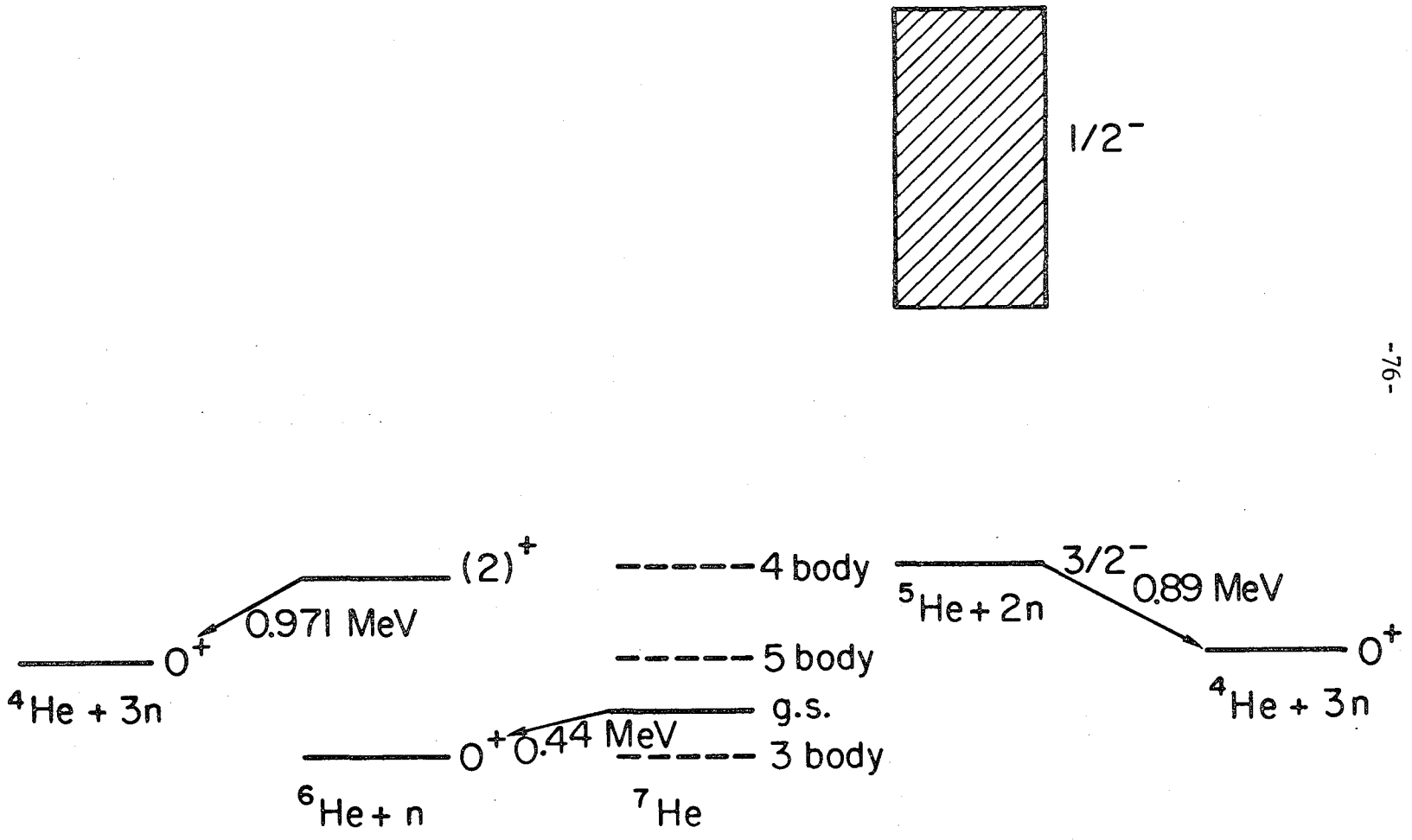

Fig. IV-10. A diagram of the decay scheme of ^{7}He indicating the relative location of the various decay channels.

if a level near 3.6 MeV excitation in ^{7}He (corresponding to the predicted $5/2^{-}$ state, which has the largest transition strength of the excited levels) has the same fraction of the ground state strength as seen in the similar ^{11}B(^{6}Li,^{8}B)^{9}Li reaction (~10%, see Table IV-6), then it would be difficult to discern if it were broader than ~1.5 MeV. Only the predicted $3/2^{-}$ ground state (see Table IV-7) should have a relatively large transition strength. The population of the ground state in this two-proton pickup reaction strongly suggests that this level has negative parity, as expected.

2. The ^{6}Li(^{6}Li,^{8}B)^{4}H Reaction

An energy spectrum of the ^{6}Li(^{6}Li,^{8}B)^{4}H reaction is shown in Fig. IV-11a. This spectrum was collected with a 93.3 MeV beam from a 0.40 mg/cm^{2} target at $\theta_{lab} = 14.7^{o}$ for 950 μC. The smooth curve in this figure corresponds to the phase-space distribution for the three-body breakup reaction $^{6}Li + {}^{6}Li \rightarrow {}^{8}B + t + n$. Four and five body breakup reactions can also contribute to the under-lying continuum above their indirected thresholds.

The observed enhancement above the three-body phase-space distribution can be attributed to the known (Fi 73) (t + n) final-state interaction, which would correspond to transitions to the 2^{-} ground state of ^{4}H along with possible contributions from transitions to probable 1^{-} and 0^{-} levels in ^{4}H, since all these states are broad. This enhancement was seen with appropriate kinemaics at all four angles studied (from $\theta_{lab} = 11^{o}$ to 17^{o}); additionally, its intensity eliminates contaminants as a cause. Assuming that all of the counts above the phase-space

Fig. IV-11. (a) An energy spectrum of the $^{6}Li(^{6}Li,^{8}B)^{4}H$ reaction collected at $\theta_{lab} = 14.7^{o}$ for 950 μC (with $E(^{6}Li) = 93.3$ MeV). These data are four channel sums and the smooth curve corresponds to three-body phase space. The excitation scale is relative to the t + n threshold. (b) An energy spectrum of the $^{7}Li(^{6}Li,^{8}B)^{5}H$ reaction collected at $\theta_{lab} = 14.7^{o}$ for 6200 μC (with $E(^{6}Li) = 93.3$ MeV). These data are four channel sums and the smooth curve corresponds to four-body phase-space. The excitation scale is relative to the t + 2n threshold and ^{10}Be and ^{14}C levels arose from target contaminants (see text).

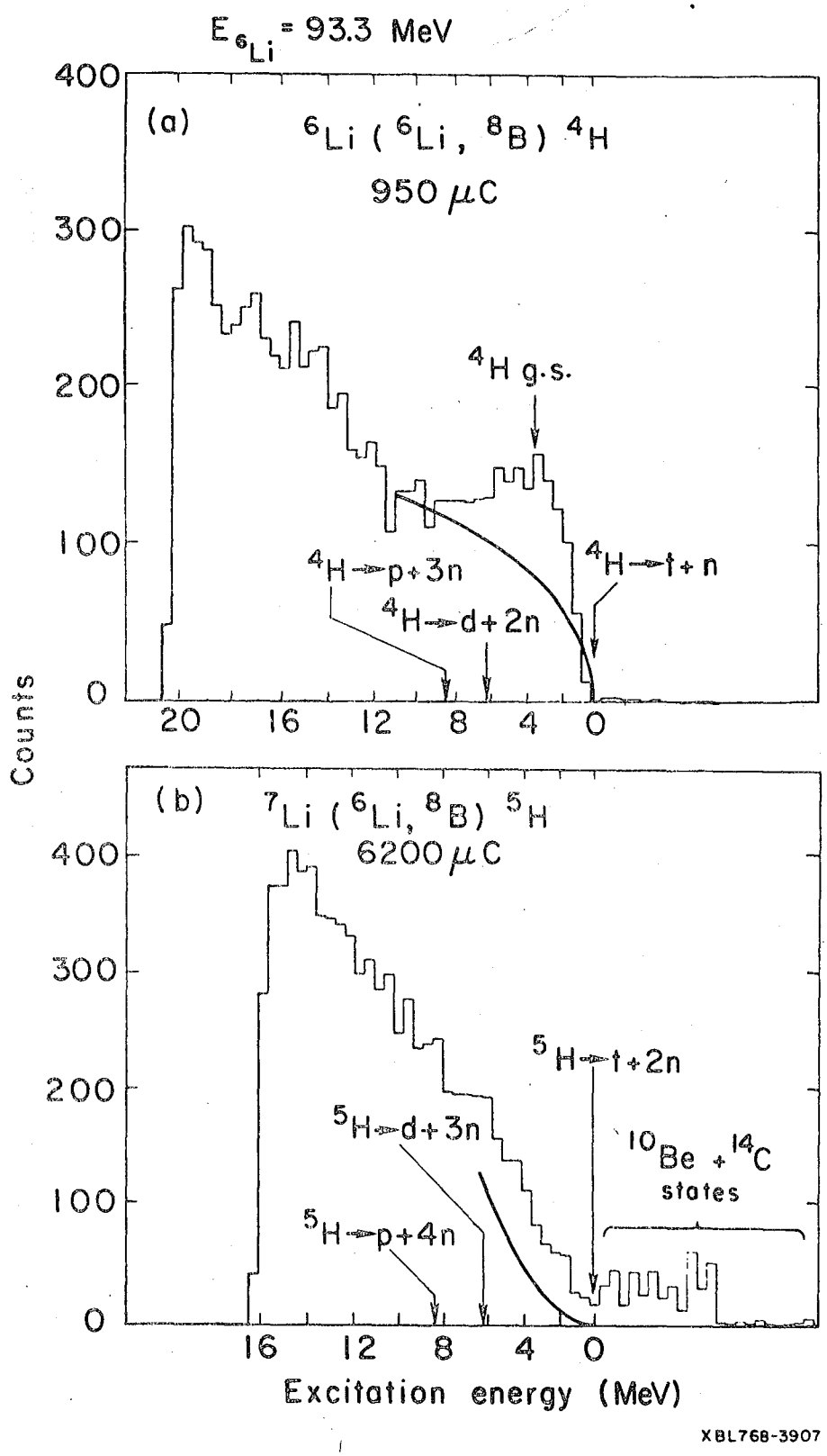
$E_{^6Li}$ = 93.3 MeV
(a)
$^6Li(^6Li, ^8B)^4H$
950 μC
^4H g.s.
$^4H \rightarrow p+3n$
$^4H \rightarrow d+2n$
$^4H \rightarrow t+n$
(b)
$^7Li(^6Li, ^8B)^5H$
6200 μC
$^5H \rightarrow t+2n$
$^5H \rightarrow d+3n$
$^5H \rightarrow p+4n$
$^{10}Be + ^{14}C$ states
Counts
Excitation energy (MeV)
XBL768-3907

Fig. IV-11.

curve correspond to this transition, then the observed yield is equivalent to 4 μb/sr (c.m.). This cross-section is roughly constant at all angles studied, although these might be a slight enhancement at more backard angles. These data can be compared to the analogous $^{6}Li(p,t)^{4}Li$ reaction (Ce 65) and both spectra show very similar structure. Although little has been established in ^{4}H, it has been studied through numerous reactions (Fi 73).

3. The $^{7}Li(^{6}Li,^{8}B)^{5}H$ Reaction

An energy spectrum of the $^{7}Li(^{6}Li,^{8}B)^{5}H$ reaction is displayed in Fig. IV-11b. This spectrum was collected with a 93.3 MeV beam from a 0.33 mg/cm^2 target at $\theta_{lab} = 14.7^{o}$ for a total of 6200 μC. The smooth curve drawn in this figure corresponds to the phase-space distribution of the four-body breakup reaction $^{6}Li + ^{7}Li \rightarrow ^{8}B + t + n + n$. The thresholds for the higher-excitation breakup channels are also indicated. Transitions to levels in ^{10}Be and ^{14}C arose from ^{12}C and ^{16}O contaminants in the target, respectively (these states provided useful calibration points). (The four-channel summing of the original data obscures these contaminant peaks, but Fig. IV-3, shown for the $^{16}O(^{6}Li,^{8}B)^{14}C$ reaction, is representative of the higher energy portion of the original spectrum.)

Counts above the phase-space curve may be attributed to either these target contaminant reactions or to other multi-body breakup channels, such as the three-body breakup $^{8}B + t + (2n)$ or $^{8}B + ^{4}H + n$. Unlike the $^{6}Li(^{6}Li,^{8}B)^{4}H$ reaction (and all the others studied in this work), no obvious evidence is seen for a strong final-state interaction in ^{5}H at any of the angles studied (from $\theta_{lab} = 11^{o}$ and 15^{o}). As a measure of the experimental sensitivity to possible ^{5}H levels, the yield at

low excitation energy above the phase-space curve corresponds to ~100 nb/sr-MeV, which may be compared with the cross-section of the final-state interaction in ^{4}H of 1 μb/sr-MeV. In summary, this investigation, as was the case in the $^{9}Be(\alpha,^{8}B)^{5}H$ data (Mc 68), the $^{3}H(t,p)^{5}H$ study (Yo 68), and pion-induced reactions on ^{7}Li targets (Mi 69), has produced no evidence for any sharp ^{5}H states below 10 MeV excitation. A negative finding was also the result of the earlier investigation of the $^{7}Li(^{7}Li,^{11}C)3n$ reaction (Ce 74), where for the lowest possible $T_z = 3/2$ nuclide--3n, there was no evidence for a narrow state below at least 10 MeV excitation.

D. The 2s-1d Shell Targets

While the remainder of this work was devoted to 1p-shell targets, these final two targets will provide an illustration of the possible extensions of this work to higher shells. The study of ^{22}Ne and ^{24}Ne is of particular interest because the neon isotopes exhibit a gradual decrease in deformation from ^{20}Ne to ^{24}Ne. This decrease in deformation with the addition of neutron pairs has also been noted in the sodium isotopes, where ^{26}Na can be successfully described by a spherical shell-model calculation (Fl 74a). Moreover, this region is valuable for allowing the comparison of various microscopic and macroscopic calculations, particularly since a spherical shell-model approach with a full 2s-1d shell basis has become feasible (Co 74a, Co 74b). While "exact" shell-model calculations can reproduce these trends in rotational character of the spectra, it would be more generally useful if this region could serve as a guide among the various Hartree-Fock calculations. To adequately explain this region in the Hartree-Fock framework it

is necessary to allow for pairing correlations (Ma 73) and possibly "shape-mixing" (or shape "co-existence") (Kh 71). Shape mixing occurs when the prolate solution (which can be associated with a small neutron energy gap and a large proton gap) has approximately the same energy as the oblate solution (corresponding to the solution with a small proton energy gap and a large neutron gap) (Kh 71). Since the reduced energy gaps enhance pairing correlations, reactions studying the two-particle configurations in these nuclei could provide an interesting test of these various theoretical models. Finally, ^{24}Ne is a $T_z = 2$ nuclide, so this study illustrates the applicability of this reaction to study such nuclei by employing $T_z = 1$ targets such as ^{14}C, ^{18}O, ^{22}Ne, ^{30}Si, etc.

1. The ^{24}Mg(^{6}Li,^{8}B)^{22}Ne Reaction

An energy spectrum of the ^{24}Mg(^{6}Li,^{8}B)^{22}Ne reaction is shown in Fig. IV-12. These data were collected with an 80.0 MeV beam from a 0.15 mg/cm^2 target; this particular spectrum is a composite of data collected between $\theta_{lab} = 10^{o}$ and 22^{o}, in which the data were kinematically shifted to $\theta_{lab} = 18^{o}$. Transitions to ^{10}Be and ^{14}C levels arose from ^{12}C and ^{16}O comtaminants in the target, respectively.

The dominant transition is to the ground state of ^{22}Ne. Also transitions were clearly resolved to the first excited state which is a 2^+ level at 1.27 MeV, the 4^+ level at 3.36 MeV, and another 2^+ state at 4.46 MeV excitation. At higher excitation the density of final states (see Table IV-8) adds ambiguity to the transition assignments, but our analysis of these data suggests that the peak near 6 MeV excitation corresponds to barely resolved transitions to the 2^+ level

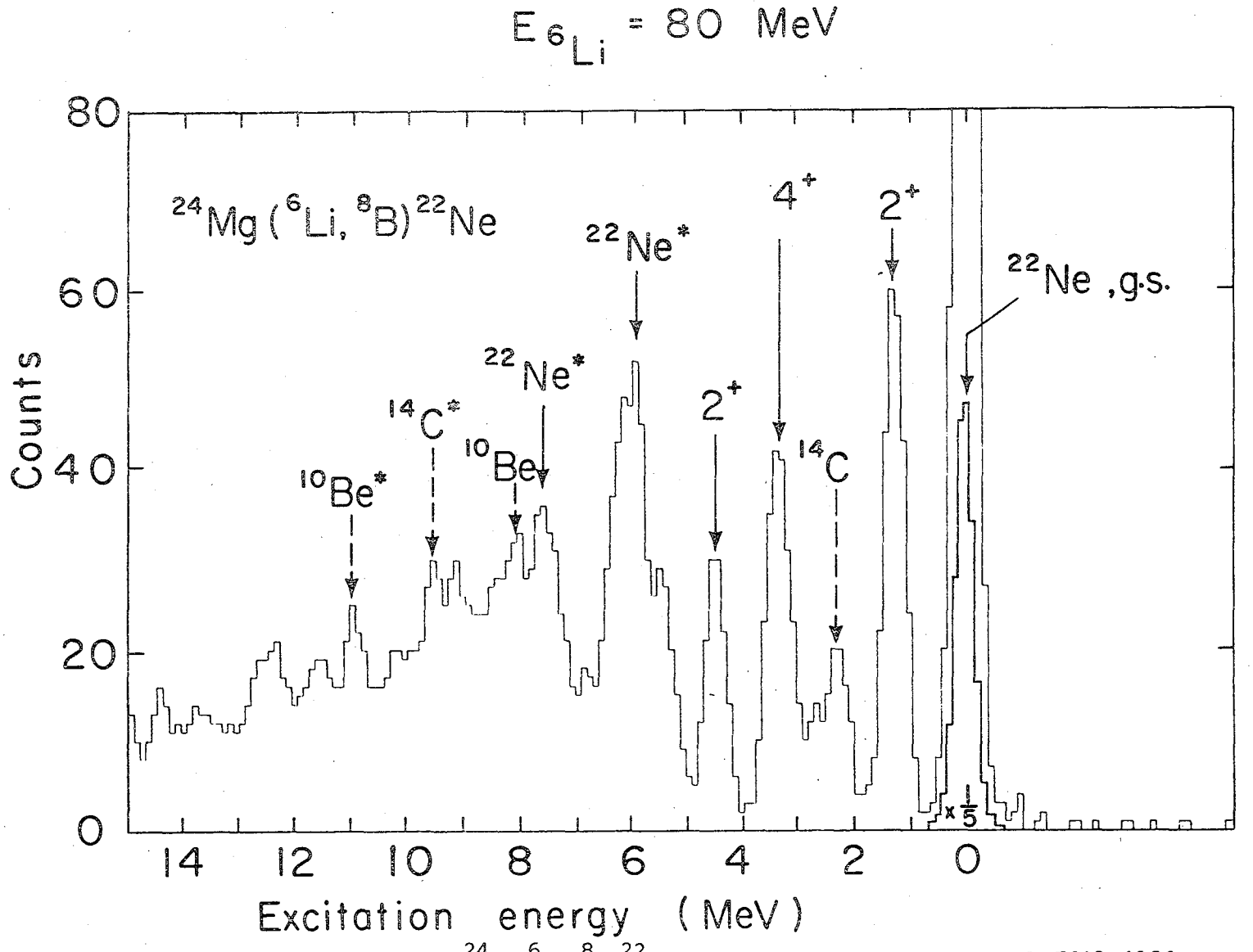

Fig. IV-12. A composite spectrum of the $^{24}Mg(^6Li, ^8B)^{22}Ne$ reaction between θ_{lab} = 10° and 22° (with E(^{6}Li) = 80 MeV), in which the data were kinematically shifted to θ_{lab} = 18°. Transitions to ^{10}Be and ^{14}C levels arose from ^{12}C and ^{16}O comtaminants in the target.

XBL7610-4286

Table IV-8. Summary of some of the experimental and theoretical results for ^{22}Ne.

Low-lying Known Levels[a]		Levels Observed in this Work		Predicted Levels					Cross Sections (c.m.)[f] $\theta_{c.m.} \sim 22^{o}$
					Freedom and Wildenthal[b]	Craig[c]	Khadkikar, Nair, and Pandya[d]	Cole, Watt, and Whitehead[e]	
J^{π}	MeV	MeV	± keV	J^{π}					μb/sr
0^+	0	0		0^+	0	0	0	0	5.5 ± 0.4
2^+	1.27	1.26	40	2^+	1.14	1.0	1.2	1.4	1.7 ± 0.2
4^+	3.36	3.36	40	4^+	3.21	2.8	3.5	3.5	1.0 ± 0.2
2^+	4.46	4.45	50	2^+	3.53	3.8	6.9	4.5	0.7 ± 0.2
2^-	5.14			3^+	4.51	4.48		5.4	
$(1,2)^+$	5.34			2^+	4.77	4.6	8.0	4.8	
2^+	5.36	5.37	70	0^+	4.95		6.4	6.0	0.7 ± 0.2
4^+	5.52			1^+	5.18	4.5		5.0	
3^+	5.64			2^+	5.43	5.1		6.0	
2^{+g}	5.91	6.0[h]	100	1^+	5.45			6.5	1.7 ± 0.2[h]
2^{+i}	6.12			4^+	5.54	4.6		5.5	
0^{+i}	6.24			6^+	6.30	5.9	7.1	6.4	
6^{+j}	6.30			0^+	6.81				
4^{+j}	6.34			3^+		6.2		6.3	
$(0-4)^+$	6.64			4^+		6.8		6.4	
(+mat)	6.69	6.69	80	2^+		6.1			0.3 ± 0.2
2^+	6.82								

Table IV-8. Continued.

Low-Lying Known Levels[a]		Levels Observed in This Work		Predicted Levels				Cross Sections (c.m.)[f] $\theta_{c.m.} \sim 22^{o}$
				Preedom and Wildenthal[b]	Craig[c]	Khadkikar, Nair, and Pandya[d]	Cole, Watt, and Whitehead[e]	
J^{π}	MeV	MeV	± keV	J^{π}				μb/sr
...[k]								
$(1-3)^{-}$	7.4							
	7.46							
1^{-i}	7.49	7.49	100					1.0 ± 0.3
	7.50							
$(4,5)^{+}$	7.54							

a Ref. En 73.
b Ref. Pr 72.
c Ref. Cr 74.
d Ref. Kh 71.
e Ref. Co 74a.
f The differential cross sections decrease monotonically with angle, see text.
g Ref. Ho 72 suggests that the 5.91 MeV level could be a 1^{-} or 3^{-} state rather than a 2^{+} level.
h This peak most likely corresponds to more than one transition.
i Based upon Ref. Fi 74b and Ho 72.
j Based upon Ref. Fi 74.
k Some known levels were omitted because of the high density of states, see Ref. a.

at 5.91 MeV and a 0^+ state at 6.24 MeV. However, while the width and centroid of this peak indicate that it corresponds to more than one transition, we cannot definitely determine its composition. Weaker transitions might correspond to the 2^+ level at 5.36 MeV, a natural parity state at 6.69 MeV, and a 3^- level at 7.49 MeV. (These assignments are consistent with the higher-lying states populated by the (α,α') reaction (Ol 70), which is to be expected, since these inelastic scattering experiments measure the deformation parameter, and this deformation arises from the quadrupole interaction, which is in turn, based upon the two-nucleon spatial correlations (and these pairing interactions are reflected in the two-nucleon transfer transition strengths) (Br 70).) These experimental results are summarized in Table IV-8; the ground state angular distribution is shown in Fig. IV-13a.

These data can be compared with those from the analogous $^{24}Mg(p,t)^{22}Mg$ reaction (Pa 74), shown in Fig. IV-14. Unfortunately, while these (p,t) data have better energy resolution than does the $(^6Li,^8B)$ reaction, the level structure of ^{22}Mg is poorly known compared to ^{22}Ne, so that this comparison suggests the spins and parities of several levels in ^{22}Mg rather than clarifying the $(^6Li,^8B)$ data by identifying the isolated analog transitions. From this analogy one can suggest that the 3.31 MeV state in ^{22}Mg (a $4^{(+)}$ (De 72)) corresponds to the analog of the 4^+ level at 3.36 MeV in ^{22}Ne, and that the state at 4.40 MeV in ^{22}Mg (a $2^{(+)}$ level) is the analog of the 2^+ state in ^{22}Ne at 4.46 MeV. As might be expected from the by-shell comparisons, this work indicates that there is a strong similarity between the selectivity of these two reactions even on the relatively more complex 2s-1d-shell targets.

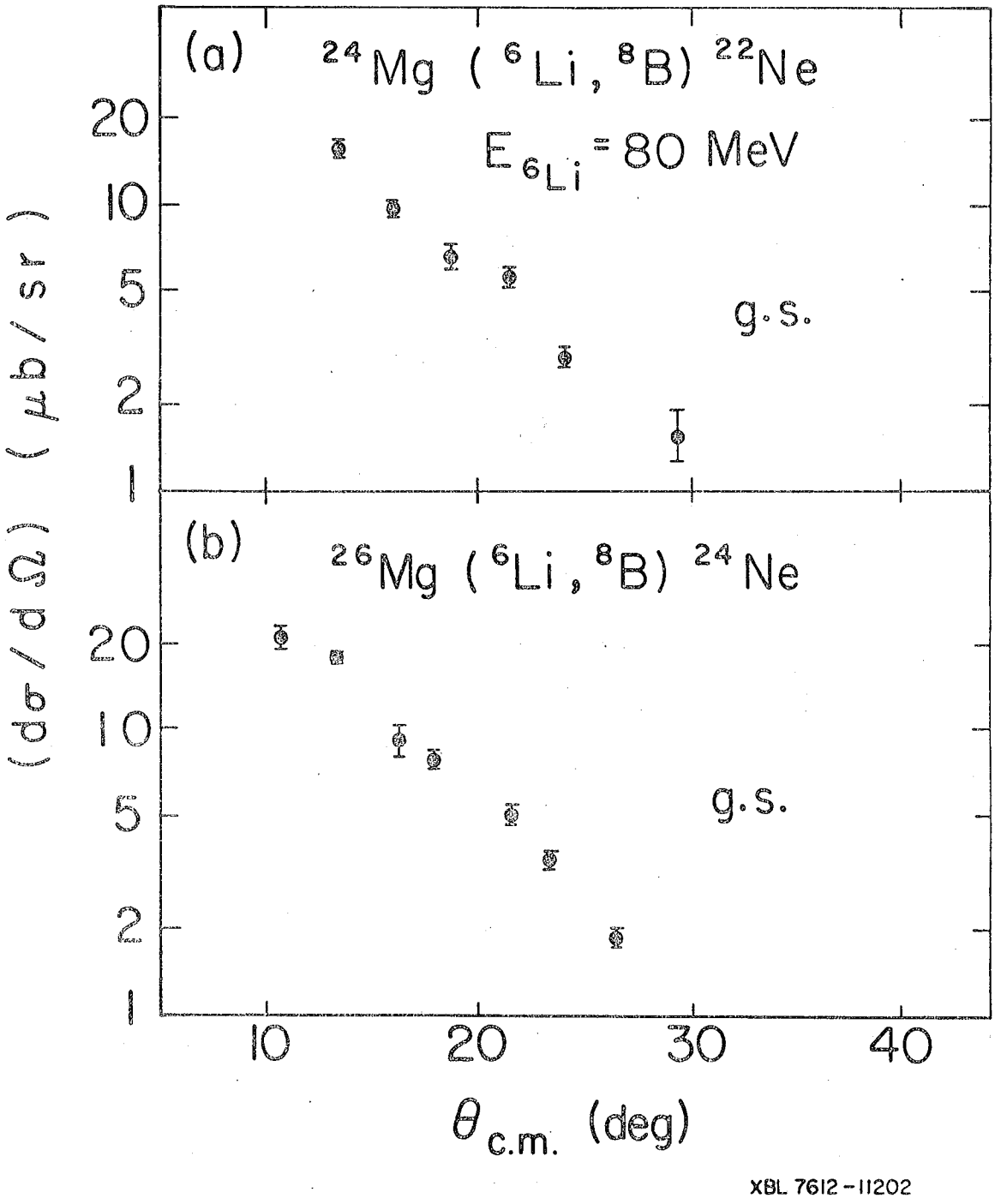

Fig. IV-13. Angular distributions for reactions induced by an 80 MeV ^{6}Li beam: (a) ^{24}Mg(^{6}Li,^{8}B)^{22}Ne, g.s., and (b) ^{26}Mg(^{6}Li,^{8}B)^{24}Ne, g.s.

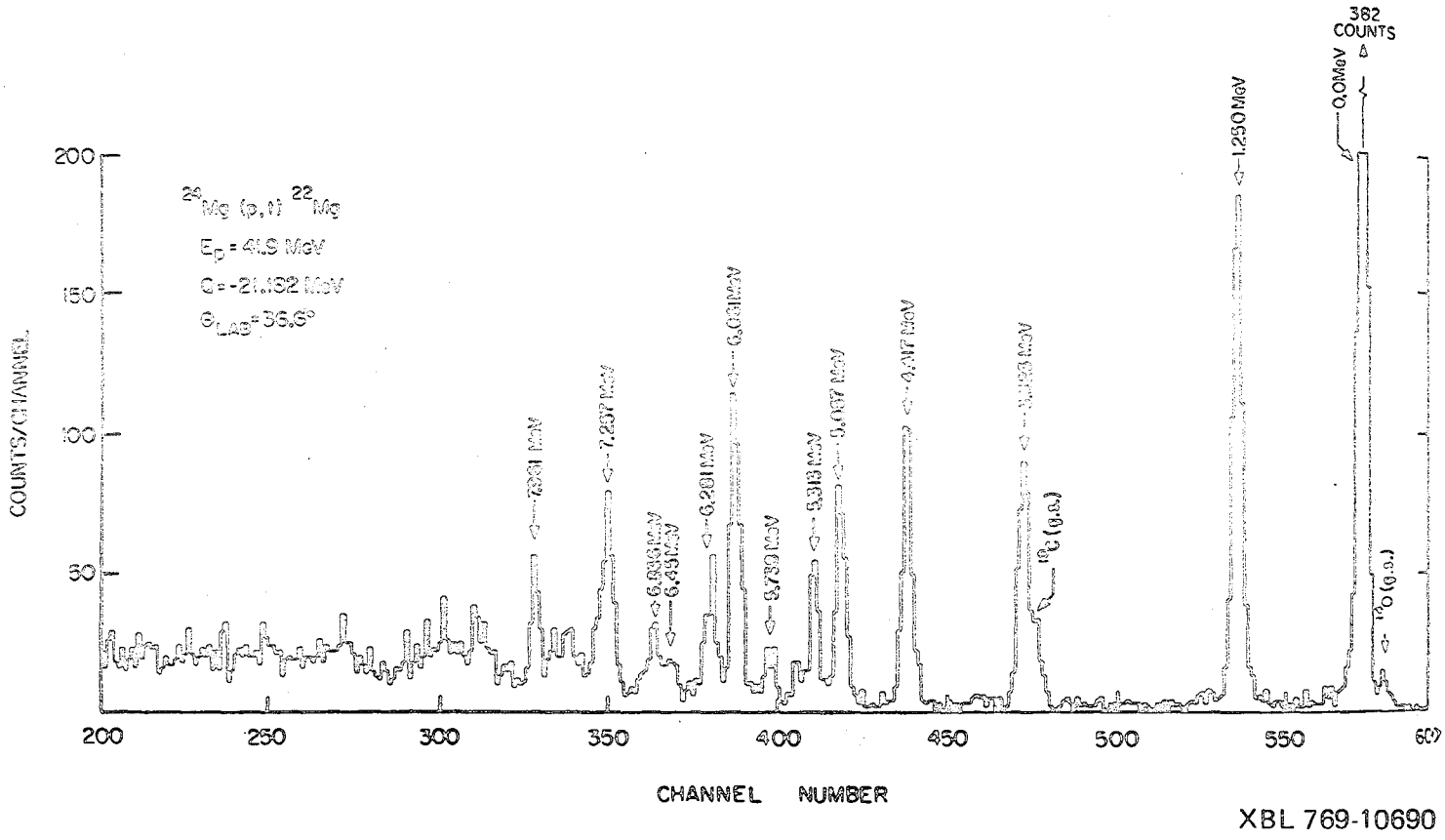

Fig. IV-14. The $^{24}Mg(p,t)^{22}Mg$ reaction induced by 41.9 MeV protons at $\theta_{lab} = 36.6^{o}$ (Pa 72). The ^{10}C and ^{14}O transitions arose from ^{12}C and ^{16}O comtaminants in the target, respectively.

Comparing the known and observed levels in Table IV-8, it is clear that this reaction is quite selective. While the resolution of this study precludes placing stringent limits on their population, no evidence is seen for the population of the multi-particle-hole levels at 5.14 MeV (a 2^- state) and 5.64 MeV (a 3^+ level), or for the 6^+ state at 6.30 MeV all of which would be forbidden in a direct single-step pickup. This selectivity will provide some bounds on the possible spin and parity of the two previously unreported levels in ^{24}Ne.

The variety of the theoretical approaches to this region can be seen in Table IV-8. Preedom and Wildenthal (Pr 72) employ an approximate shell-model approach, while Cole et al. (Co 74a) use a spherical shell-model with a full 2s-1d shell basis. Craig (Cr 74) uses a Nilsson model. Khadkikar et al. (Kh 71) employ a Hartree-Fock framework with shape-mixing. This list is by no means exhaustive of the theoretical approaches to ^{22}Ne. The state at 5.92 MeV is generally considered to be an intruder level (Cr 74, Pr 72) and the 2^+ state at 6.12 MeV is considered to be a 2s-1s shell state, which might disagree with our results. However, there is a large uncertainty in the results at this excitation because of the difficulties in unfolding the overlapping transitions. Alternatively, it has been suggested that the state at 5.92 MeV is either a 1^- or a 3^- level (Ho 73). It would be difficult to believe that there is such a large component of a cross-shell level in the ^{24}Mg ground state. If the level at 5.92 MeV excitation were a 3^- octupole vibration, then its strong population by this reaction is possible (as is the case in the ^{54}Fe(^{6}Li,^{8}B)^{52}Cr reaction (We 75)).

This possibility is supported by the inelastic scattering data (Ol 70).

2. The $^{26}Mg(^{6}Li,^{8}B)^{24}Ne$ Reaction

An energy spectrum of the $^{26}Mg(^{6}Li,^{8}B)^{24}Ne$ reaction is shown in Fig. IV-15. These data were collected with an 80.0 MeV beam from a 0.45 mg/cm^2 target; this particular spectrum is a composite of data collected between $\theta_{lab} = 8^{o}$ and 21^{o}, in which the data were kinematically shifted to $\theta_{lab} = 17^{o}$. Levels of ^{10}Be and ^{14}C arose from the ^{12}C and ^{16}O contaminants in the target, respectively.

The dominant transition is to the 0^+ ground state. Along with a weaker transition to the first excited level, which is a 2^+ state at 1.98 MeV excitation, a peak is observed to 3.88 MeV, which probably corresponds to both members of the 2^+, 4^+, doublet near this energy (while the measured excitation energy agrees well with the 2^+ level, this peak is noticably broader than the other transitions in a high resolution preliminary observation of this reaction (We 75)). Transitions to two unreported states (En 73) at 7.47 and 8.86 MeV are also observed. Finally, some evidence is seen for the weak population of the known level at 5.58 MeV, but the contaminant peaks in this region precluded a definite confirmation of its kinematic shift. These experimental results are summarized in Table IV-9. The angular distributions of some of these levels are shown in Fig. IV-16, from which (as before) it is apparent that these distributions do not offer a means of discriminating among the possible spin changes of the various transitions. It is of some interest that the ground state transitions to ^{22}Ne and ^{24}Ne have almost identical cross-sections (and angular distributions),

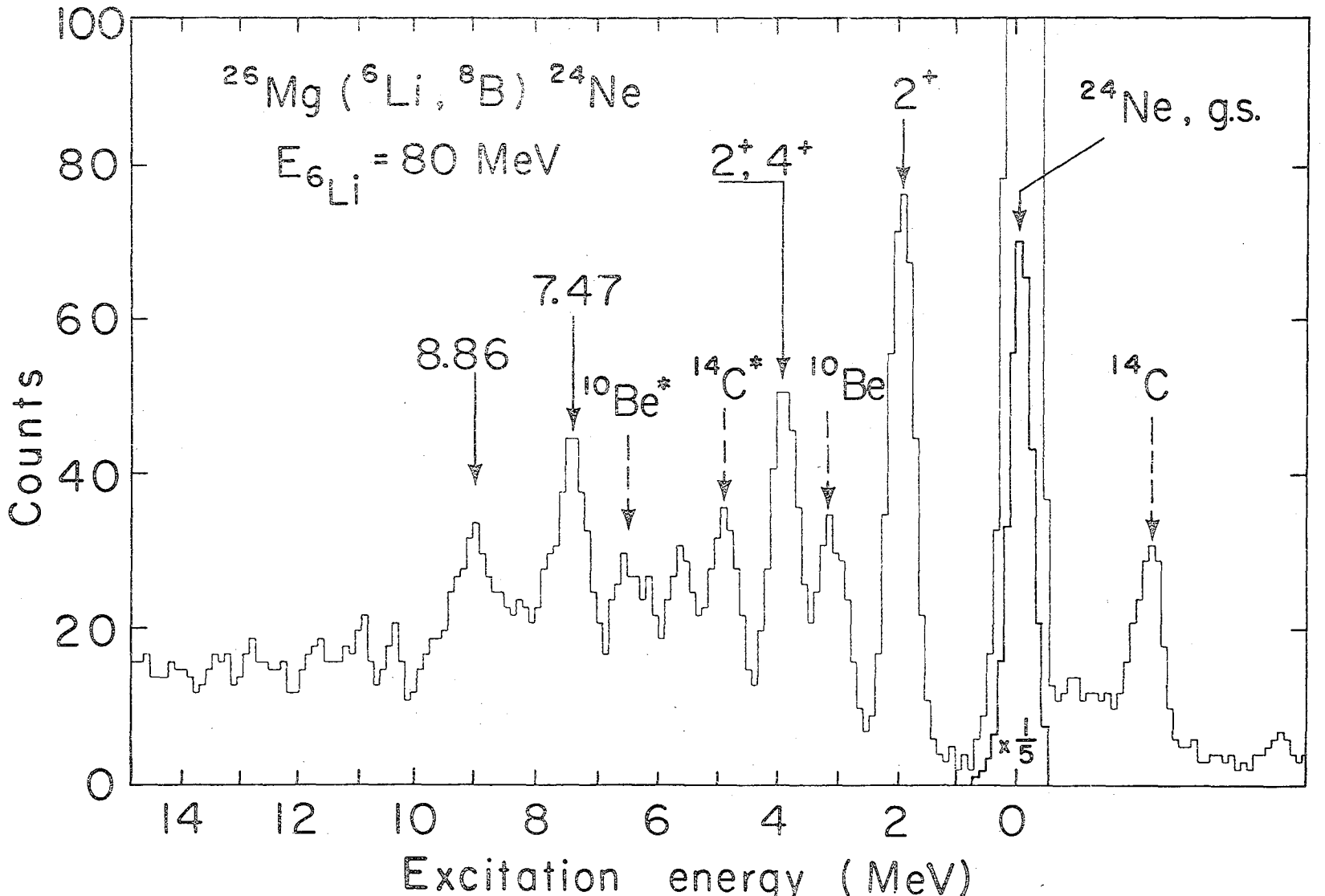

Fig. IV-15. A composite spectrum of the ^{26}Mg(^{6}Li, ^{8}B)^{24}Ne reaction between θ_{lab} = 8° and 21° (with E(^{6}Li) = 80 MeV), in which the data were kinematically shifted to θ_{lab} = 17°. Transitions to ^{10}Be and ^{14}C levels arose from ^{12}C and ^{16}O comtaminants in the target.

XBL 762-2257A

Table IV-9. Summary of experimental and some of the theoretical results for ^{24}Ne.

Known Levels[a]		Levels Observed in This Work		Predicted Levels					Structure Amplification	Cross Sections (c.m.)[g] $\theta_{c.m.} \sim 22^{\circ}$
				Macdonald, Morrison, and Watt[b]	Khadkikar, Nair, and Pandya[c]	Cole, Watt, and Whitehead[d]	Robertson and Wildenthal[e]			
J^{π}	MeV	MeV	± keV	J^{π}					Factor[f]	μb/sr
0^+	0	0		0^+	0	0	0	0	0.36	1.9 ± 0.2
2^+	1.98	1.97	35	2^+	1.5	1.4	1.8	2.24	0.015	0.4 ± 0.2
2^+	3.87	3.88	50	2^+	2.8	6.0	4.8	4.27	0.09	0.3 ± 0.1
4^+	3.93			4^+	3.8	3.9	4.7	4.94	0	
0^+	4.76			4^+	4.1	3.8	3.8	4.41	0.03	
	4.99			4^+	6.1	7.5		5.06	0.03	
2	5.50	(5.5)	100	0^+		5.6		5.36	0.01	(0.03 ± 0.04)
	(5.64)			0^+		7.2		5.83	0	
	6.03			2^+				5.83	0	
		7.07	50	2^+				6.07	0.003	0.29 ± 0.10
		8.35	70	4^+				6.33	0.04	0.10 ± 0.05
				2^+				7.77	0	
				2^+				7.93	0.025	
				4^+				8.02	0.004	
				4^+				8.20	0	
				4^+				8.84	0.006	

a Ref. En 73.
b Ref. Ma 73.
c Ref. Kh 71.
d Ref. Co 74b.
e Ref. Ro 73.
f From Ref. f.
g The differential cross sections decrease monotonically with angle, see text.

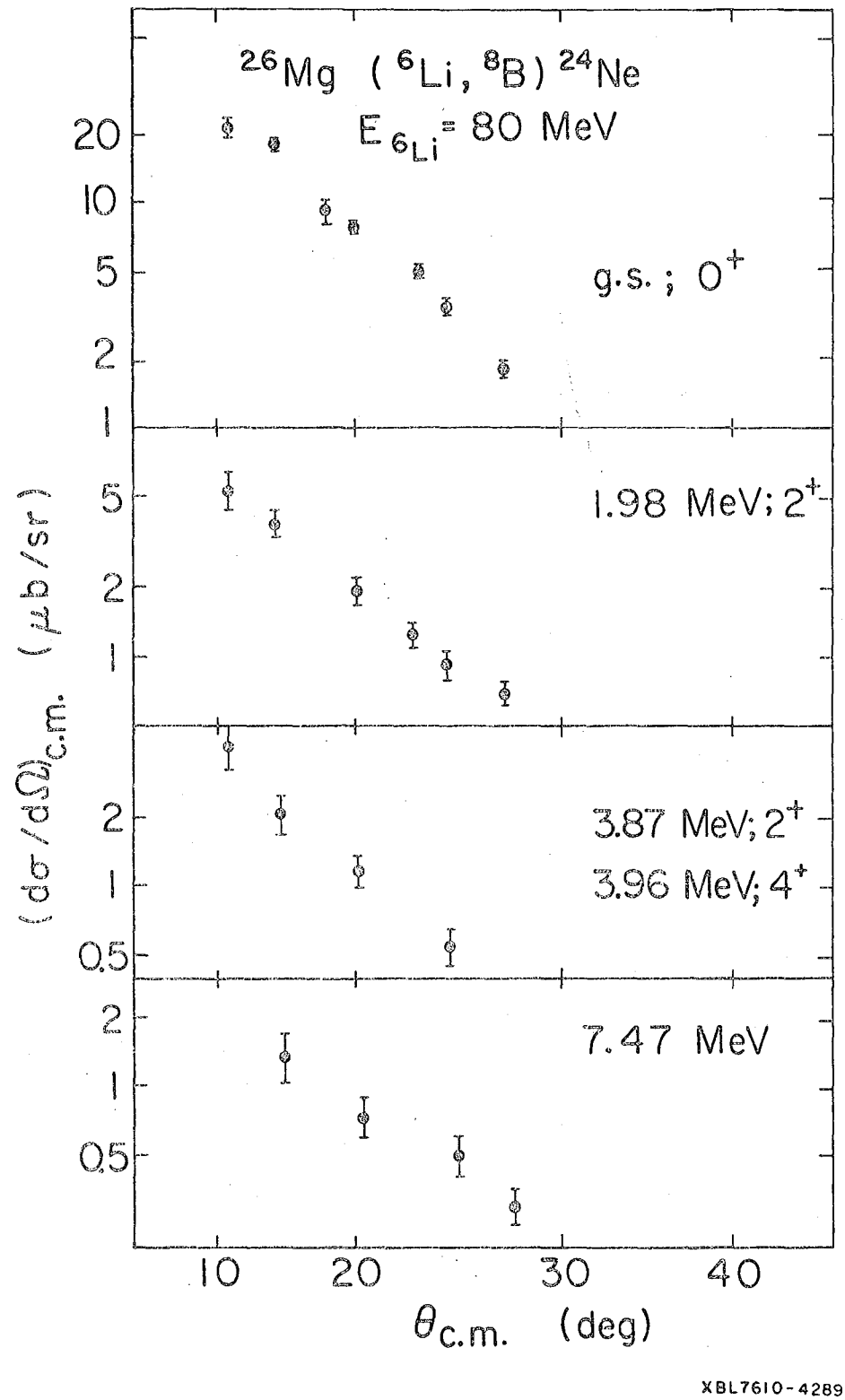

Fig. IV-16. Angular distributions for transitions induced by an 80 MeV ^{6}Li beam in the $^{26}Mg(^{6}Li,^{8}B)^{24}Ne$ reaction: (a) g.s., 0^+; (b) 1.98 MeV, 2^+; (c) unresolved transitions to the 3.87 MeV, 2^+, state and 3.96 MeV, 4^+, level, and (d) 7.47 MeV.

although the Q values differ by ~5 MeV. A simple DWUCK calculation reproduces this trend. These experimental results can be compared with those of the $^{22}Ne(t,p)^{24}Ne$ reaction (Ho 70), which identified all the known levels, but could not have observed the two higher-lying states.

Some of the theoretical predictions for ^{24}Ne are also summarized in Table IV-9. Cole et al. (Co 74b) employ a spherical shell-model calculation with a complete 2s-1d-shell basis, while Robertson and Wildenthal (Ro 73) use a spherical shell-model calculation with a truncated basis. Khidkikar et al. (Kh 71) employ a Hartree-Fock calculation with shape-mixing, while Macdonald et al. (Ma 73) use a Hartree-Fock-Bogoliubov calculation (which includes pairing effects) with number projection. The two levels found in this work might provide an interesting test for these various models, if their spins and parities could be determined. However, we can only limit them to having spins ≤ 4 and natural parity (which is the only allowed possibility for the transfer of two identical 2s-1d-shell nucleons).

The structure amplification factors of Robertson and Wildenthal (Ro 73) are compared with the observed transition strengths in Fig. IV-17. Several higher-lying levels are predicted that might be observed in this reaction. (Again one should note that slight admixtures in the ground state wave function might have a dramatic effect on these predicted "transition strengths" for weak transitions.) It should be noted that the Preedom-Wildenthal interaction (which was employed in this calculation) predicts too high an excitation for low-lying levels and too low an excitation for high-lying ones in ^{22}Ne,

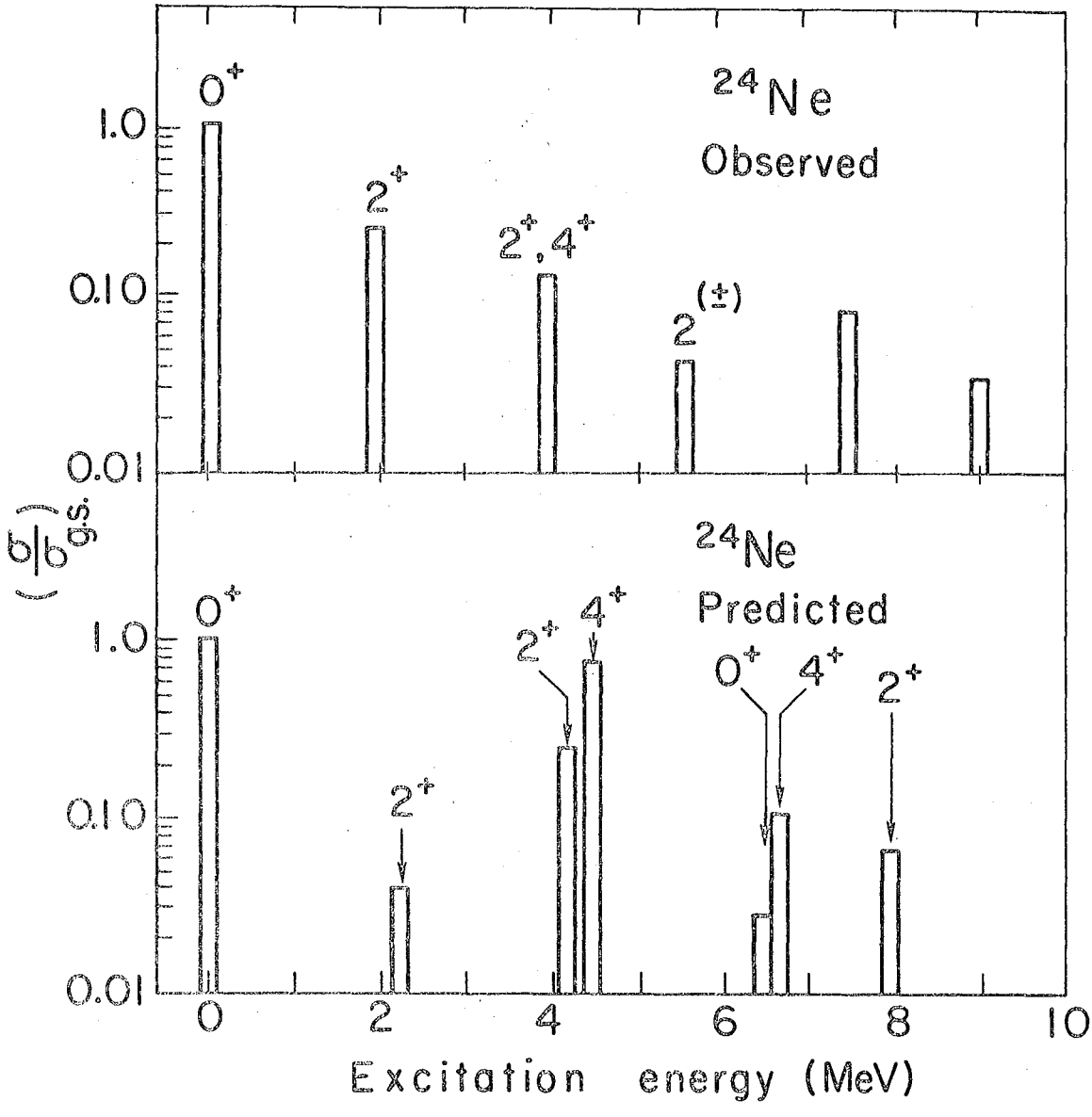

XBL 762-2256

Fig. IV-17. A comparison between the observed relative yields of the ^{26}Mg(^{6}Li,^{8}B)^{24}Ne reaction (with E(^{6}Li) = 80 MeV) and the predicted relative structural amplification factors (Ro 73).

and if this were the case in ^{24}Ne, then the agreement with our results would be reasonable.

E. Comparisons With Other Reactions

In principle, there could be rather dramatic differences in the population of levels in the final nuclei between the (^{6}Li,^{8}B) and (p,t) reactions since the differing wave functions of the outgoing particles could select different cluster configurations from the target ground state wave functions. However, the observed similarities between the spectroscopic selectivities of these two reactions for the $T_z = 0$ ^{12}C, ^{16}O, ^{10}B, ^{6}Li, and ^{24}Mg targets demonstrate a related simple pickup reaction mechanism and suggest that any differences in the relative yields simply arise from the two reactions sampling the ^{1}S cluster probability density at different interaction radii (and over different ranges of radii).

Agreement in the comparisons between the (^{6}Li,^{8}B) and (t,p) reactions producing the same final nuclei (e.g., ^{11}Be, ^{9}Li, and ^{24}Ne) leads to the anticipated complementary nature of their spectroscopic selectivities in studies of neutron-excess nuclei. Any differences in the population of levels in final nuclei between these two reactions indicate possible configuration differences (e.g., predominant particle or hole states).

Investigations of two-proton pickup reactions are still rather sparse, so that only limited comparisons are now feasible. As the lightest experimentally feasible two-proton pickup reaction, (^{6}Li,^{8}B) is best suited to studies of 1p-shell targets and these targets provide a convenient means of determining the reaction mechanism. We have also obtained data from two heavier targets—^{24}Mg and ^{26}Mg—to

facilitate cross-comparisons with this particular reaction.

The usefulness of these various reactions is measured by the combination of experimental difficulty, the presence of bound excited states, spectroscopic selectivity, and relative yield. As mentioned, particle identification based upon counter telescopes is particularly suitable for the (^{6}Li,^{8}B) reaction since both ^{7}B and ^{9}B are particle unstable. A requirement that the outgoing particle not have any bound excited states would eliminate several possible reactions, as can be seen from Table IV-10 which also lists the spectroscopic amplitudes (Co 70) and two-proton separation energies. While the (^{18}O,^{20}Ne) has a relatively high yield, its spectra are complicated by the large transition strength of the bound 2^{+} and 4^{+} "shadow peaks" (Si 72, Ch 73, Ke 76). Experimental results are available for the ^{26}Mg(^{11}B,^{13}N)^{24}Ne reaction (Sc 74a). Comparing data from the (^{6}Li,^{8}B) and (^{11}B,^{13}N) reactions on the ^{26}Mg target:

- both reactions have similar spectroscopic selectivity,
- the (^{11}B,^{13}N) reaction has a (c.m.) yield about three times higher than the (^{6}Li,^{8}B) reaction (however, the (^{11}B,^{13}N) reaction data were collected at the grazing angle).

The higher relative yield of the (^{11}B,^{13}N) reaction might be expected from the larger spectroscopic amplitude, more positive Q-value, and greater proton pair binding energy in the outgoing particle for the (^{11}B,^{13}N) reaction (see Table IV-10). Similarly, either the (^{10}B,^{12}N) or the (^{12}C,^{14}O) reactions might have a higher yield than the (^{6}Li,^{8}B) reaction, while still lacking any shadow peak ambiguity.

Table IV-10. Comparison among some of the possible two-proton pickup reactions.

Reaction	J_i	J_f	Bound Excited States	Two-Proton Separation Energy* (MeV)	Strengths** SMAG	DMAG
$(^{6}Li,^{8}B)$	1^+	2^+	No	- 5.744	0	0.032
$(^{9}Be,^{11}C)$	$3/2^-$	$3/2^-$	Yes	-15.277	0	0.747
$(^{10}B,^{12}N)$	3^+	1^+	No	- 9.287	0	1.354
$(^{11}B,^{13}N)$	$3/2^-$	$1/2^-$	No	-17.901	0	2.061
$(^{12}C,^{14}O)$	0^+	0^+	No	- 6.570	0.597	0
$(^{13}C,^{15}O)$	$1/2^-$	$1/2^-$	Yes	-14.843	1.002	0
$(^{14}C,^{16}O)$	0^+	0^+	Yes	-22.335		
$(^{18}O,^{10}Ne)$	0^+	0^+	Yes	-20.838		

*Calculated as $\Delta_f - \Delta_i - \Delta_{2p}$.

**The notation and values are from Co 70, except for $(^{6}Li,^{8}B)$ which is from Ku 75.

F. Comparisons With Semi-Classical Reaction Theory

We have already seen that the (^{6}Li,^{8}B) reaction strongly populates only those levels with a significant predicted two-nucleon spectroscopic amplitude and that these transition strengths reasonably reflect gross differences in the predicted relative yields. However, several transition strengths appear to be significantly different from their predicted relative yield. In particular, some configurations with rather large predicted transition strengths seem to be fragmented among several states. (Of course, this splitting would be most obvious if the configuration possessed a particularly large transition strength.) Several configurations that had rather small predicted transition strengths were noticably populated, probably indicating the effect of configuration mixing in the target ground state wave function.

As previously mentioned, the transition matrix element can be described as depending upon both the spectroscopic amplitude and a transfer amplitude factor. We have attempted to describe this kinematic dependence by a semi-classical reaction theory (Br 72, An 74) with the computer code HIFROB (Hu 75). This approach involves in part the description of the target and outgoing particle (for pickup reactions) as core plus cluster systems with the spins of the core and the cluster coupling with their relative internal angular momentum (L) to form the total angular momentum (J). In Table IV-11, we list the observed relative transition strengths along with the predicted transition strength, the relative kinematic hindrance, and the total predicted relative transition strengths for some spin zero targets. These results are less than impressive, which seems to indicate that this approach has

Table IV-11. Comparisons between the observed and predicted relative transition strengths.

Nuclide	Final MeV	Level J^π	Observed $\frac{d\sigma/d\Omega}{(d\sigma/d\Omega)_{g.s.}}$	SMAG[a]	DMAG[a]	Relative Kinematic Hindrance	Predicted $\frac{d\sigma/d\Omega}{(d\sigma/d\Omega)_{g.s.}}$
^{10}Be	0	0^+	1.	2.75	0	1.	1.
	3.36	2^+	0.60	0	1.22	0.48	0.21
	5.96	2^+	0.26 } 0.36[b]	0	4.54	0.35	0.58
	7.54	2^+	0.10 }			0.28	
	9.4	(2^+)	0.15	0	0.004	0.22	3.2×10^{-4}
	11.8	(0^+)	0.11	0.004	0	0.18	2.6×10^{-4}
^{14}C	0	0^+	1.0	2.21	0	1.	1.
	7.01	2^+	0.35 }			0.34	
	8.32	2^+	0.16 } 0.61[b]		12.71	0.29	1.73
	10.4	2^+	0.10 }			0.23	
^{22}Ne	0	0^+	1.0		c	1.	1.
	1.27	2^+	1.			0.68	
	3.36	4^+	0.18			0.34	
	4.46	2^+	0.12			0.27	
	5.36	2^+	0.13			0.25	
	6.0		0.3				
					Structure Amplification[d] Factor		
^{24}Ne	0	0^+	1.		0.36	1.	1.
	1.98	2^+	0.22		0.015	0.42	0.018
		2^+			0.09	0.27	0.068 } 0.086
	3.9	4^+	0.17		0.03	0.21	0.018 }
	5.6	(2^+)	0.04		0.003	0.19	0.016
		0^+			0.01	0.32	0.009
	7.5	4^+	0.13		0.04	0.12	0.013
	8.9	2^+	0.05		0.025	0.13	0.009

a From Ref. Co 70. b Predicted strength is fragmented. c Not available.
d From Ref. Ro 74.

limited utility for this reaction, and accordingly we have not attempted any more complicated spin situations.

It is possible that this semi-classical approach is inappropriate for this particular situation because of low values of η. Further it is likely that this poor agreement reflects the inappropriateness of functional forms of Q-value dependence in this particular approach. This possibility is supported by the Oxford approach of empirically varying the input parameters to shift the relative probability curves vs excitation energy to achieve satisfactory agreement (Me 76). No variation of the input parameters was attempted in this work. This possible deficiency can be generalized to the inadequacy of the assumed Gaussian functional form of the kinematic matching criteria.

V. CONCLUSIONS AND SUMMARY

Results from the first broad survey of a two-proton pickup reaction have been presented in Section IV. This study was undertaken to determine the utility of the (^{6}Li,^{8}B) reaction as a spectroscopic probe of neutron-excess nuclei. A systematic feature of these data is that the (^{6}Li,^{8}B) reaction populates strongly only states for which a significant two-nucleon cfp is predicted. The spectroscopic selectivity of the (^{6}Li,^{8}B) reaction on T_z = 0 targets resembles that of the analogous (p,t) reaction. The observed selectivity in the population of states in the final nuclei demonstrates that the (^{6}Li,^{8}B) reaction proceeds primarily through a direct, single-step pickup of two protons. Moreover, these data indicate that the predominant configuration of the two-proton cluster is a relative ^{1}S state. No evidence was seen for the transfer of the proton pair coupled to a spatially anti-symmetric configuration.

By establishing an understanding of the observed spectroscopic selectivity with T_z = 0 targets, it has been possible to employ this reaction on T_z > 0 targets to locate low-lying 1p-shell levels in relatively inaccessible T_z = 3/2 nuclei, such as ^{11}Be, ^{9}Li, and ^{7}He. However, no evidence was seen for any narrow excited states in ^{7}He. Also, no indication was observed for a strong final-state interaction in ^{5}H, although the known t + n interaction corresponding to the ^{4}H ground state was readily apparent. Two previously unreported levels (at 7.47 $\pm$ 0.05 MeV and 8.86 $\pm$ 0.07 MeV) were identified in the T_z = 2 nuclide ^{24}Ne.

The measured angular distributions were all rather featureless

and decrease monotonically with increasing angle. This feature can be explained by a semi-classical approach to the reaction kinematics in terms of the localization of the incoming wave packet at a relatively large interaction radius without strong focusing into a particular Coulomb trajectory. Similarly, simple DWBA calculations indicate that the angular distributions should not be very oscillatory, although these calculations do not describe very well the envelope of the observed distributions. Both the semi-classical reaction theory and the DWBA calculations indicate that the kinematic term in the transition matrix should be only slightly dependent upon the transferred angular momentum. However, while the observed relative transition yields agree qualitatively with the spectroscopic predictions of Cohen and Kurath (Co 70), good quantitative agreement was not obtained. This could indicate the inappropriateness in the present situation of either the semi-classical reaction theory or its approximation for the functional form of the Q-value dependence.

The (^{6}Li,^{8}B) two-proton pickup reaction has been demonstrated to be well suited to counter-telescope techniques and most appropriate on light targets. However, due to the higher yield one might expect that future studies of two-proton pickup on heavier targets will employ other techniques, such as the (^{11}B,^{13}N) reaction. Now that this work has demonstrated the broad utility of two-proton pickup reactions, one might also expect further two-nucleon transfer studies to focus on two-proton transfer reactions. For example, two-proton pickup reactions can be employed in investigations of neutron-excess systems for mass measurement studies with neutron-excess targets such as ^{36}S and ^{70}Zn

as well as spectroscopic studies of the levels of $T_z = 2$ nuclides by reactions on $T_z = 1$ targets. Finally, spectroscopic studies on heavier targets might permit investigation of proton pairing-vibration states by studying a series of targets such as ^{48}Ca, ^{50}Ti, ^{52}Cr, and ^{54}Fe or ^{140}Ce, ^{142}Nd, and ^{144}Sm.

ACKNOWLEDGEMENTS

I would like to express my appreciation to:

My research advisor, Dr. Joseph Cerny, for his interest and support over the years and, perhaps more important, for his patience and wisdom in providing me both the time and space to grow both as a nuclear physicist and, eventually, as an ERGie;

The senior staff of Building 88, Dr. Bernard Harvey, Dr. David Hendrie, Dr. H. E. Conzett, Dr. David Scott, and Dr. David Clark, for their interest and encouragement in my work and for providing a milieu of interesting and excellant physics;

The various post-docs with whom I have had the pleasure of working, Dr. Hans Harney, for his guidance and friendship during my formative days, Dr. Nick Jelley, for his assistance, advice, and companionship over the years and miles, Dr. Rick Gough, Dr. Dan Ashery, Dr. Gary KeKelis, Dr. Rainer Jahn, and Dr. Charles Mcguire, for their aid and example;

Dr. Mike Zisman, whose enthusiasm and dedication were always both inspiring and helpful, first, as a senior graduate student guiding me through my orals and, second, as a post-doc suffering through a few experiments, numerous drafts of papers, and finally numerous drafts of this thesis;

The past and present graduate students, John Esterl, George Goth, Joe Sherman, John Macdonald, Rich Sextro, Leonard Ho, Dave Vieira, Dieter Stahel, and Dennis Moltz, for numerous owl shifts, good times,

and their support in countless ways;

My collaborator on these experiments, Ken Wilcox, for sharing these years in many ways;

My faithful office-mate, Gordon Wozniak, for his friendship, example, assistance, and parties;

Creve Maples, for countless computer programs and interesting conversations;

The cyclotron crew and other support people for making Building 88 such a pleasant place to work, particularly John Bowen, for his long hours developing lithium beams; Roy Burton, for his assistance with design work and for supplying the mermaids; Claude Ellsworth, for the targets; Frank Hart and the Accelerator Technicians, Manny Enos and the electricians, Ted Reynolds, Lou Bish, and the maintenance machinists, for their aid; Carol Adams, for crack-typing, dynamic phone pages, and general exuberance; Fred Goulding and Don Landis, for their elegant electronics; Ed Lampo and Glenn Skipper, for their patient assistance in the care and feeding of electronics and computers; Jack Walton and Heinrich Sommer, for their beautiful detectors; and John Flambard and Evelyn Grant, for their wondrous illustrations;

To my family, for their support and confidence in my future;

To Cheryl, for her love, comfort, and warm ways over the years, particularly for her support and assistance during my thesis months in the typing of the countless drafts, and for the Tekies that made this work possible;

To Suzanne, Shadow, the Grateful Dead, and Richard Brautigan, for both joy and a joyeous perspective;

To Carl Blumstein and the unbearable multitude (particularly Kent Anderson), for harassing me to complete this task;

And to the U. S. Energy Research and Development Administration who supported this work.

APPENDIX A. UNBOUND FINAL SYSTEMS

An additional element of complexity occurs in reactions of the type

$$1 + 2 \rightarrow 3 + 4 + \ldots + n$$

(where 1 is the beam, 2 is the target, 3 is the detected particle, and 4 through n are unobserved). While these reactions obey the same laws of conservation of energy, linear momentum, and angular momentum as do two-body reactions, the multi-body nature of the final state means that measurement of the angle and energy of particle 3 no longer completely specifies the reaction kinematics. In an ordinary two-body final system, the energy and laboratory angle, θ, of one of the particles uniquely determines the energy and angle of the unobserved particle. For multi-body final systems, the additional complexity is that the center-of-mass energy of the final system is distributed among three or more nuclides, and for any detected energy and angle of one particle, the unobserved nuclei can experience a range of relative energies.

The consequences of this added freedom in the residual system can be explored by writing the differential cross section of the observed particle as

$$\frac{d\sigma}{dE_3 d\Omega_3} = \frac{8\pi^2}{h^2} \frac{\mu_1}{k_1} |M(E_3,\Omega_3)|^2 \rho(E_3,\Omega_3) \qquad \text{(A1)}$$

where μ_1 is the reduced mass of the initial system, k_1 is the relative momentum between the target (2) and the projectile (1), $|M(E_3,\Omega_3)|^2$ is the matrix element determining the interaction, and $\rho(E_3,\Omega^3)$ is the phase space or density of final states (see Go 71 and references

therein for a more detailed discussion). One might expect that effects due to the multi-body nature of the final state could arise through either the phase space factor or the matrix element. We will discuss each in turn below.

1. Phase Space

One can see from Eq. (A1) that the cross section is proportional to the density of final states. The division of the available energy between the unobserved particles can be considered (in a simple picture) to depend not on the residual nuclei, but on the number of ways in which this division can be accomplished. (Of course, a strong interaction among these nuclei can cause an enhancement of the yield above this simple statistical distribution through the matrix element; such as enhancement could indicate the existence of a state at this relative energy (see Section 2 below).)

For a system such as the 3n final state, there are very few orientations allowed which provide low relative energy among all three neutrons, while still conserving linear and angular momentum with the observed particle. On the other hand, there are many ways of distributing 10 MeV excitation among these three neutrons. Accordingly, one would expect the yield at 10 MeV excitation to be greatly enhanced over that at 0 MeV. From this simple argument, one can derive an expression for this relative enhancement by counting the number of values of the linear momentum permitted the observed particle while integrating over the coordinates of the unobserved nuclei within the limits of the conservation laws (see Ha 69 and Go 71 for some simple examples of this derivation). This result is generally familiar from

β-decay, where the shape of the detected electron spectrum is simply that of three-body phase space.

In the case of non-relativistic particles, the phase space distribution in an n-particle final state can be solved in general. In the center-of-mass frame

$$\left(\frac{\partial^2 N}{\partial E_3 \partial \Omega_3}\right)_{c.m.} \propto (E_3)^{1/2}_{c.m.} \cdot \left(E - \frac{M_t}{(M_t \cdot M_3)} \cdot (E_3)_{c.m.}\right)^{\left(\frac{3}{2n} - 4\right)} \qquad (A2)$$

where

$$E = Q + (M_2/M_1 + M_2) \cdot E_1$$

is the energy available in the center of mass frame; $(E_3)_{c.m.}$ is the center-of-mass energy of the detected final particle; and M_t is the total mass of all the particles in the final system (Ba 73). To convert this quantity from the center-of-mass to the laboratory frame of reference, one uses simply the inverse of the Jacobian.

At some excitation, most systems become unbound to several decay channels. For example, ^{5}H is unbound to (d + 3n) at 6.3 MeV above its threshold for breakup into (t + 2n), while at 8.5 MeV, it becomes unbound to (p + 4n). The ratio of the appropriate phase space distributions with more than one channel open will be equal to the ratio of the decay widths. For the systems that we have investigated (i.e., ^{4}H, ^{5}H, and ^{7}He), the ratio of these decay channels as a function of energy is unknown. One would expect that the opening of additional breakup modes will reduce the normalization of the previous phase space

distribution, on the assumption that the cross section is either a constant or smoothly varying function of the excitation energy. Because of these complexities, we have not attempted phase space fits that are a composite of several of these distributions, but have only fit the less ambiguous portions of the spectra. Such a fit is achieved by an arbitrary normalization of the expected shape to the experimental spectrum. Even with fixed proportions of the various distributions, it would be difficult to perform composite fitting with much confidence, since in a situation of several breakup modes, the regions near the various thresholds may be distorted by the additional final state interactions.

Deviations from these phase space distributions can arise from either a final state interaction, or from the reaction mechanism. As an example, the reaction could have a knock-out mechanism.

2. Final State Interactions

An enhancement of the yield above phase space is often called a final state interaction. Any state will cause such an enhancement, but not all of these final state interactions correspond to states in the system to interest or to only one particular level. (A resonance will also cause an enhancement, but then is typically described as a resonant interaction rather than a final state interaction.) For example, if one were studying the $^{7}Li(^{6}Li,^{8}B)^{5}H$ reaction and saw an enhancement above phase space, then this effect, if it were not an artifact of the reaction mechanism, would be a final state interaction. However, this additional yield could arise from the matrix element corresponding to the t + n + n interactions (^{5}H), or to the n + n

interaction (corresponding to ^{2}n), or to the t + n interactions (^{4}H), or it might be a combination of all of these systems. Similarly, at the higher breakup thresholds, enhancements might arise from d + n or p + n interactions, respectively. Also in ^{4}H there is known final state interaction between the t + n, but it is felt to correspond to, not only the ground state of ^{4}H, but also to the three other low-lying levels (since all these states are quite broad).

There are two ways of removing this ambiguity. Interactions in the mass 2, or 4, or 5 systems all have characteristic kinematic shifts so that by collecting data at several angles one should be able to decide which interaction is present. Alternatively, if one employs a coincidence experiment, in which all but one of the final particles is observed, then one would note on correlation plots that the enhancement corresponds to particular relative energies between some group or groups of particles.

APPENDIX B. REACTION DYNAMICS

1. Definitions and Relationships of Some of the Kinematic Parameters

We will employ the following subscript convention

$$T(I,O)\ F$$

where T is target, I is the incident beam, O is the outgoing particle, and F is the final system. Then for these calculations

$$E_{c.m.} = M_T \cdot E_{lab}/(M_I + M_T) \tag{B.1}$$

$$k_I = (2 \cdot M_I \cdot E_{c.m.})^{1/2}/\hbar \tag{B.2}$$

$$\lambda_I = 1/k_I \tag{B.3}$$

$$\eta_I = Z_I \cdot Z_T \cdot k_I \cdot e^2/2E_{c.m.} \tag{B.4}$$

$$v_I = k_I \cdot \hbar/m_I \tag{B.5}$$

$$R_{int} = 1.65(A_I^{1/3} + A_T^{1/3}) \tag{B.6}$$

$$\theta_c/2\theta = \sin^{-1}(1/((R_{int} \cdot k_I)/\eta_I) \quad 1) \tag{B.7}$$

$$L_I(\theta_c) = \eta_I \cot(\theta_c/2) \tag{B.8}$$

$$L(0^o) = k_I \cdot R_{int} \tag{B.9}$$

$$\Delta\theta_{min}(\theta_c) = (2/\eta_I) \cdot \sin(\theta_c/2) \tag{B.10}$$

$$Q_{eff} = Q_o - ((Z_o Z_f \quad Z_I Z_T) \cdot e^2)/R_I \tag{B.11}$$

$$Q_{opt} = (Z_o Z_f - Z_I Z_T) \cdot E_{c.m.}/Z_I Z_T \tag{B.12}$$

In Brink's formalism

$$K_o = m_k \cdot V/\hbar \tag{B.13}$$

where: m_k = transferred mass

V = the relative velocity.

2. Tables of Kinematic Parameters for the (^{6}Li,^{8}B) reaction at 80.0 MeV on Some Representative Targets

****

9BF(6LI,8B)7HF

0 MEV

****

CM ENERGY IN (MEV) 48.04	MOMENTUM IN (FM-1) 3.71	VELOCITY IN (C) .131
CM ENERGY OUT (MEV) 13.76	MOMENTUM OUT (FM-1) 2.30	VELOCITY OUT (C) .061

Q (MEV) -23.60	Q OPTIMUM (MEV) -8.01	BRINK'S Q EFFECTIVE (MEV) -23.15

RC X K IN	22.86	AETA IN .67	CLASSICAL L IN 23.19
RC X K OUT	14.81	AETA OUT 1.20	CLASSICAL L OUT 13.57
QR TRANSFERRED AT 0 DEG.	9.05		DELTA L AT GRAZING ANGLE 9.62

R TOUCHING IN (FM) 6.43	WAVELENGTH IN (FM-1) .27
R TOUCHING OUT(FM) 6.45	WAVELENGTH OUT (FM-1) .44

GRAZING ANGLE IN (DEG) 3.30	MINIMUM ANGULAR UNCERTAINTY IN 8.07
GRAZING ANGLE OUT (DEG) 10.11	MINIMUM ANGULAR UNCERTAINTY OUT 18.44

****

12C(6LI,8B)10BE

0 MEV

****

CM ENERGY IN (MEV) 53.37	MOMENTUM IN (FM-1) 3.91	VELOCITY IN (C) .138
CM ENERGY OUT (MEV) 23.03	MOMENTUM OUT (FM-1) 2.97	VELOCITY OUT (C) .079

Q (MEV) -21.44	Q OPTIMUM (MEV) 5.93	BRINK'S Q EFFECTIVE (MEV) -21.87

RC X K IN 26.50	AETA IN .95	CLASSICAL L IN 25.54
RC X K OUT 20.34	AETA OUT 1.86	CLASSICAL L OUT 18.41
QR TRANSFERRED AT 0 DEG. 6.16		DELTA L AT GRAZING ANGLE 7.13

R TOUCHING IN (FM) 6.77	WAVELENGTH IN (FM-1) .26
R TOUCHING OUT (FM) 6.85	WAVELENGTH OUT (FM-1) .34

GRAZING ANGLE IN (DEG) 4.26	MINIMUM ANGULAR UNCERTAINTY IN 8.74
GRAZING ANGLE OUT (DEG) 11.51	MINIMUM ANGULAR UNCERTAINTY OUT 16.87

****

16O(6LI,8B)14C

0 MEV

****

CM ENERGY IN (MEV) 58.23 MOMENTUM IN (FM-1) 4.09 VELOCITY IN (C) .144
CM ENERGY OUT (MEV) 34.36 MOMENTUM OUT (FM-1) 3.63 VELOCITY OUT (C) .096

Q (MEV) -16.59 Q OPTIMUM (MEV) 14.56 BRINK'S Q EFFECTIVE (MEV) -17.80

PC X K IN 29.23 AETA IN 1.21 CLASSICAL L IN 28.00

PC X K OUT 26.37 AETA OUT 2.28 CLASSICAL L OUT 24.01

QR TRANSFERRED AT 0 DEG. 2.87 DELTA L AT GRAZING ANGLE 3.99

R TOUCHING IN (FM) 7.15 WAVELENGTH IN (FM-1) .24

R TOUCHING OUT(FM) 7.27 WAVELENGTH OUT (FM-1) .28

GRAZING ANGLE IN (DEG) 4.96 MINIMUM ANGULAR UNCERTAINTY IN 9.01

GRAZING ANGLE OUT (DEG) 10.85 MINIMUM ANGULAR UNCERTAINTY OUT 14.35

****

26MG(6LI,8B)24NE

0 MEV

****

CM ENERGY IN (MEV) 65.05	MOMENTUM IN (FM-1) 4.32	VELOCITY IN (C) .153
CM ENERGY OUT (MEV) 40.94	MOMENTUM OUT (FM-1) 3.96	VELOCITY OUT (C) .105

Q (MEV) -19.10	Q OPTIMUM (MEV) 25.30	BRINK'S Q EFFECTIVE (MEV) -21.66

RC X K IN	34.05	BETA IN	1.72
RC X K OUT	31.88	BETA OUT	3.48
CLASSICAL L IN	32.29		
CLASSICAL L OUT	28.24		
OR TRANSFERRED AT 0 DEG.	2.17	DELTA L AT GRAZING ANGLE	4.06

R TOUCHING IN (FM)	7.88	WAVELENGTH IN (FM-1)	.23
R TOUCHING OUT (FM)	8.05	WAVELENGTH OUT (FM-1)	.25

GRAZING ANGLE IN (DEG)	6.10	MINIMUM ANGULAR UNCERTAINTY IN	9.30
GRAZING ANGLE OUT (DEG)	14.06	MINIMUM ANGULAR UNCERTAINTY OUT	15.03

****

142ND(6LI,8B)140CE

0 MEV

****

CM ENERGY IN (MEV) 76.76	MOMENTUM IN (FM-1) 4.69	VELOCITY IN (C) .166
CM ENERGY OUT (MEV) 68.97	MOMENTUM OUT (FM-1) 5.14	VELOCITY OUT (C) .136

Q (MEV) -6.71	C OPTIMUM (MEV) 46.91	BRINK'S Q EFFECTIVE (MEV) -20.38

RC X K IN 54.41	AETA IN 7.93	CLASSICAL L IN 45.97
RO X K OUT 60.89	AETA OUT 15.55	CLASSICAL L OUT 43.31
QR TRANSFERRED AT Q EFF. -6.48		DELTA L AT GRAZING ANGLE 2.66

R TOUCHING IN (FM) 11.55	WAVELENGTH IN (FM-1) .21
R TOUCHING OUT (FM) 11.85	WAVELENGTH OUT (FM-1) .19

GRAZING ANGLE IN (DEG) 19.56	MINIMUM ANGULAR UNCERTAINTY IN 13.83
GRAZING ANGLE OUT (DEG) 39.51	MINIMUM ANGULAR UNCERTAINTY OUT 19.64

REFERENCES

Aj 72. F. Ajzenberg-Selove, R. F. Casten, O. Hansen, T. J. Mulligan, Phys. Lett. 40B, 205 (1972).

Aj 73. F. Ajzenberg-Selove, H. G. Bingham, and J. D. Garrett, Nucl. Phys. A202, 152 (1973).

Aj 74. F. Ajzenberg-Selove and T. Lauritzen, Nucl. Phys. A227, 1 (1974) and references therein.

Aj 75. F. Ajzenberg-Selove, Nucl. Phys. A248, 1 (1975) and references therein.

Al 69. D. E. Alburger, E. K. Warburton, A. Gallmann, and D. H. Wilkinson, Phys. Rev. 185, 1242 (1969).

An 72. Argonne Physics Division Informal Report, PHY-1972H, "Symposium on Two-Nucleon Transfer and Pairing Excitations," (1972).

An 74. N. Anyas-Weiss, J. C. Cornell, P. S. Fisher, P. N. Hudson, A. Menchaca-Rocha, D. J. Millener, A. D. Panagiolou, D. K. Scott, D. Strottman, D. M. Brink, B. Buck, P. J. Ellis, and T. England, Phys. Report 12C, 201 (1974).

As 75. D. Ashery and M. S. Zisman, private communication.

As 76. D. Ashery, M. S. Zisman, G. W. Goth, G. J. Wozniak, R. B. Weisenmiller, and J. Cerny, Phys. Rev. C 13, 1345 (1976) and private communication.

Ba 66. F. C. Barker, Nucl. Phys. 83, 418 (1966).

Ba 71. A. D. Bacher, E. A. McClatchie, M. S. Zisman, T. A. Weaver, and T. A. Tombrello, Nucl. Phys. A181, 453 (1971).

Ba 73. A. D. Bacher, private communication.

Be 67. W. Benenson, G. M. Crawley, J. D. Dreisbach, and W. P. Johnson, Nucl. Phys. A97, 510 (1967).

Bi 67. J. Birnbaum, J. C. Overley, and D. A. Bromley, Phys. Rev. 157, 787 (1967).

Bo 64. A. N. Boyarkina, Akademiia Nauk, SSSR (English translation) Physical Series 28, 255 (1964).

Br 60. T. A. Brody, and M. Moshinsky, "Table of Transformation Brackets," Monografias del Instituto de Fisica, Mexico (1960).

Br 70. G. Bruge, J. C. Faivre, H. Faraggi, and A. Bussiere, Nucl. Phys. A146, 597 (1970).

Br 71. R. A. Broglia, C. Riedel, and T. Udagawa, Nucl. Phys. A169, 255 (1971).

Br 72. D. M. Brink, Phys. Lett. 40B, 37 (1972).

Br 73. R. A. Broglia, O. Hansen and C. Riedel, Advances in Nuclear Physics, M. Baranger and E. Vogt, eds. (Plenum Publishing Co., NY, 1973), Vol. 6, p. 287.

Ce 64. J. Cerny and R. H. Pehl, "Nuclear Spectroscopy with Direct Reactions," Argonne National Laboratory Report, ANL-6848, March 1964, p. 208.

Ce 65. J. Cerny, C. Detráz, and R. H. Pehl, Phys. Rev. Lett. 15, 300 (1965).

Ce 66a. J. Cerny, S. W. Cosper, G. W. Butler, H. Brunnader, R. L. McGrath, and F. S. Goulding, Nucl. Instr. and Meth. 45, 337 (1966).

Ce 66b. J. Cerny, C. Detráz, and R. H. Pehl, Phys. Rev. 152, 950 (1966).

Ce 68. J. Cerny, Ann. Rev. Nucl. Sci. 18, 27 (1968) and references therein.

Ce 74. J. Cerny, R. B. Weisenmiller, N. A. Jelley, K. H. Wilcox, and G. J. Wozniak, Phys. Lett. 53B, 247 (1974).

Ch 73. P. R. Christensen, V. I. Manko, F. D. Becchetti, and R. J. Nickles, Nucl. Phys. A207, 33 (1973).

Cl 72. D. J. Clark, J. Stayaert, J. Bowen, A. Carneiro, and D. Morris, AIP Conf. Proc., No. 9, Cyclotrons—1972. (Intern. Cyclotron Conference, Proc. of the 6th, Vancouver, 1972, J. J. Burgeryin and A. Strathdee, eds. (AIP, NY, 1972)), p. 265.

Co 70. S. Cohen and D. Kurath, Nucl. Phys. A141, 145 (1970).

Co 74a. B. J. Cole, A. Watt, and R. R. Whitehead, J. Phys. A: Math., Nucl. Gen. 7, 1374 (1974).

Co 74b. B. J. Cole, A. Watt, and R. R. Whitehead, J. Phys. A: Math., Nucl., Gen. 7, 1399 (1974).

Cr 74. C. Craig, Nucl. Phys. A225, 493 (1974).

Da 73. S. Dahlgren, P. Grafström, B. Höistad, and A. Åsberg, Nucl. Phys. A204, 53 (1973).

De 73. R. M. De Vries, Phys. Rev. C 8, 951 (1973).

Do 65. L. R. Dodd and K. R. Greider, Phys. Rev. Lett. 14, 959 (1965).

Do 66. L. R. Dodd and K. R. Greider, Phys. Rev. 146, 671 (1966).

En 73. P. M. Endt and C. van der Leun, Nucl. Phys. A214, 1 (1973) and references therein.

Fi 73. S. Fiarman and W. E. Meyerhof, Nucl. Phys. A206, 1 (1973) and references therein.

Fi 74. L. K. Fifield, R. W. Zürmuhle and D. P. Balamuth, Phys. Rev. C 10, 1785 (1974).

Fl 71. D. G. Fleming, J. C. Hardy, and J. Cerny, Nucl. Phys. A162, 225 (1971) and unpublished data.

Fl 74a. E. R. Flynn and J. D. Garrett, Phys. Rev. C 9, 210 (1974).

Fl 74b. E. R. Flynn, O. Hansen and O. Nathan, Nucl. Phys. A228, 189 (1974).

Gl 63. N. K. Glendenning, Ann. Rev. Nucl. Sci. 13, 191 (1963)

Gl 65. N. K. Glendenning, Phys. Rev. 137, B102 (1965).

Gl 71. Y. A. Glukhov, B. G. Novatskii, A. A. Ogloblin, S. B. Sakuta, D. N. Stephanov, and V. I. Chufv, Yad. Fiz. 13, 277 (English trans. Sov. J. Nucl. Phys. 13, 154 (1971)).

Gl 75. N. K. Glendenning, Nuclear Spectroscopy and Reactions, J. Cerny, ed. (Academic Press, NY, 1975), p. 317, part D.

Go 64. F. S. Goulding, D. A. Landis, J. Cerny, and R. H. Pehl, Nucl. Instr. and Meth. 31, 1 (1964).

Go 66. F. S. Goulding, D. A. Landis, J. Cerny, and R. H. Pehl, IEEE Trans. Nucl. Sci. 13, 514 (1966).

Go 71. G. W. Goth, Lawrence Berkeley Laboratory Report LBL-224, Ph. D. Thesis, 1971 (unpublished).

Gr 70. K. R. Greider, Nuclear Reactions Induced by Heavy Ions, R. Bock and W. R. Hering, eds. (North-Holland, Amsterdam, 1970), p. 217.

Go 75. D. A. Goldberg, J. G. Cramer, M. S. Zisman, and R. M. DeVries, private communication.

Ha 69. B. G. Harvey, Introduction to Nuclear Physics and Chemistry, (Prentice-Hall, Englewood Cliffs, NJ, 2d, 1969), p. 213.

Hi 69. R. E. Hintz, F. B. Selph, W. S. Flood, B. G. Harvey, F. G. Resmini, and E. A. McClatchie, Nucl. Instr. and Meth. 72, 61 (1969).

Ho 70. A. J. Howard, R. G. Hirko, D. A. Bromley, K. Bethge, and J. W. Olness, Phys. Rev. C 1, 1446 (1970).

Ho 72. A. J. Howard, R. G. Hirko, D. A. Bromley, K. Bethge, and J. W. Olness, Il Nuovo Cimento 11, 575 (1972).

Hu 75. The Fortran program HIPROB was provided by Dr. P. H. Hudson, Oxford University, Oxford, England.

Je 74. N. A. Jelley, K. H. Wilcox, R. B. Weisenmiller, G. J. Wozniak and J. Cerny, Phys. Rev. C 9, 2067 (1974).

Ka 71. G. Kaschl, G. Mairle, H. Mackh, D. Hartwig, and U. Schwinn, Nucl. Phys. A178, 275 (1971).

Ke 76. G. KeKelis, M. S. Zisman, D. K. Scott, D. L. Hendrie, R. B. Weisenmiller, and J. Cerny, unpublished data.

Kh 71. S. B. Khadkikar, S. C. K. Nair, and S. P. Pandya, Phys. Lett. 36B, 290 (1971).

Ku 56. D. Kurath, Phys. Rev. 101, 216 (1956).

Ku 72. D. Kurath, Comments on Nuclear and Particle Physics V2, 55 (1972).

Ku 74a. The Fortran program DWUCK (March 1974 version DWUCK IV) was provided by Dr. P. D. Kunz, University of Colorado, Boulder, CO.

Ku 74b. N. Kumar, Nucl. Phys. A225, 221 (1974).

Ku 75. D. Kurath, Argonne National Laboratory, private communication.

Ku 76. D. Kurath, Argonne National Laboratory, private communication.

Li 72. S. Lie, Nucl. Phys. A181, 517 (1972).

Li 73. R. H. Lindsay, W. Toews, and J. J. Veit, Nucl. Phys. A199, 513 (1973).

Lk 70. O. Lkhagva and I. Rotter, Yad. Fiz. 11, 1037 (Sov. J. Nuc. Phys. 11, 576 (1970)).

Ma 70. The Fortran program LZY was provided by Dr. C. C. Maples, Lawrence Berkeley Laboratory.

Ma 71. C. C. Maples, Lawrence Berkeley Laboratory Report LBL-253, Ph. D. Thesis, September 1971 (unpublished).

Ma 74. The Fortran program CHAOS was provided by Dr. C. C. Maples, Lawrence Berkeley Laboratory.

Mc 68. R. L. McGrath, J. Cerny, and S. W. Cosper, Phys. Rev. 165, 1126 (1968).

Me 76. A. Menchacca-Rocha, University of Mexico, private communication.

Mi 69. R. C. Minehart, L. Coulson, W. F. Grubb, III, and K. Ziock, Phys. Rev. 177, 1455 (1969) and references therein.

Mo 66. J. Moss and G. C. Ball, UCRL-17124, 1966 (unpublished).

Na 73. K. Nagatini, D. H. Youngblood, B. Kennefick, and J. D. Bronson, in Symposium on Heavy-Ion Transfer Reactions (Argonne, March, 1973). Argonne Physics Division Informal Report, PHY 1973B (1973), p. 623.

No 71. J. L. Norton and P. Goldhammer, Nucl. Phys. A165, 33 (1971).

Ol 71. R. W. Ollerhead, G. F. R. Allen, A. M. Baxter, B. W. J. Gillespie, and J. A. Kuehner, Can. J. Phys. 49, 594 (1971).

Pa 72. R. A. Paddock, Phys. Rev. C 5, 485 (1972).

Po 76. A. M. Poskanzer, Lawrence Berkeley Laboratory, private communication.

Pr 72. B. M. Preedom and B. H. Wildenthal, Phys. Rev. C 6, 1633 (1972).

Ri 68. G. Ripka, Advances in Nuclear Physics, M. Baranger and E. Vogt, eds. (Plenum Press, NY, 1968), Vol. 1, p. 183.

Ro 73. R. G. H. Robertson and B. H. Wildenthal, Phys. Rev. C 8, 241 (1973) and private communication.

Sc 73. D. K. Scott, in LBL-1991, and in Intern. Conf. on Nuclear Physics, Munich, 1973, Proc. by J. de Boor and H. J. Mang, eds. (North Holland/American Elsevier Publ. Co., Inc., 1973), p. 215.

Sc 74a. D. K. Scott. B. G. Harvey, D. L. Hendrie, L. Kraus, C. F. Maguire, J. Mahoney, Y. Terrien, and J. K. Yagi, Phys. Rev. Lett. 33, 1343 (1974) and private communication.

Sc 74b. D. K. Scott, in LBL-3434, and in Classical and Quantum Mechanical Aspects of Heavy Ion Collisions, H. L. Harney and C. K. Gelbke, eds. (Springer-Verlag, 1975), p. 165.

Sc 75. D. K. Scott, in Intern. Conf. on Cluster Structure of Nuclei and Transfer Reactions Inducted by Heavy-Ions (Tokyo, Japan, 1975), also in LBL-3495.

Si 72. R. H. Siemssen, C. L. Fink, L. R. Greenwood, and H. J. Körner, Phys. Rev. Lett. 28, 626 (1972).

Sø 74. B. Sørensen, Phys. Lett. 53B, 285 (1975).

Sq 70. G. T. A. Squier, A. R. Johnston, E. W. Spiers, S. A. Harbison, and N. M. Stewart, Nucl. Phys. A141, 158 (1970).

St 67. R. H. Stokes and P. G. Young, Phys. Rev. Lett. 18, 611 (1967).

Ta 60. I. Talmi, and I. Unna, Phys. Rev. Lett. 4, 469 (1960).

To 69. I. S. Towner and J. C. Hardy, Adv. Phys. 18, 401 (1969).

Tr 63. W. W. True, Phys. Rev. 130, 1530 (1963).

Wa 75. J. Walton, Lawrence Berkeley Laboratory, private communication.

We 75. R. B. Weisenmiller, unpublished data.

Wi 74. K. H. Wilcox, L. Ho, N. A. Jelley, R. B. Weisenmiller, G. J. Wozniak, and J. Cerny, unpublished data.

Yo 68. P. G. Young, R. H. Stokes, and G. G. Ohlsen, Phys. Rev. 173, 949 (1968).

Yo 71. P. G. Young, and R. H. Stokes, Phys. Rev. C 4, 1597 (1971).

Yo 73. D. H. Youngblood, K. Nagatani, R. Kenefick, and J. D. Bronson, in Symp. on Heavy-Ion Transfer Reactions, (Argonne, 1973), Vol. II. Argonne Physics Division Informal Report, PHY-1973B (1973), p. 689 and Phys. Rev. Lett. 31, 250 (1973).

This report was done with support from the United States Energy Research and Development Administration. Any conclusions or opinions expressed in this report represent solely those of the author(s) and not necessarily those of The Regents of the University of California, the Lawrence Berkeley Laboratory or the United States Energy Research and Development Administration.

TECHNICAL INFORMATION DIVISION
LAWRENCE BERKELEY LABORATORY
UNIVERSITY OF CALIFORNIA
BERKELEY, CALIFORNIA 94720